In-vivo studies of new vector velocity and adaptive spectral estimators in medical ultrasound

Hansen, Kristoffer Lindskov; Nielsen, Michael Bachmann; Jensen, Jørgen Arendt

Publication date:
2011

Document Version
Publisher's PDF, also known as Version of record

In-vivo studies of new vector velocity and adaptive spectral estimators in medical ultrasound

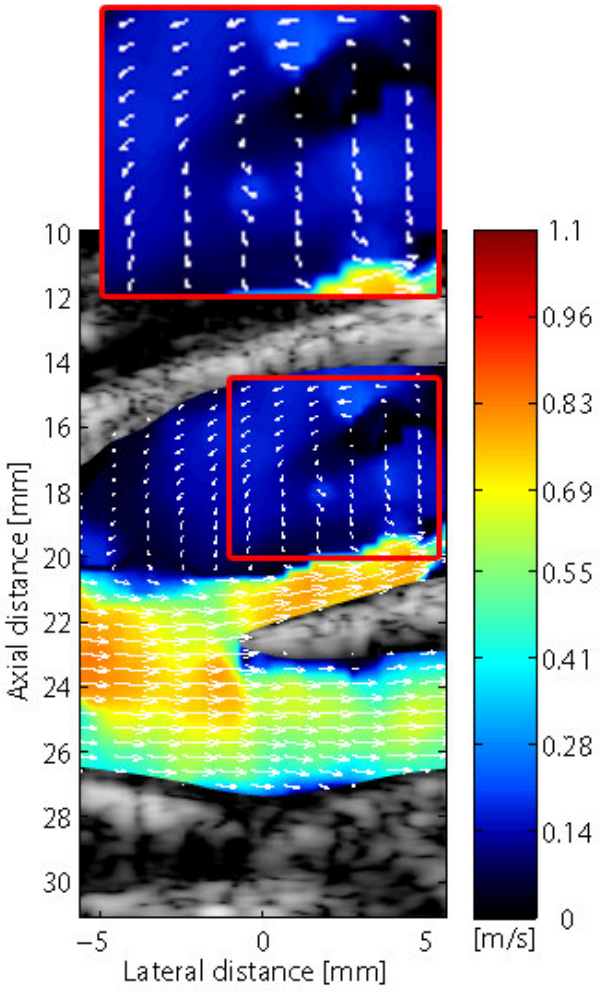

Ph.D. thesis

Kristoffer Lindskov Hansen, M.D.
Department of Radiology
Rigshospitalet
Denmark

Faculty of Health Sciences, University of Copenhagen

Main supervisor

Michael Bachmann Nielsen, M.D., Ph.D., Dr.Med., Professor, Department of Radiology, Section of Ultrasound, Rigshospitalet, Blegdamsvej 9, DK-2100 Kbh. Ø, Denmark

Project Supervisor

Jørgen Arendt Jensen, M.Sc. Ph.D., Dr.Techn., Professor, DTU Elektro, Building 349, Room 222, Technical University of Denmark, DK-2800 Kgs. Lyngby, Denmark

Evaluating committee

Liselotte Højgaard, M.D., Dr.Med., Professor, Department of Clinical Physiology and Nuclear Medicine and PET, Rigshospitalet, Blegdamsvej 9, DK-2100 Kbh. Ø, Denmark

Hans Nygaard, M.Sc., Dr.Med., Professor, Aarhus University Hospital, Department of Cardiothoracic and Vascular Surgery T, Skejby Sygehus, DK-8200 Aarhus N, Denmark

Ola Björgell, M.D., Dr.Med., Docent, Department of Radiology, Universitetssjukhuset MAS, 205 02 Malmö, Sweeden

Front page illustration: Vortex formation in the bulb of the internal carotid artery visualized with the vector method Plane Wave Excitation.

Contents

Acknowledgements

I am grateful to the volunteers who generously participated in the studies included in the thesis.

Without my supervisors Michael Bachmann Nielsen and Jørgen Arendt Jensen, who introduced me to clinical research, this thesis would never have become reality. I am truly grateful for their effort, guidance and patience. I would like to fully thank my assistant supervisor Jesper Udesen for introducing me to the fascinating world of signal processing in ultrasound and for his never yielding support and optimism. I have benefited greatly from his advises and guidance. Also I would like to thank my unofficial supervisor Carsten Thomsen for constructive discussions, guidance and manuscript revisions in the studies concerning magnetic resonance imaging. In addition I would like to thank all my colleagues at Rigshospitalet and the Technical University of Denmark for inspiring collaborations. In particular, I thank Fredrik Gran, Niels Oddershede, Lasse Henze and Iben K. Holfort, with whom I simply could not have worked without and my research fellows Mads M. Pedersen, Caroline Ewertsen, Kristina R. Nielsen, Hanne Sønder, Thomas Skaarup Kristensen, Ester Belmaati, Søren Heerwagen, Anders Ohlhues, Klaus S. Andersen, Henrik Andresen and David Bæk. I would like to thank Jon Hyett and Andrew Child for letting me stay at the Department of Obstetric Ultrasound and Fetal Medicine at Royal Prince Alfred Hospital in Sydney, Australia as part of CADUCEUS - The Danish-Australasian ultrasound exchange program. A big thank-you shall also go to Linda Schumann, Elna Sørensen and Bettina Jepsen.

Additionally, I thank

- The Department of Radiology and especially the sections of ultrasound and MRI, Rigshospitalet, Copenhagen for letting me use the equipment.
- Paul E. Nilsson, Head of the Department of Radiology, Rigshospitalet, Copenhagen for making this work possible financially.

The studies were supported by grant 26-04-0024 from the Danish Science Foundation and by B-K Medical A/S, Herlev, Denmark.

Project summary

In this PhD project new ultrasound techniques for blood flow measurements have been investigated *in-vivo*. The focus has mainly been on vector velocity techniques and four different approaches have been examined: Transverse Oscillation, Synthetic Transmit Aperture, Directional Beamforming and Plane Wave Excitation. Furthermore two different adaptive spectral estimators have been investigated: Blood spectral Power Capon method (BPC) and Blood Amplitude and Phase Estimation method (BAPES).

The novel techniques investigated in this thesis are developed to circumvent some of the main limitations in conventional Doppler ultrasound. That is angle dependency, reduced temporal resolution and low frame rate.

Transverse Oscillation, Synthetic Transmit Aperture and Directional Beamforming can estimate the blood velocity angle independently. The three methods were validated *in-vivo* against magnetic resonance phase contrast angiography when measuring stroke volumes in simple vessel geometry on 11 volunteers. Using linear regression and Bland-Altman analyses good agreements were found, indicating that vector velocity methods can be used for quantitative blood flow measurements.

Plane Wave Excitation can estimate blood velocities angle independently with a high frame rate. Complex vessel geometries in the cardiovascular system were explored *in-vivo* on four volunteers using the technique. Flow patterns previously visualized with magnetic resonance angiography and predicted by models of computational fluid dynamics, were shown for the first time with ultrasound. Additionally, new information on complex flow patterns in bifurcations and around venous valves was discovered.

BPC and BAPES are adaptive spectral estimators which can produce spectrograms with a high temporal resolution. Spectrograms obtained *in-vivo* with the two techniques on ten volunteers were evaluated quantitatively and qualitatively and compared to the conventional spectral Doppler method. Descriptive statistics, kappa statistics and multiple t-tests were performed and it was shown that BAPES and BPC can produce useful spectrograms with a narrower observation window compared to the conventional spectral Doppler method.

The thesis shows, that novel information can be obtained with vector velocity methods providing quantitative estimates of blood flow and insight in to the complexity of fluid dynamics. This could give the clinician a new tool in assessment and treatment of cardiovascular diseases. Also solutions to produce spectrograms with fewer emissions per estimate were given. This could potentially bring improvements to spectral blood estimation as an increase of the temporal resolution of the spectrogram or as an increase of the frame rate for the interleaved B-mode images.

Dansk resumé

I dette PhD projekt er nye ultralydmetoder til måling af blodets hastighed blevet undersøgt *in-vivo*. I alt er seks metoder undersøgt. Fire forskellige vektorultralydsteknikker: Transverse Oscillation, Synthetic Transmit Aperture, Directional Beamforming og Plane Wave Excitation og to forskellige adaptive spektralestimatorer: Blood spectral Power Capon method (BPC) og Blood Amplitude and Phase Estimation method (BAPES).

De nye teknikker belyst i denne afhandling er udviklet i forsøget på at løse nogle af de begrænsninger, der findes i konventionel Dopplerultralyd: vinkelafhængighed i hastighedsestimering, lav temporal opløsning og lav frame rate.

Transverse Oscillation, Synthetic Transmit Aperture og Directional Beamforming er tre vektorteknikker, der er kendetegnet ved at kunne estimere blodets hastighed vinkeluafhængigt. De tre metoder blev valideret *in-vivo* med magnetisk resonans fase kontrast angiografi ved måling af slagvolumen i en simpel kargeometri på 11 forsøgspersoner. Ved hjælp af lineær regression og Bland-Altman analyser blev det vist, at der var god overensstemmelse med reference metoden, hvilket indikerer, at vektorteknikker i ultralyd kan benyttes til at måle volumenflow.

Plane Wave Excitation er en vektorteknik, der vinkeluafhængigt og med høj frame rate kan måle blodets bevægelse. Komplekse kargeometrier blev skannet *in-vivo* hos fire forsøgspersoner. Flowmønstre, der før er visualiseret med magnetisk resonans og beregnet ud fra computer genereret fluid modeller, blev for første gang vist med ultralyd. Desuden blev ny information opsamlet om blodet komplekse bevægelser i bifurkaturer og omkring veneklapper.

BPC og BAPES er adaptive spektralestimatorer, som kan generere spektrogrammer med en høj temporal opløsning. Ti forsøgspersoner blev skannet *in-vivo.* Spektrogrammer beregnet med de adaptive metoder og den konventionelle metode blev sammenlignet kvantitativt og kvalitativt. Deskriptiv og kappa statistik samt multipel t-test viste, at BAPES og BPC kunne producere brugbare spektrogrammer med et smallere observationsvindue i forhold til den konventionelle metode.

Denne afhandling viser, at ny kvantitativ og kvalitativ viden om blodets bevægelse kan opsamles med vinkeluafhængige vektorteknikker og give en øget forståelse af blodets komplekse flowmønstre. Dette kunne blive et brugbart redskab for klinikeren i bestemmelse og behandling af kadiovaskulære lidelser. Samtidig viser afhandlingen at adaptive spektralestimatorer kan generere brugbare spektrogrammer med færre data end den konventionelle metode. Dette vil kunne forbedre anvendeligheden af spektral Doppler enten ved at øge den temporale opløsning i spektrogrammet eller ved at øge frame rate for B-mode sekvensen.

List of papers

Journal papers:

1. Hansen K.L., Udesen J., Thomsen C., Jensen J.A., Nielsen M.B., *In-vivo* validation of a blood vector velocity estimator with MR angiography, IEEE UFFC, vol. 56 pp 91 - 100, 2009 (appendix 1)

2. Hansen K.L., Udesen J., Oddershede N., Henze L., Thomsen C., Jensen J.A., Nielsen M.B., *In-vivo* comparison of three ultrasound vector velocity techniques to MR phase contrast angiography, accepted for publication, Ultrasonics, 2009 (appendix 2)

3. Hansen K.L., Udesen J., Gran F., Jensen J.A., Nielsen M.B. *In-vivo* examples of flow patterns with a fast vector velocity ultrasound method, accepted for publication, Ultraschall in Med., 2009 (appendix 3)

4. Hansen K.L., Gran F., Pedersen M.M., Holfort I.K., Jensen J.A., Nielsen M.B., *In-vivo* validation of fast spectral velocity estimation techniques, submitted, 2009 (appendix 4)

Conference papers:

1. Hansen K.L., Udesen J., Thomsen C., Jensen J.A., Nielsen M.B., Validation of Transverse Oscillation Vector Velocity Estimation *In-Vivo*, Proc IEEE Ultrason Symp, pp. 1093-1096, 2007 (appendix 5)

2. Hansen K.L., Udesen J., Oddershede N., Henze L., Thomsen C., Jensen J.A., Nielsen M.B., *In-vivo* evaluation of three ultrasound vector velocity techniques with MR angiography, Proc IEEE Ultrason Symp, pp. 1060-1063, 2008 (appendix 5)

3. Hansen K.L., Udesen J., Gran F., Jensen J.A., Nielsen M.B., Fast Blood Vector Velocity Imaging using ultrasound: *In-vivo* examples of complex blood flow in the vascular system, Proc IEEE Ultrason Symp, pp. 1068 – 1071, 2008 (appendix 5)

4. Hansen K.L., Gran F., Pedersen M.M., Holfort I.K., Jensen J.A., Nielsen M.B., *In-vivo* validation of fast spectral velocity estimation techniques - preliminary results, Proc IEEE Ultrason Symp, pp. 1615-1618, 2008 (appendix 5)

List of abbreviations

BAPES: Blood Amplitude and Phase Estimation method
BPC: Blood spectral Power Capon method
CFU: Center of Fast Ultrasound Imaging
DB: Directional Beamforming
DTU: Technical University of Denmark
FWHM: Full-width-at-half-maximum
KLH: Kristoffer Lindskov Hansen
MRA: Magnetic resonance angiography
OW: Observation window
PWE: Plane Wave Excitation
RASMUS: Remotely Accessible Software configurable Multi-channel Ultrasound Sampling
SARUS: Synthetic Aperture Real-time Ultrasound System
STA: Synthetic Transmit Aperture
TO: Transverse Oscillation
US: Ultrasound
W.BOX: Welch's method with boxcar window
W.HAN: Welch's method with Hanning window

Introduction

The thesis is a collaborative work between the Section of Ultrasound in the Department of Radiology located in Rigshospitalet, and Center of Fast Ultrasound Imaging (CFU) located at the Technical University of Denmark.

The studies were focused on evaluations of new methods for blood flow measurements developed at CFU. The methods have previously been evaluated in simulations and in flow phantoms. This work concerns *in-vivo* validation which is an important investigational stage before any new method can be implemented into commercially available scanners.

The methods are all thought as possible solutions to some of the inherent limitations found in conventional Doppler ultrasound. Firstly, modern scanners of today can only estimate blood velocities angle dependently and this introduces an operator dependent angle correction. The angle correction is build upon the assumption of laminar flow, which is a gross simplification. Secondly, the frame rate of the B-mode image and the temporal resolution of the velocity estimation suffer when several ultrasound modalities are performed simultaneously as in duplex and triplex scan mode. In the thesis angle independent vector velocity estimators and fast adaptive spectral estimators are investigated.

The experimental scanner RASMUS (1;2) developed at CFU has made it possible to realize the *in-vivo* clinical trials as full control is achieved of how signals are sent out and how the scattered signals are received. In several of the studies, magnetic resonance was used as the reference modality and this took place in the MR department of Rigshospitalet. All the studies were carried out on healthy young volunteers found among colleagues and friends.

Apart from the studies enrolled in the thesis, I have helped colleges with clinical scans necessary for their projects. This has resulted in a number of co-authored papers:

- Gran F., Hansen K.L., Jensen J.A., Nielsen M.B., Preliminary *In-vivo* Results For Spatially Coded Synthetic Transmit Aperture Ultrasound Based On Frequency Division, IEEE Ultrasonics Symposium, 2006, pp 1087-1090
- Henze L., Holfort I.K., Kortbek J., Hansen K.L., Jensen J.A., *In vivo* vector flow imaging using improved Directional Beamforming, IEEE Ultrasonics Symposium, 2007 , pp 2438-2441
- Udesen J., Gran F., Hansen K.L., Jensen J.A., Thomsen C., Nielsen M.B., Fast Blood Vector Velocity Imaging: Simulations and Preliminary In Vivo Results, IEEE Ultrasonics Symposium, 2007, pp 1005-1008
- Oddershede N., Hansen K.L., Nielsen M.B., Jensen J.A., *In-vivo* examples of synthetic aperture vector flow imaging, Proc SPIE Medical Imaging, 2007, Vol. 6513, 65130A
- Udesen J., Gran F., Hansen K.L., Jensen J.A., Thomsen C., Nielsen M.B., High frame-rate blood vector velocity imaging using plane waves: simulations and preliminary experiments, IEEE UFFC, 55(8), 2008, pp 1729-43

Background

Definition of blood flow

Blood flow is defined as the flow of blood in the cardiovascular system. Flow can be described as laminar, disturbed/complex or turbulent flow. The transition of flow from laminar to turbulent is dependent on a number of factors, e.g. vessel geometry, velocity, pulsation and plaque involvement. In healthy individuals only laminar and disturbed/complex flow patterns are present while turbulent flow is a symptom of vessel disease. The type of flow is described numerically by the Reynolds number and usually turbulence occurs when the Reynolds number exceeds 2500 (3). Flow can be measured as a velocity (meters per second) or a quantity (liters per second or liters per stroke). Flow measurements can be done invasively or non-invasively. In this thesis are only used non-invasive methods for blood flow estimation. Nevertheless, a brief introduction to some of the invasive methods is presented below.

Invasive techniques

Invasive techniques for measuring blood flow are mostly based on the indicator dilution technique, where an indicator, such as radioisotopes, iodinated agents, dyes, cold saline ect., injected into the blood stream, makes it possible to record changes of indicator concentration in the region or vessel of interest over time (4;5)

Swan-Ganz catheter, used for estimating cardiac output, is based on a thermo dilution method using cold saline as indicator (6). Positron Emission Tomography (PET) and Single Photon Emission Computed Tomography (SPECT) use unstable isotopes in imaging and measure mainly blood flow in the brain (4). Iodinated agents are used as indicators in conventional contrast-enhanced perfusion computed tomography (CT) and can provide both qualitative and quantitative estimates (7). Digital subtractions angiography also uses iodinated agents to enhance the attenuation in vessels, however the method only provides qualitative information (8). Contrast enhanced magnetic resonance imaging using gadolinium chelates as the indicator agent is used for both imaging and quantifying blood flow. The bolus of contrast creates, in contrast to iodinated agents, a drop in signal intensity in the voxel, which can be related to the blood flow (9).

Electromagnetic flowmeter does not use the indicator dilution principle albeit it is an invasive method for flow measurement. A magnetic field is applied over the vessel of interest. In the vessel, a catheter with two electrodes mounted on the tip is inserted. Knowing the electric and the magnetic field, the blood velocity can be estimated (5).

Non-invasive techniques

Non-invasive techniques for blood flow measurement in vessels can be performed with a number of different techniques: laser Doppler flowmetry,

plethysmography, magnetic resonance phase contrast angiography and Doppler ultrasound.

Laser Doppler flowmetry solely measures microcirculation down to 1 mm in the dermis and only as a blood flux in arbitrary perfusion units. Laser Doppler flowmetry is primarily used as an evaluation tool of endothelial function (10). Plethysmography is used for investigation of limb blood flow, yielding a global blood arterial inflow for the investigated limb (11), while the selective evaluation of small vessels, sections of vessels, blood flow in the major vessels and cerebral blood flow are only feasible non-invasively with magnetic resonance angiography and ultrasound Doppler techniques (5).

The techniques used in magnetic resonance for non-invasive blood flow measurements are mainly the time-of-flight and the phase contrast sequences even though a lot of novel sequences are emerging such as blood oxygenation level dependent (BOLD) and arterial spin labeling techniques (12). In this thesis is only used the phase contrast technique, which ECG-triggered can provide quantitative blood flow measurements. The method is accepted as the gold standard for non-invasive cerebral blood flow estimation and has been validated accordingly both *in-vivo* and *in-vitro* (13-18). Phase contrast angiography is a subtraction technique where two images are obtained with different gradients and subtracted from each other (19). The contrast between blood and surrounding tissue is achieved by manipulating the magnetization of moving and stationary spins. The phase of the magnetization from the stationary spin is zero and the phase of the magnetization from the moving spin is non-zero. Thereby, direction and velocity of the moving blood can be derived from the obtained phase velocity maps (20).

The assessment of blood flow with magnetic resonance angiography regardless of the applied sequence is time-consuming, the equipment is expensive and non-mobile, the evaluation is not performed in real time and the estimates are not instantaneous. Conversely, Doppler ultrasound, which is the clinical method of choice for real time assessment of blood velocities is an easily manageable and fast technique, the equipment is mobile, relatively inexpensive, and providing instantaneous estimates. However, the current Doppler systems suffer from several limitations. In this thesis two main limitations are sought to be solved: the angle dependency and the relatively low frame rate.

Doppler ultrasound

In conventional Doppler methods pulses with 4-8 cycles are emitted at frequencies of 2-12 MHz. The ultrasound, scattered by the moving blood cells, are received by the transducer as echoes and then converted to a voltage signal. On the basis of time-of-flight from emission of the signal to reception of the echo, the position of the moving blood cell can be determined while the velocity of the motion is found from a measured phase shift (21;22). The velocity estimate is only found along the ultrasound beam direction, i.e. in the axial direction. Formally, this can be described as,

$$v_z = \frac{f_p c}{2 f_o} \quad (1),$$

where v_z is the axial velocity, f_p is the Doppler frequency, f_0 is the centre frequency of the emitted ultrasound pulse and c is the speed of sound. As transverse flow to the beam direction is not found, the operator is impelled to achieve an acceptable angle of insonation (< 70°) to record the blood motion.

In color flow mapping no angle correction is performed and thus, no correct velocities are given. Consequently, color flow mapping is only used as a qualitative method for visualizing flow. In Fig. 1 the common carotid artery with an angle of insonation of 90° is shown.

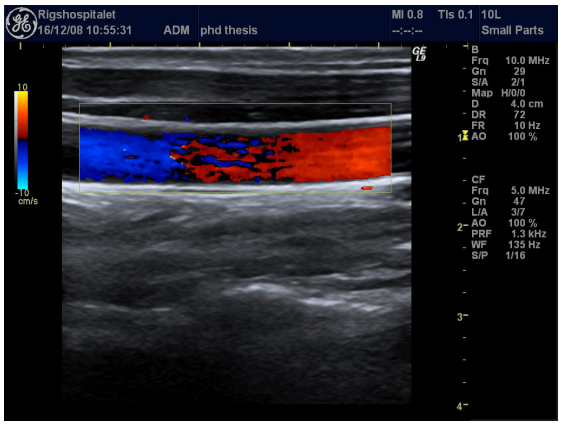

Figure 1: Color flow mapping of the common carotid artery is shown. It can only be used for qualitative evaluation. Note that with an angle of insonation of 90° no velocities are measured.

Angle dependency

In spectral Doppler examination angle correction is applied on blood velocities estimated within the range gate. The spectral Doppler method is used quantitatively as it is believed that true velocities are displayed after angle correction. This can be seen from the relationship between the axial velocity v_z given by (1) and the true velocity of the blood v given by,

$$v = \frac{v_z}{\cos\theta} = \frac{f_p c}{2 f_o \cos\theta} \quad (2),$$

where θ is the angle between the ultrasound beam and the blood flow. All variables in (2) can be estimated if the operator manually supplies the scanner with the angle θ assuming blood flow parallel to the vessel wall. When performing angle correction in spectral Doppler examination, it is compulsory to achieve an angle of insonation below 70°. When the angle approaches 90° reliable velocity estimates cannot be obtained with (2) as $\cos(90) \sim 0$ and small deviations between the angle estimated visually by the operator and the correct angle between blood flow and beam direction result in large errors when calculating the velocity v.

However, not even an acceptable angle of insonation is a guarantee for correct velocity estimation. Tola et al. showed differences of 24-25% for peak

systolic and end-diastolic velocities between measurement obtained with fixed angles of 45° and 60° (23) and Hoskins showed an overestimation of maximum velocity by 20% at 50°, 15-30% at 60° and 24-46% at 70° (24).

Not only poses the angle of insonation a problem in the velocity estimation, also the necessary assumption made by the operator concerning the direction of the blood flow is problematic. In the ideal situation, the rigid and straight vessel encompasses a laminar flow parallel to the vessel boundaries, and the angle correction scheme can be made. Vessels are curving and highly elastic creating skewed velocity profiles (25-27) with secondary velocity components (28-32), which makes such an assumption a source of measurement error (33). Thus, it is in general impossible to predict the direction of a blood scatterer based on the B-mode image (24;34-36).

The problem becomes even more evident when examining vessels with complex geometries as the flow profile in these areas always are multidirectional. At bifurcations, branchings, valves or any kind of constrictions the pulsative nature of human blood flow will give rise to disturbed or even turbulent flow, where flow direction rapidly changes within the heart cycle. Correcting for the angle would therefore imply that the operator has an a priori knowledge of the direction of the blood scatterers at any location for any image, which clearly is impossible.

In conclusion, an error will always be associated with the conventional Doppler methods with or without angle correction due to angle dependency, and information on the complex flow patterns kept unrevealed (37;38).

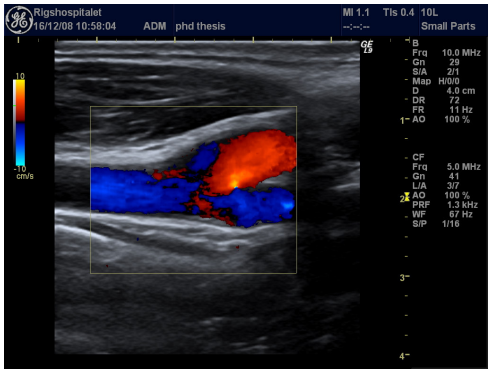

Figure 2: Color flow mapping of the carotid bifurcation is shown. The complex flow patterns are only visualized as a confusing blend of colors.

Accuracy and reproducibility of Doppler ultrasound

Precise information of blood flow is desirable and especially of the blood flow in complex geometries with disturbed flow and vortices as these regions have predilection for atherosclerotic lesions (37-40). The limitation of conventional Doppler ultrasound has been reflected in several papers concerning the validity and reproducibility. Hoskins showed that velocity parameters such as maximum blood velocity, mean blood velocity and volumetric flow had errors up to 100% depending especially on angle of insonation and blood velocity (41), Krams et al. investigated volume flow estimation assuming parabolic flow

and showed 24% error compared to a computational fluid dynamic model (33). However, studies showing the opposite have also been published e.g. Walker et al. using a string phantom reported only up to 5% overestimation of mean velocity (42) and Deane et al. reported 5% error in volume flow estimation with a commercial multi-gated Doppler system (43). Stewart et al. reported that the color Doppler accuracy was significantly dependent on transducer type, angle of insonation, the actual blood velocity and instrument settings such as pulse repetition frequency and wall filter frequency (44). Also operator and centre dependency have been addressed and several studies actually recommended centre specific validation to normalize for interequipment variation (45-47). Paivansalo carried out an *in-vivo* interobserver and interequipment study and showed variation of up to 61% for equipment and up to 42% variation between observers. In the study it was recommended in addition to centre specific validation, the use of the same operator and equipment for follow-up measurements to reduce the variability of estimates (48). Likewise, Henry-Feugeas et al. explored the variability on the operator and equipment level. While no equipment dependency was found, it was recommended to repeat measurements to reduce a significant operator variability (49).

Vector velocity imaging

The estimate of blood motion in more than the axial direction is termed a vector velocity (24). Several authors have tried to bypass the angle dependency in conventional Doppler systems and efforts have been made to create such an ultrasound system. Daigle et al. used a multi transducer pulsed Doppler system (50), Fox applied two beams (51), Trahey et al. and Bohs et al. used speckle tracking (52;53), Newhouse et al. used the total bandwidth of the received signal (54), Bonnefous worked with several beamformers in parallel (55), Dunmire et al. proposed a cross-beam technique (56) and Overbeck et al. used an ultrasound unit with a single transmitting and two receiving transducers (57). However, these techniques have neither been evaluated in clinical trials nor have they made it into commercial systems. In this thesis four vector velocity methods all developed at CFU, DTU were investigated: Transverse Oscillation, Synthetic Transmit Aperture, Directional Beamforming and Plane Wave Excitation.

Frame rate and temporal resolution

The other limitations in conventional Doppler systems examined in this thesis are frame rate and temporal resolution. Frame rate is mainly governed by the number of pulses used per frame and by the distance each pulse has to travel between transducer and target. It means that scanning depth, pulse repetition frequency and the number of modalities used simultaneously, affect frame rate performance (21;58). Also the placement and size of the color box in color flow imaging as well as the placement of the range gate in spectral Doppler dictate the data acquisition time (59). The larger and deeper placed the color box and the deeper placed the range gate, the lower the frame rate will be. B-mode

images on high-end scanners are acquired with frame rates up to 50 Hz and can be reduced down to 8-10 Hz in 2-D duplex mode (B-mode combined with color flow mapping), which clearly is unsuitable for visualizing rapid temporal changes in the blood flow as pointed out by Ferrara (60). The problem is aggravated in 2-D triplex mode (B-mode image, color flow mapping and spectral Doppler) and will be a major hurdle in 3-D duplex/triplex scanning.

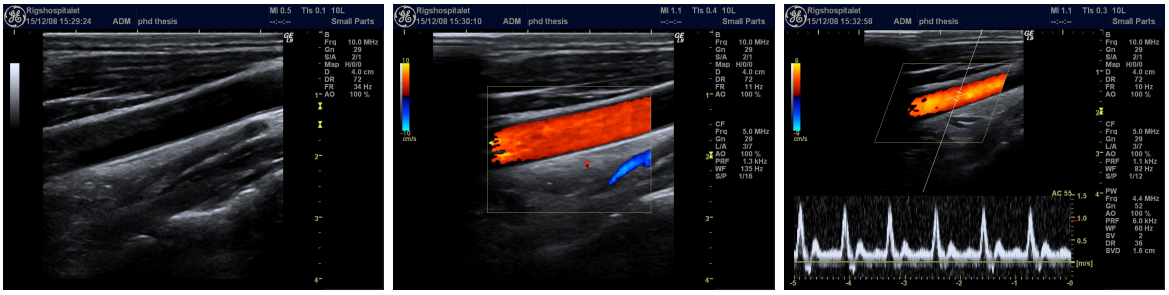

Figure 3: Frame rate decreases from 34 Hz to 10 Hz when adding color flow mapping and spectral Doppler to B-mode imaging. Frame rate is on the screen denoted FR.

A typical B-mode frame consists of about 100 image lines where each line is generated from a number of emissions. Whether the technique is color flow mapping, power Doppler or spectral Doppler the axial velocity of blood is found by imaging the same image line repeatedly. In spectral Doppler the estimates are angle corrected by the operator and presented as blood velocities plotted against time denoted a spectrogram (Fig. 3). In most commercial scanners Welch's method is used for estimation of the spectrogram (61) and to obtain an acceptable spectral resolution, a window of up to 256 consecutive emissions is used for each velocity estimate (58).

The temporal resolution of the conventional spectrogram can be impaired to the point where the rapid changes of blood velocities in the systole are difficult to measure. The events of upstroke, peak velocity and downstroke lie temporally so close that the different phases are merged together due to the long observation window (62). Furthermore, the frame rate of the interleaved B-mode images can be decreased to the point where the examination is difficult to perform (58;60). The operator can experience difficulties in placing the range gate in the vessel of interest. The reasons are often respiratory movement by the patient or involuntary transducer movements by the operator, which are not realized and corrected as the B-mode image used for navigation is not updated adequately.

The problem of inadequate processing power especially in 2-D triplex scan mode is in several commercial scanners solved by reducing triplex to a pseudo-triplex scan mode. All three modalities are present on the working screen ex. B-mode image, color flow mapping and spectral Doppler but only two modalities are running simultaneously thus reducing the computational demands. On the commercial scanner, which generated the frames shown in Fig. 3, triplex mode is implemented as such.

In different experimental setups and by several groups, the limitations in frame rate and temporal resolution have been tried solved. Coats et al. used offline computation combined with a recursive spectral estimation approach (62), Tanaka et al. used selected phase information (63), Udesen et al. proposed a method with chirp excitation signal and frequency splitting (64), Gran et al. proposed a similar method but with Barker and Golay code excitation signal (65), Oddershede et al. used multi-frequency encoding (66) and Jensen used sparse data sequences (67). Also adaptive filtering have previously been tried by Li et al. (68), Herment et al. (69) and Vaikus (70;71). In this thesis two approaches for high frame rate/temporal resolution are investigated: Plane Wave Excitation and adaptive filtering on spectral velocity data using the BAPES and BPC approaches.

Aim of studies

Study I and II concerned angle independent ultrasound vector velocity techniques. Stroke volume measurements were obtained *in-vivo* with three different experimental vector velocity ultrasound techniques: Transverse Oscillation, Synthetic Aperture Transmit and Directional Beamforming, and compared to magnetic resonance imaging using phase contrast angiography. The aims of the studies were to validate *in-vivo* the ultrasound vector velocity methods to magnetic resonance angiography in terms of measured stroke volume.

Study III concerned yet another angle independent ultrasound vector velocity technique called Plane Wave Excitation that can obtain vector velocity estimates with a high frame rate. The aim of the *in-vivo* study was to investigate flow patterns in complex geometries of the human cardiovascular system in healthy volunteers and compare the results to the literature.

Study IV focused on the two adaptive spectral estimators BAPES and BPC. The estimators can generate spectrograms with a shortened observation window and thereby consequently with a higher temporal resolution. The aim of the study was to validate quantitatively and qualitatively BAPES and BPC *in-vivo* against the conventional method for spectral estimation.

Materials, methods and results

All studies can be found unabridged in appendices I-IV. The studies were all performed after approval by The Danish National Committee on Biomedical Research Ethics (Date:30-05-6, J.nr:(KF)07307579).

In study I and II, the same eleven healthy volunteers (seven males and four females, 24 – 44 y, mean age: 32 y) were included after informed consent. The right common carotid artery was examined in all volunteers using ultrasound and magnetic resonance angiography. The volunteer rested supine on the examination table 15 min prior to all examinations.

In study III, four healthy volunteers (three males and one female, 26 – 45 y, mean age: 34 y) were included after informed consent. Complex vessel geometries were scanned in supine or standing position depending on scan location.

In study IV, ten healthy volunteers (nine males and one female, 24-36 y, mean age: 29 y) were included after informed consent. The right common carotid artery was examined in all volunteers using ultrasound.

All scans whether ultrasound or magnetic resonance angiography in the studies were carried out by KLH. All the *in-vivo* results obtained with the experimental methods were recorded with the experimental scanner RASMUS (1;2) and post-processed using MATLAB (Mathworks, Natick, MA, USA) on a 100 CPU Linux cluster. This combination gave a very flexible and unique environment for emitting, receiving and processing signals from an experimental point of view, but the processing time was considerable for all methods. It took seconds to acquire the data, hours to store and up to two full days to process. Obviously this affected the logistics and reduced the number of samples that realistically could be enrolled into the study populations.

	study I	study II	study III	study IV
no. of volunteers	11	11	4	10
mean age	32	32	34	29
male/female	7/4	7/4	3/1	9/1
experimetal method(s)	TO	TO/STA/DB	PWE	BAPES/BPC
reference method	MRA	MRA	none	spectral US (Welch)

Table 1: Overview of volunteers included in to the four studies

Before the studies are described in detail a brief introduction to the techniques is given below. Full details can be found in the manuscripts in appendices I-IV.

Transverse Oscillation method

The Transverse Oscillation method has been proposed by Jensen and Munk (72;73) and evaluated in simulations, in flow rig and *in-vivo* by Udesen et al. (36;74). The Transverse Oscillation method tracks scatterer motion along two orthogonal axes by emitting a pulse identical to conventional Doppler. The

velocity component in the axial direction is found exactly as in conventional Doppler ultrasound. An oscillation in the transverse direction is created by changing sensitivity of the receiving elements and the velocity along the transverse direction is found from the frequency content of this oscillation. By combining the velocity component along the two axes, vector velocities are achieved.

Directional Beamforming method

The Directional Beamforming method has been proposed by Jensen and Bjerngaard (75;76), evaluated in simulations (77;78) and examined in flow rig and *in-vivo* by Holfort et al. (79). In Directional Beamforming a focused pulse is emitted with the focal point placed below the depth of interest. Hence, the acoustic energy around the scatterer is sufficient for beamforming echo lines in a star-shaped pattern with the scatterer of interest as the centre. Lines are compared through a normalized cross-correlation across matching angles for consecutive pulses (80). The highest normalized cross-correlation is ideally found for the correct angle. When the correct angle is known, the magnitude of the motion along the correct echo line is found through cross-correlation for consecutive pulses.

Synthetic Transmit Aperture method

The Synthetic Transmit Aperture method has been proposed by Jensen and Nikolov (81) and evaluated in simulations, in flow rig and *in-vivo* (82-85). A Synthetic Transmit Aperture image is acquired by emitting a spherical unfocused wave from a few elements and receiving the scattered signal with all elements. Since the position for the emission is known, the precise origin of the received scattered signal can be calculated from time-of-flight for all elements and used in focusing. The Synthetic Transmit Aperture approach generates one low-resolution image for every emitted pulse. A high-resolution image is constructed by adding a number of consecutive low-resolution images. For every emission, a high-resolution image can be created by applying a recursive approach, where the oldest transmission event is replaced by the newest. The Synthetic Transmit Aperture method can therefore yield a frame rate equal to pulse repetition frequency with focus in all image points.

An approach to estimate vector velocities, identical to Directional Beamforming is computed. Echo lines in a star-shaped pattern are created to every point of interest and compared between emission-identical high-resolution images for every angle. The normalized cross-correlation peaks for the right angle. The magnitude is found through cross-correlation across echo-lines of the right angle for consecutive pulses.

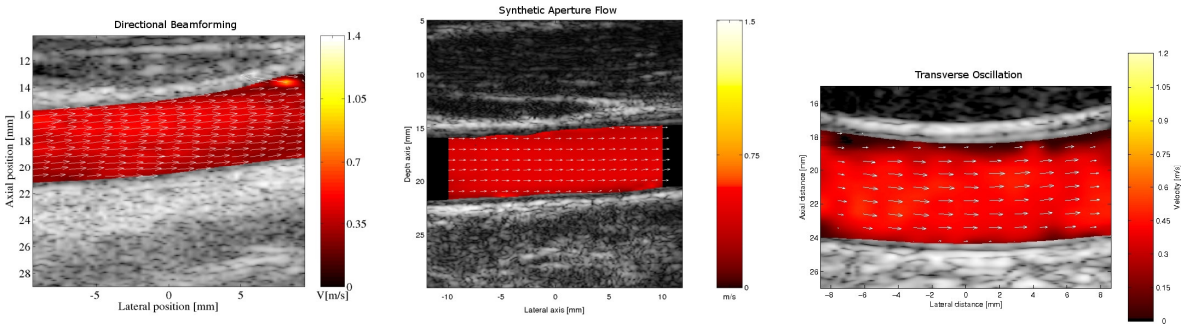

Figure 4: Frames obtained with Directional Beamforming, Synthetic Transmit Aperture and Transverse Oscillation are shown. The frames are obtained from different volunteers and to different time. The vector arrows, superimposed onto color flow maps, delineate magnitude and direction of the moving blood scatterers.

Plane Wave Excitation method

The Plane Wave Excitation method has been proposed by Udesen et al., and simulations, flow rig and *in-vivo* evaluations have been reported (86;87). In Plane Wave Excitation all elements of the transducer are excited at the same time thereby creating a pressure wave with a nearly plane front. The unfocused pulse covers the entire imaging plane with acoustic energy and a full speckle image is obtained for every emission. To increase the penetration of the signal into the tissue, a 13 bit Barker code is used instead of a conventional pulse (65). The angle independent vector velocity estimates are found when tracking speckle motion between consecutive speckle images by using a speckle tracking approach called sum of squared differences (52;88). The frame rate of the vector velocity images obtained with Plane Wave Excitation in study III was 100 Hz. However, matching receive and transmit channels in RASMUS would give a frame rate of 200 Hz without degrading the quality of the vector velocity estimates.

Blood spectral Power Capon method

The BPC method has been proposed by Stoica et al. (61;89), evaluated in simulations by Jensen et al. (77;78), and in flow rig and *in-vivo* by Gran et al. (90).The BPC method is a spectral estimator using adaptive filtration on data. Unique filters are designed to every velocity component in the data set. Hence, a unique matched filterbank is generated for each specific data set where the total power of the filters for each velocity of interest is minimized while not distorting the signal of interest.

Blood Amplitude and Phase Estimation method

The BAPES method has been proposed by Gran et al. (91) and evaluated in simulations by Jensen et al. (77;78), and in flow rig and *in-vivo* by Gran et al. (90). The BAPES method is based on a matched filterbank framework as BPC (61;92). However, in the BAPES method the filtered noise power is minimized fulfilling the constraint that the signal of interest is not distorted.

Previous simulations and phantom studies carried out by Gran et al. (90) have indicated that the two adaptive methods BPC and BAPES can obtain spectrograms with sufficient spectral resolution and contrast using fewer data than the conventional method for spectral Doppler estimation.

Magnetic resonance angiography method

In study I and II magnetic resonance angiography was used as the reference method. The examinations were performed with a 1.5 Tesla whole body scanner (Magnetom Vision, Siemens AG). A prospective ECG triggered phase contrast sequence using a cervical coil was employed. (Phase interval: 29 ms, echo time: 7 ms, flip angle: 30°, FOV: 100 mm, slice thickness: 6 mm, VENC: +/-1.5 m/s, pixel resolution: 0.52 x 0.39 mm in a matrix of 192 x 256 pixels interpolated up to 256 x 256 pixels).

Welch's method

In study IV the Welch's method was used as the reference method. Two different weighting schemes were applied on data, which resulted in different performances: Welch's method with a Hanning window (W.HAN) and Welch's method with a boxcar window (W.BOX). According to the basic principles in digital processing (93), W.HAN has a good contrast at the expense of spectral resolution, while W.BOX has a good spectral resolution at the expense of contrast. W.HAN is the preferred conventional spectral estimator.

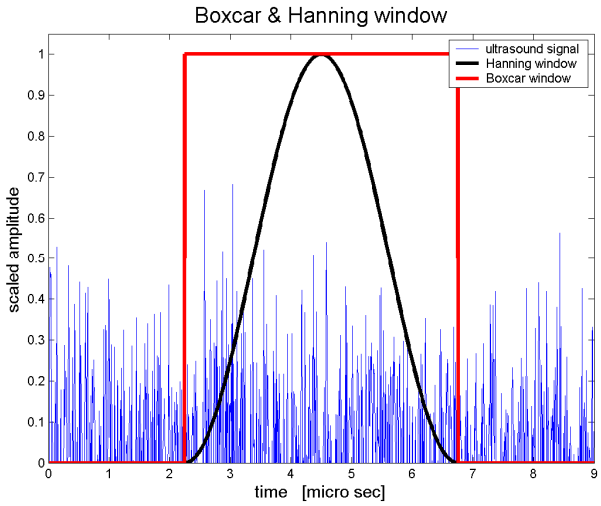

Figure 5: The scattered signal is multiplied in the time domain with a bell-shaped Hanning window or with a rectangular boxcar window. Thus, the blood signal used for velocity estimation is found under the curve corresponding to the chosen window

Study I:

In-vivo validation of a blood vector velocity estimator with MR angiography (appendix I)

Study I concerned *in-vivo* validation of the angle independent ultrasound vector velocity technique Transverse Oscillation. Stroke volume measurements of the common carotid artery were obtained *in-vivo* on 11 healthy volunteers and compared to measurements obtained with magnetic resonance imaging using phase contrast angiography.

The Transverse Oscillation measurements were performed with angles of insonation of approximately 90°, i.e. when the conventional Doppler method fails to estimate any blood velocities, and the vessel of interest was scanned approximately two cm upstream of the bifurcation to prevent confounding complex flow. For each vector velocity image, the vessel region was automatically identified from the B-mode image by an algorithm described by Udesen et al. (36). The volume flow per second in each vector velocity image was estimated by integrating the delineated 2-D vessel up to form a 3-D vessel. The mean volume flow per second in each vector velocity image was found as an average of the volume flows per second estimated to all different lateral positions in the vector velocity image. This yielded a volume profile for every sequence. A detailed description of the calculations is given by Hansen et al. (27).

The volume flow obtained with magnetic resonance angiography was found in the scan plan perpendicular to the right common carotid artery and two cm upstream of the bifurcation as in Transverse Oscillation. For each velocity map an anatomic image was calculated. A threshold pixel value defined the region of interest on the anatomic images in order to discriminate between the pixel values of blood and vessel boundaries. The region of interest encompassing the lumen of the vessel was used as a window on the phase velocity maps to ensure that velocity values from the vessel surroundings representing e.g. vena jugularis were ignored in the volume flow measurement. A region near the common carotid artery was selected to correct the phase off-set (94). The volume flow to each frame was found by multiplying the velocity with the area it occupied i.e. the pixel area and then adding up all the pixel derived volume flows encompassing the region of interest. The volume flow profile was given by the estimated volume flows of the full sequence of frames.

Assumption

To investigate the assumptions of circular geometry and rotationally symmetric blood flow necessary for computing stroke volume from the vector velocity estimates obtained with Transverse Oscillation, an additional approach was carried out. The assumptions were tested by taking out lines from the phase velocity maps to every angle. The lines of velocity values were treated as if they were obtained with Transverse Oscillation, i.e. in the longitudinal scan plane. Thus, for every angle the 1-D line taken from the phase velocity

map was integrated up to form a 2-D circle resulting in a volume flow estimate. For every volunteer a stroke volume range encompassing the stroke volume variation over all angles was found. This was compared to the actual magnetic resonance angiography stroke volume measurement where the velocities of the entire region of interest were used and no assumptions were made.

Statistics

A descriptive statistical analysis was computed on the stroke volume data for the two modalities finding mean value, standard deviation and stroke volume range. The stroke volume data obtained with Transverse Oscillation was then compared to stroke volume data obtained with magnetic resonance angiography using linear regression analysis with two-tailed significance value given and $p<0.05$ considered significant. The correlation coefficient, regression equation, and confidence interval using Fisher's r-to-z-transformation were calculated. Finally a Bland-Altman plot was made to illustrate the difference of stroke volume estimated by Transverse Oscillation and magnetic resonance angiography.

Results

The mean stroke volume +/- one standard deviation for Transverse Oscillation was 5.5 ml +/- 1.7 ml with the range of 3.4 – 9.5 ml. Respective estimates for magnetic resonance angiography were 5.8 ml +/- 2.0 ml with the range 3.0 – 10.8 ml.

The correlation between the stroke volume estimated by Transverse Oscillation and magnetic resonance angiography is illustrated in Fig. 6 as a scatterplot. R was 0.91 ($p<0.01$; 95 % confidence interval: 0.69 to 0.98) and the least squares (MRA = 1.1 * TO - 0.4) was found to be close to unity. The range of magnetic resonance angiography stroke volume assuming rotationally symmetric flow and circular vessel geometry is shown as a bar for every volunteer in the scatterplot.

In Fig. 7 the Bland-Altman plot is constructed. The mean difference is 0.24 ml with limits of agreement at -1.41 ml and 1.90 ml (95% confidence interval for mean difference: -0.32 ml to 0.81 ml).

In Fig. 8 the stroke volume range as percentages of the actual magnetic resonance angiography stroke volume is plotted for all volunteers, giving a mean ratio of 24.3%. One volunteer (no. 7) presented a ratio between the magnetic resonance angiography stroke volume range and the actual magnetic resonance angiography stroke volume of 48.3%. The angle dependent stroke volume with a range of 3.2 ml to 5.1 ml for this volunteer is depicted in Fig. 9. By examining the phase velocity maps of this particular volunteer, it was seen that a substantially asymmetric flow was present, while the vessel had an approximately circular geometry.

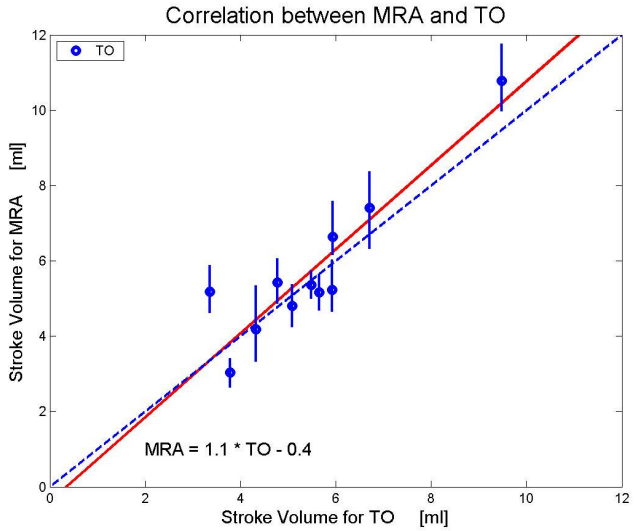

Figure 6: Correlation between magnetic resonance angiography and Transverse Oscillation. Line of best fit (solid line) and line of perfect fit (dashed line) are drawn. The range of magnetic resonance angiography stroke volume assuming circular geometry and rotationally symmetric flow is shown for every volunteer as a bar.

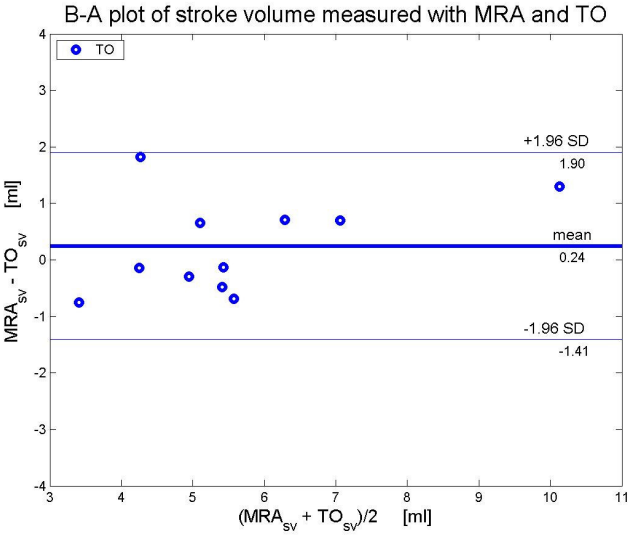

Figure 7: Bland-Altman plot of stroke volume measured with magnetic resonance angiography and Transverse Oscillation showing mean (thick solid line) +/- 1.96 standard deviations (thin solid line).

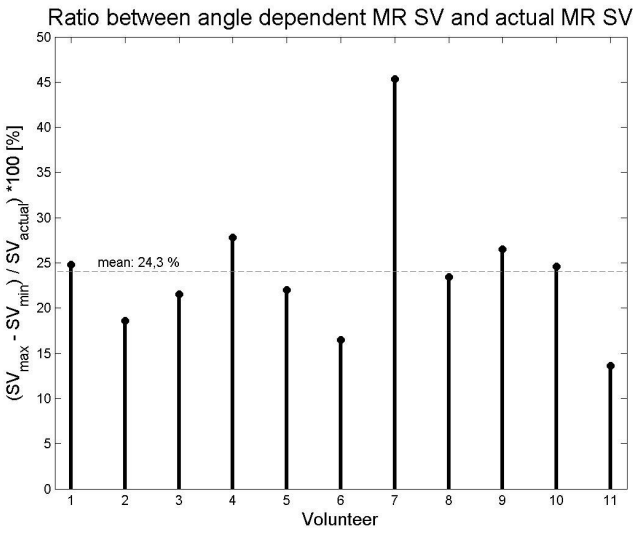

Figure 8: Stroke volume ratio was estimated by the range, found as the difference between the maximal and minimal angle dependent stroke volume, divided with the actual magnetic resonance angiography stroke volume and given in percentage. The mean ratio was 24.3 %.

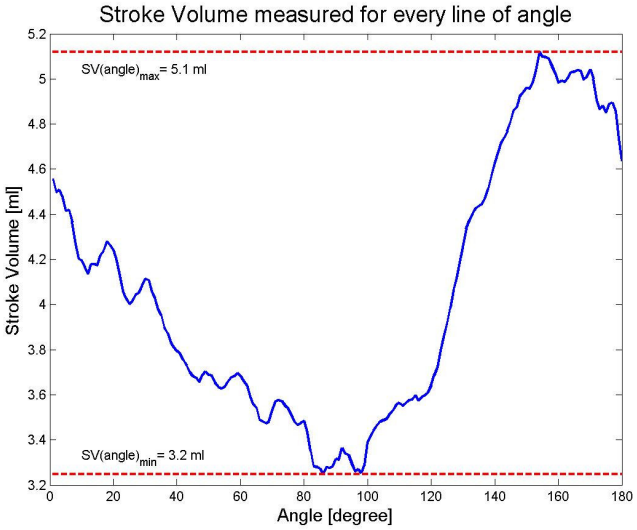

Figure 9: Stroke volume measured for every line of angle for one volunteer. The maximal and minimal angle dependent stroke volume estimates are shown as dashed lines.

In conclusion volume flow measurements were obtained *in-vivo* with the angle independent blood vector velocity method Transverse Oscillation. The results validated against volume flow measurements obtained with magnetic resonance angiography were found to be comparable for stroke volume using correlation, regression and Bland-Altman analyses. With Transverse Oscillation a method has been introduced to obtain quantitative blood flow measurements from the entire frame.

Study II:

In-vivo comparison of three ultrasound vector velocity techniques to MR phase contrast angiography (appendix II)

In this study Directional Beamforming, Synthetic Transmit Aperture and Transverse Oscillation were validated against magnetic resonance angiography in a setup similar to study I. Stroke volume measurements of the common carotid artery were obtained *in-vivo* on 11 healthy volunteers and compared to measurements obtained with magnetic resonance phase contrast angiography. Transverse Oscillation was included to compare the performances between the three vector velocity ultrasound methods.

The ultrasound measurements were performed with angels of insonation of approximately 90° and two cm upstream of the bifurcation. The volume flow estimates deriving from measurements of the three vector velocity methods were calculated in an approach similar to the approach described in study I. The magnetic resonance angiography data was identical to the data used in study I and was treated accordingly. Also the statistics were identical to study I using descriptive statistical and linear regression analyses as well as Bland-Altman plots.

Results

The stroke volume in the right common carotid artery was measured for the 11 volunteers with the three ultrasound methods and magnetic resonance angiography. The results are displayed in Table 2 along with mean, standard deviation and range for each modality.

In Fig. 10 the scatter plots are given showing the correlation between the each of the three ultrasound techniques and magnetic resonance angiography, with Directional Beamforming vs. magnetic resonance angiography: R=0.84 (p<0.01, 95% confidence interval: 0.49 to 0.96); Synthetic Transmit Aperture vs. magnetic resonance angiography: R=0.71 (p<0.05, 95% confidence interval: 0.19 to 0.92) and Transverse Oscillation vs. magnetic resonance angiography: R=0.91 (p<0.01, 95% confidence interval: 0.69 to 0.98). No significant differences were observed for any of the three comparisons (Directional Beamforming vs. magnetic resonance angiography: p=0.65; Synthetic Transmit Aperture vs. magnetic resonance angiography: p=0.24; Transverse Oscillation vs. magnetic resonance angiography: p=0.36). The resultant Bland-Altman plots are shown in Fig. 11. The mean difference, with confidence interval and limits of agreement are given for all plots in Table 3. The confidence interval for the mean differences overlapped zero for all three methods and was narrowest for Transverse Oscillation and broadest for Synthetic Transmit Aperture (Transverse Oscillation: 1.13 ml; Directional Beamforming: 1.56 ml; Synthetic Transmit Aperture: 1.97 ml). This also applied to the limits of agreement (Transverse Oscillation: 3.31 ml; Directional Beamforming: 4.55 ml; Synthetic Transmit Aperture: 5.74 ml). In terms of

mean differences in the Bland-Altman plots, Directional Beamforming was the most precise method followed by Transverse Oscillation and Synthetic Transmit Aperture (Directional Beamforming: 0.17 ml; Transverse Oscillation: 0.24 ml; Synthetic Transmit Aperture: -0.55 ml).

Volunteer no.	DB [ml/heart beat]	STA [ml/heartbeat]	TO [ml/heartbeat]	MRA [ml/heartbeat]
Volunteer 1	4.81	5.58	3.78	3.03
Volunteer 2	5.02	7.45	5.65	5.17
Volunteer 3	6.48	6.95	5.93	6.64
Volunteer 4	9.31	6.74	6.71	7.41
Volunteer 5	6.00	5.83	4.78	5.43
Volunteer 6	9.53	9.70	9.48	10.78
Volunteer 7	3.92	4.16	4.32	4.18
Volunteer 8	3.66	4.24	5.09	4.80
Volunteer 9	4.08	8.50	5.92	5.23
Volunteer 10	3.72	5.25	3.36	5.18
Volunteer 11	4.85	4.89	5.49	5.36
mean SV +/- SD	5.58 +/- 2.10	6.30 +/- 1.76	5.30 +/- 1.65	5.75 +/- 2.02
range	3.72 - 9.53	4.16 - 9.70	3.36 - 9.48	3.03 - 10.78

Table 2: Stroke volume measurements for all volunteers, mean stroke volume +/- one standard deviation and stroke volume range obtained with Directional Beamforming, Synthetic Transmit Aperture, Transverse Oscillation and magnetic resonance angiography.

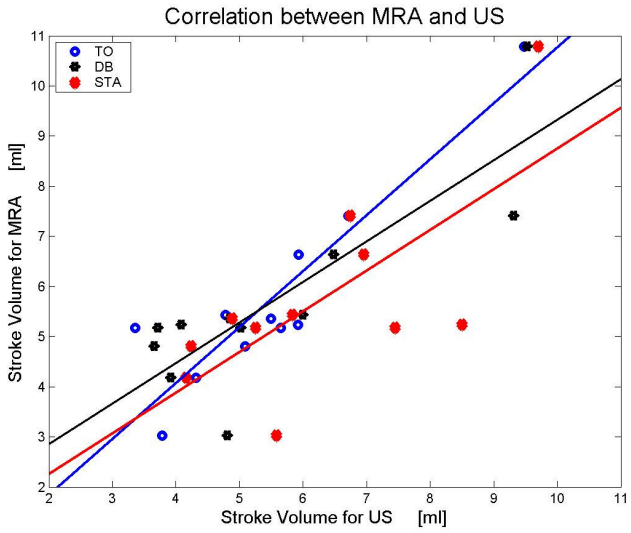

Figure 10: Graph showing the correlation between magnetic resonance angiography and the three ultrasound methods. The line of best fit is drawn for each comparison.

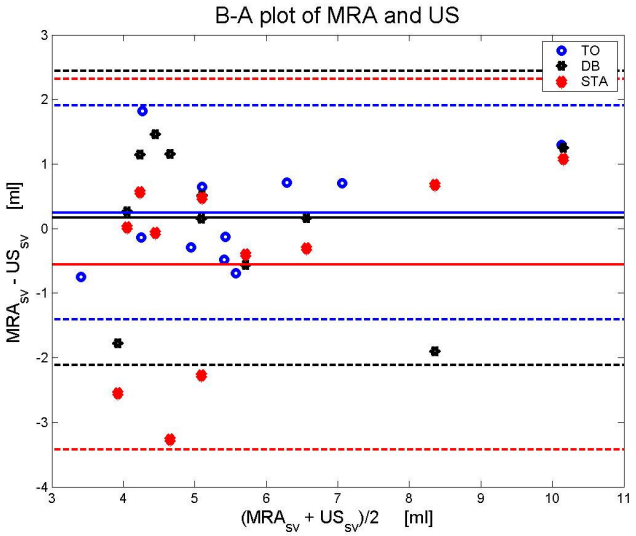

Figure 11: Bland-Altman plots of stroke volume measurements comparing magnetic resonance angiography with each of the three ultrasound methods showing mean +/- 2 standard deviations as solid and dashed lines, respectively.

Method	Mean [ml] (95% CI)	Lower limit [ml]	Upper limit [ml]
DB vs. MRA	0.17 (-0.61 to 0.95)	-2.11	2.44
STA vs. MRA	-0.55 (-1.54 to 0.43)	-3.42	2.32
TO vs. MRA	0.24 (-0.32 to 0.81)	-1.41	1.90

Table 3: Mean of difference with confidence interval, upper and lower limits of agreement given for the Bland-Altman plots.

In conclusion study II showed that it was possible to obtain reliable quantitative measurements *in-vivo* with the three different angle-independent 2-D vector velocity methods, Directional Beamforming, Synthetic Transmit Aperture, and Transverse Oscillation when compared to magnetic resonance angiography.

Study III:

In-vivo examples of flow patterns with a fast vector velocity ultrasound method (appendix III)

In study III different vessel locations were examined with the Plane Wave Excitation method. Four healthy volunteers with no history of cardiovascular disease were scanned on locations with complex vessel geometries encompassing multidirectional blood motion. Scan sequences were acquired of two carotid bifurcations, two femoral bifurcations, the bifurcation at the brachiocephalic trunk, the bifurcation of the subclavian artery as well as the internal jugular vein and the great saphenous vein, both with venous valves.

The scans were all recorded with the volunteers in supine position except the scan of the great saphenous vein, where the volunteer was in standing position while performing dorsal and plantar flexion to simulate walking.

In Fig. 12 the vortex formation in the carotid bulb of two different volunteers is shown. In the left frame the internal carotid artery is seen as the superficial vessel while in the right frame it is seen as the deep vessel. For both volunteers a vortex with low velocities in the carotid bulb was present during the entire heart cycle. Apart from the vortical recirculation in the bulb no retrograde flow was present.

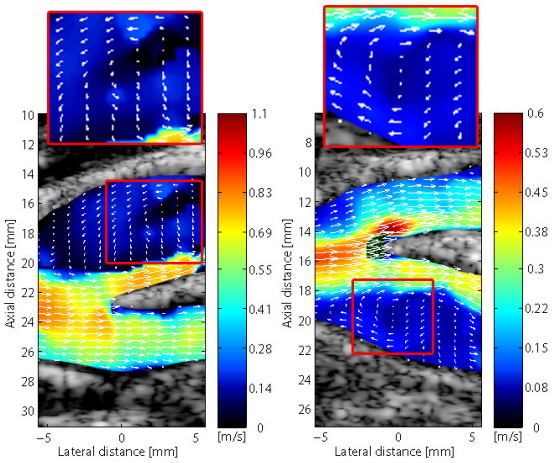

Figure 12: In the bulb of the internal carotid artery a vortex was present during the entire heart cycle. The depicted frames were both taken from systole.

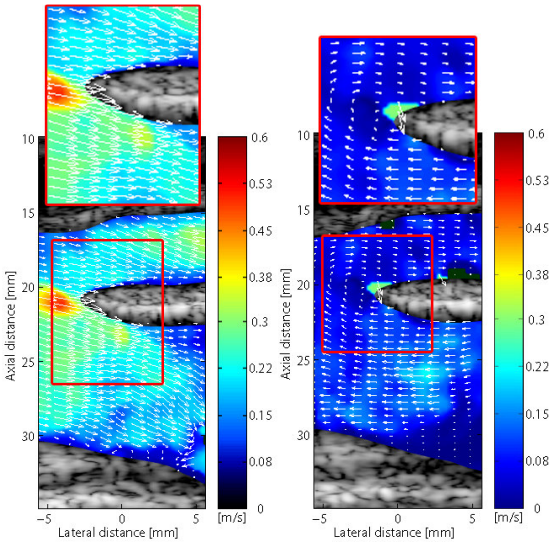

Figure 13: No vortex was seen in the brachiocephalic trunk during systole (left frame). The diastolic flow was going from the subclavian artery (deep vessel) to the common carotid artery (superficial vessel) (right frame).

In Fig. 13, the brachiocephalic trunk is shown. No vortex was present in systole but disturbed flow was seen in the subclavian artery when flow reversed at end-systole and end-diastole. In diastole the flow was filling the common carotid artery (superficial vessel) from the subclavian artery (deep vessel). Thus, the diastolic flow was retrograde in the subclavian artery and antegrade in the common carotid artery.

The same volunteer was scanned on the right side bifurcation of the thyrocervical trunk and the vertebral artery. Two frames are shown in Fig. 14. During peak systole the flow propagated without disturbed flow from the subclavian artery to the vertebral artery (superficial vessel) and the thyrocervical trunk (deep vessel) as seen in the left frame. Vortices in the subclavian artery scanned in the cross-sectional plane were visible right after peak systole and throughout diastole (right frame). The secondary flow swept from the superficial part of the subclavian artery and downwards in an s-shaped pattern creating two vortices.

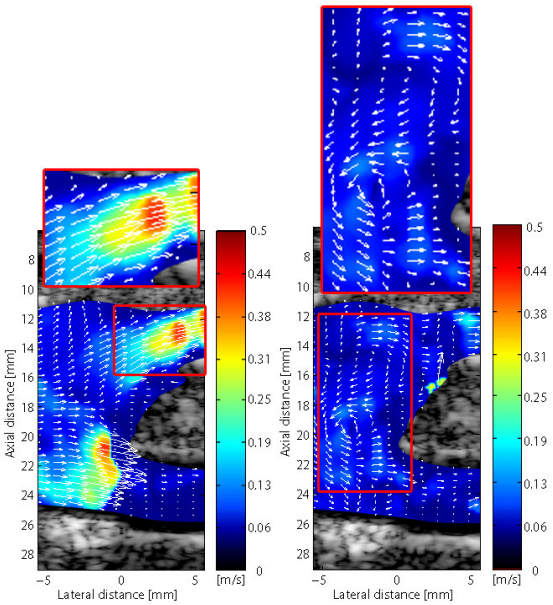

Figure 14: No disturbed flow in the vertebral artery (superficial vessel) and the thyrocervical trunk (deep vessel) was present during peak systole (left frame). In the subclavian artery vortices were present after peak systole and throughout diastole. The frame is taken from the beginning of diastole (right frame).

In Fig. 15, frames of two femoral bifurcations taken from examinations on two different volunteers are shown. Laminar flow was seen during the entire heart cycle with reversed flow in the superficial branch in the beginning of diastole.

The venous valves of the great saphenous vein and internal jugular vein were scanned. In Fig. 16, a venous bulb of the saphenous vein is depicted. Although the valves were not visible, the effect of the valves on the flow was obvious. During opening of the valves the flow was squeezed to form a jet.

Furthermore, vortices were formed in the pockets behind the valves. No retrograde flow was present and during the closed phase bidirectional blood motion was seen with the competent valves as a separator.

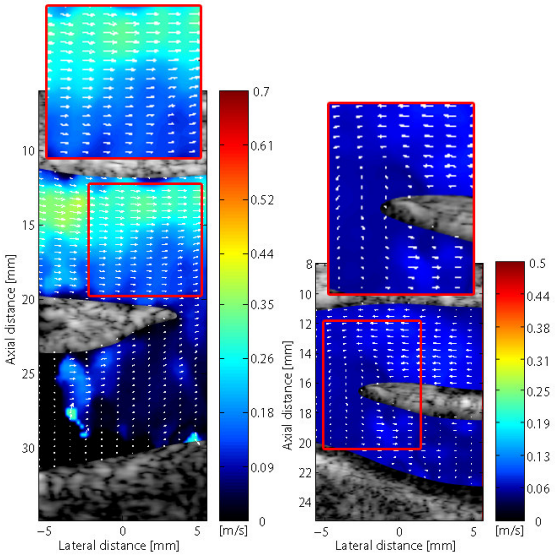

Figure 15: During diastole reversed flow in the superficial branches of the femoral arteries for two volunteers were present.

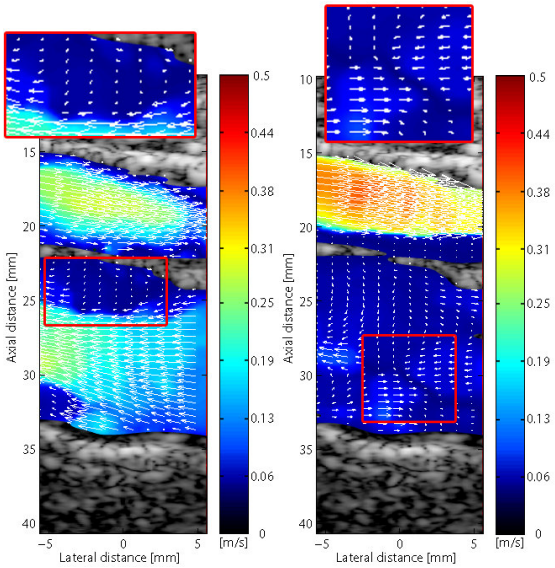

Figure 16: In the great saphenous vein (deep vessel) a jet was formed during antegrade flow between the valves, and vortices were formed behind the valves (left frame). The valves were competent and no retrograde flow was present (right frame). The femoral artery is seen as the superficial vessel in both frames.

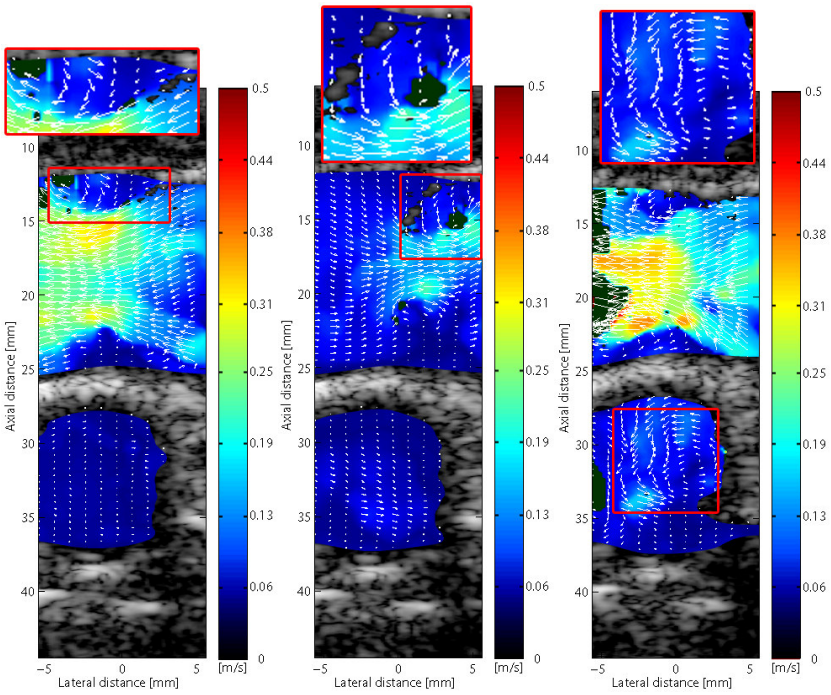

Figure 17: In the jugular vein (superficial vessel) the flow was squeezed by incompetent venous valves forming a jet during antegrade and retrograde flow (left and middle frame, respectively). Vortices were formed in the pockets behind the valves during antegrade flow and upstream of the valves during retrograde flow. In the carotid artery (deep vessel) secondary flow was seen during systole when scanned in the short axis (right frame).

The valves of the jugular vein are visible in Fig. 17. The flow pattern around the valves was similar to the flow pattern observed in the great saphenous vein except that retrograde flow was observed due to incompetent valves. Vortices were formed in the pockets behind the valves and a jet was formed between the valves during the opened phase (left frame). During retrograde flow a jet was formed between the valves with vortices upstream of the valves (middle frame). The common carotid artery was scanned in the cross-sectional plane, and a secondary flow was observed during systole (right frame).

Volunteer no.	Gender	Age	Location	Findings
Volunteer 1	male	34	carotid bifurcation	stable vortex in the bulb
-	-	-	femoral bifurcation	retrograde flow in the superficial branch, antegrade flow in the deep branch
-	-	-	femoral vein	vortices in the pockets, competent valves
Volunteer 2	female	45	carotid bifurcation	stable vortex in the bulb
Volunteer 3	male	26	jugular vein	vortices down- and upstream of the incompetent valves, secondary flow in the carotid artery
-	-	-	brachiocephalic trunk	retrograde flow in the subclavian artery, antegrade flow in the carotid artery
-	-	-	subclavian bifurcation	S-shaped secondary flow in the subclavian artery
Volunteer 4	male	31	femoral bifurcation	retrograde flow in the superficial branch, antegrade flow in the deep branch

Table 4: Overview of the findings with data given on gender, age and location.

In conclusion study III showed that the Plane Wave Excitation method can visualize complex flow patterns with a high frame rate. The results indicate that novel information on fluid dynamics can be achieved with Plane Wave Excitation and may in the future be a tool for cardiovascular disease assessment. Even though widespread anatomic variations of the arterial as well as the venous system dictate individual flow patterns not to be generalized, the results obtained with Plane Wave Excitation are glimpses of a far more complex blood dynamics than previously reported. Table 4 provides an overview of the findings with data given on gender, age and scan location.

Study IV:

In-vivo validation of fast spectral velocity estimation techniques (appendix IV)

In study IV adaptive filtering in spectral Doppler was investigated and compared to conventional algorithms for spectral Doppler estimation.

Ten healthy volunteers were scanned on the right common carotid artery. One data set was recorded for each volunteer and post processed using the four different methods; W.HAN, W.BOX, BPC and BAPES. For each method, spectrograms were estimated using different observation windows (OW): 128, 64, 32, 16, 8, 4 and 2 emissions/estimate. Thus, from every data set, were calculated 28 spectrograms giving in total 280 spectrograms for all volunteers.

To investigate the methods quantitatively, a spectrum corresponding to end-diastole was found for each spectrogram. For each data set, the time instant was chosen by visually examining the spectrogram obtained with W.HAN at OW 128. To the chosen time, spectra to all 28 spectrograms of the same data set were found. End-diastole was chosen to be the time of interest as it is easy to indentify and used clinically for calculating resistive index and systolic-diastolic ratio (95). From each spectrum, two parameters were calculated: the full-width-at-half-maximum (FWHM) and the ratio between main and side lobe levels. The FWHM was found as the width of the velocity distribution of the main lobe at half of the maximum amplitude. Thus, the FWHM given in m/s is a measure of spectral resolution. The ratio was found as the relative difference between the side-lobe level and the peak amplitude. The side-lobe level was found as the median value of the distributed amplitudes outside the main-lobe, outlined by the FWHM. The ratio, given in decibel (dB), is a measure of contrast in the spectrogram.

To investigate the methods qualitatively, nine experienced radiologists evaluated in a blinded trial the 280 randomized spectrograms by scoring each spectrogram useful or not useful. Intra- and interobserver variations were additionally found. The intra-observer variability was assessed by comparing the scores given twice by three radiologists with >14 days between each

session. The sequence of spectrograms was randomized to each session so judgment bias was minimized.

Statistics

A descriptive statistical analysis was computed on FWHM and ratio estimates of the 280 spectra finding mean value and standard deviation for each combination of method and window. The scores given by the radiologists were pooled by method and window. Useful and not useful were coded with the dummy variables 1 and 0, respectively. Before data analysis, Kolmogorov-Smirnov normality test and the Levene variance homogeneity test were applied to the data. No data transformation was needed. Bonferroni adjusted tests for multiple comparisons paired on volunteer level with $p<0.05$ considered significant were performed (96). The intra- and interobserver variability were investigated using Cohen's and Fleiss' kappa, respectively (97;98). Statistical analyses were performed using SAS (SAS Institute, Cary, NC, USA) and MATLAB (Mathworks, Natick, MA, USA).

Results

From a data set of one volunteer with three systoles recorded, examples of spectrograms generated with the four methods at OW 128 and 16 are presented in Fig. 18. The gaps in the spectrograms represent the necessary pulse emissions used for generating the interleaved B-mode images.

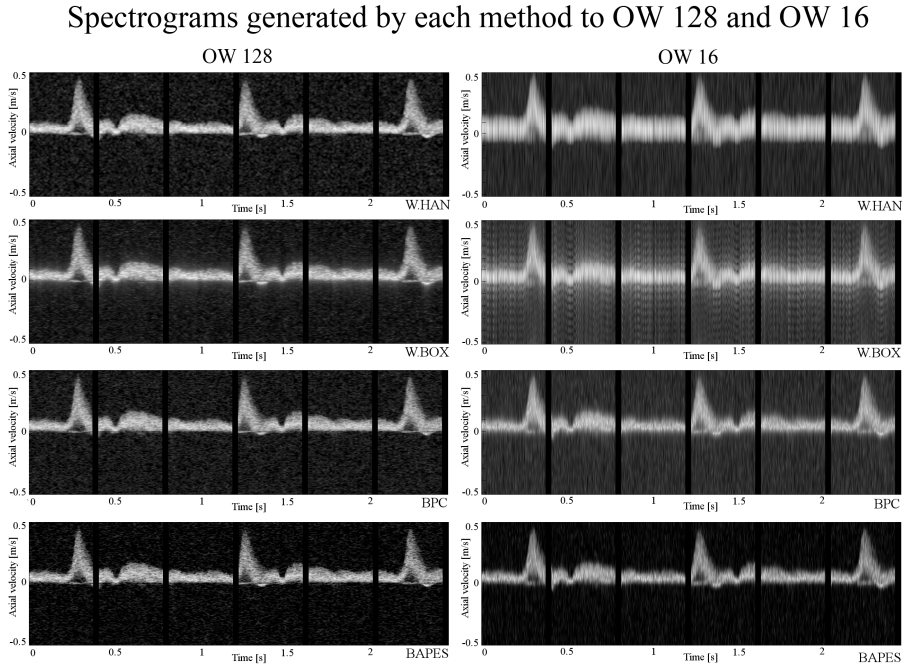

Figure 18: Spectrograms were found using the four methods with an OW 128 (left frames) and 16 (right frames). At OW 128 all methods displayed good performances. At OW 16, W.HAN and W.BOX estimated spectrograms with decreased quality compared to BPC and BAPES.

Examples of spectra obtained at end-diastole to time 2.2 s from the spectrograms shown in Fig. 18 are presented in Fig. 19. Mean and standard deviation of FWHM and ratio for the 280 spectra pooled by method and window are displayed in Table 5 and plotted in Fig. 20. The overall result of the scores given for each combination of method and window is displayed in Table 6 and illustrated in Fig. 21. The result of the Bonferroni adjusted tests for multiple comparisons paired on volunteer level is shown in Table 7 and illustrated in Fig. 22.

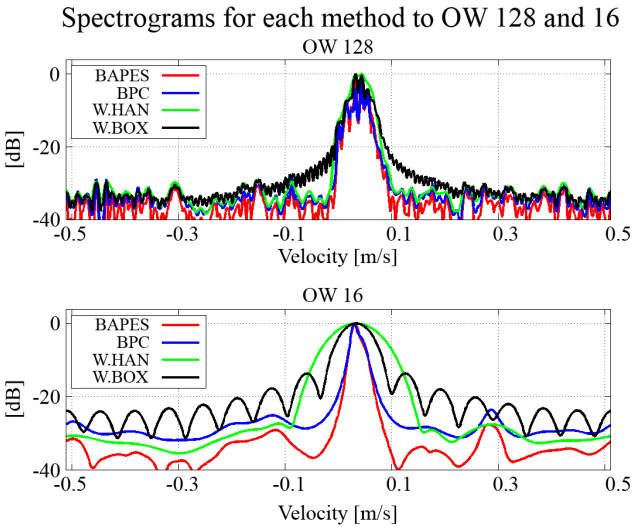

Figure 19: From the same volunteer at one time instant, spectra were generated using the four methods with an OW 128 and 16.

OW	Parameter	BAPES	BPC	W.HAN	W.BOX
128	FWHM [m/s]	0.029 (0.01)	0.026 (0.01)	0.034 (0.01)	0.029 (0.01)
	ratio [dB]	37.06 (3.19)	33.64 (3.16)	34.47 (3.20)	32.80 (2.45)
64	FWHM [m/s]	0.025 (0.01)	0.032 (0.01)	0.050 (0.01)	0.040 (0.01)
	ratio [dB]	35.81 (3.91)	29.89 (2.76)	31.53 (2.63)	29.31 (1.87)
32	FWHM [m/s]	0.034 (0.02)	0.033 (0.02)	0.074 (0.01)	0.055 (0.01)
	ratio [dB]	34.02 (4.47)	28.71 (2.94)	30.67 (4.63)	26.60 (2.25)
16	FWHM [m/s]	0.029 (0.01)	0.027 (0.01)	0.124 (0.00)	0.082 (0.01)
	ratio [dB]	33.27 (5.24)	29.03 (4.41)	29.63 (5.81)	22.99 (1.73)
8	FWHM [m/s]	0.034 (0.01)	0.033 (0.02)	0.230 (0.00)	0.159 (0.01)
	ratio [dB]	31.26 (5.17)	26.01 (4.18)	26.49 (5.33)	17.85 (0.81)
4	FWHM [m/s]	0.065 (0.02)	0.053 (0.03)	0.412 (0.01)	0.319 (0.00)
	ratio [dB]	26.73 (4.73)	22.23 (4.01)	20.51 (3.29)	13.20 (0.60)
2	FWHM [m/s]	0.145 (0.03)	0.113 (0.06)	0.688 (0.01)	0.688 (0.01)
	ratio [dB]	23.38 (4.13)	18.94 (4.18)	11.21 (0.51)	11.21 (0.51)

Table 5: Mean (and standard deviation) of FWHM and ratio given for each combination OW/method over ten volunteers.

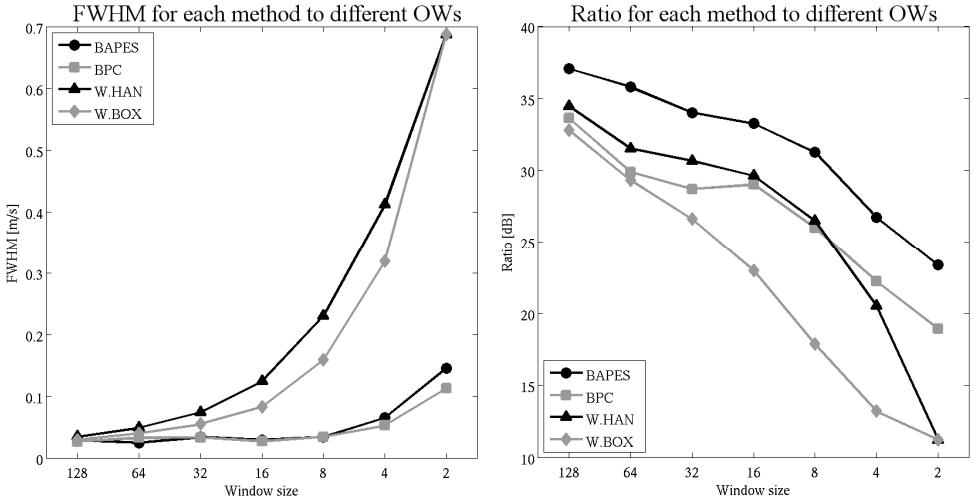

Figure 20: FWHM (left frame) and ratio (right frame) are plotted against OW for each method.

OW	BAPES	BPC	W.HAN	W.BOX
128	72 (80 %)	73 (81.1 %)	73 (81.1 %)	62 (68.9 %)
64	73 (81.1 %)	78 (86.7 %)	75 (83.3 %)	55 (61.1 %)
32	80 (88.9 %)	77 (85.6 %)	34 (37.8 %)	23 (25.6 %)
16	70 (77.8 %)	50 (55.6 %)	5 (5.6 %)	5 (5.6 %)
8	31 (34.4 %)	13 (14.4 %)	0 (0.0 %)	0 (0.0 %)
4	6 (6.7 %)	6 (6.7 %)	0 (0.0 %)	0 (0.0 %)
2	0 (0.0 %)	0 (0.0 %)	0 (0.0 %)	0 (0.0 %)

Table 6: Each cell consists of the total sum of scores given by nine radiologists on 10 volunteers in the range 0 to 90 (and percentage) for the combination method/OW.

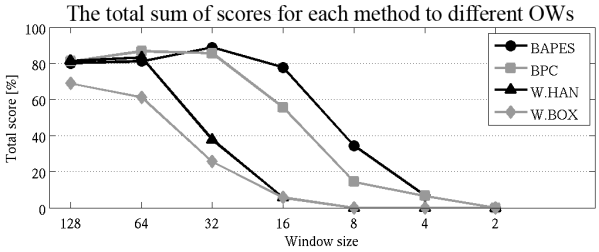

Figure 21: The total sum of scores in percentage for each method to different OWs

	BAPES	BPC	W.HAN	W.BOX	95% CI	p-value
128 emissions/estimate	7.2 (0.91)	7.3 (0.65)	7.3 (0.95)	6.2 (1.23)		
BAPES vs. BPC	x	x			(-1.03;0.83)	1.0
BAPES vs. W.HAN	x		x		(-1.03;0.83)	1.0
BAPES vs. W.BOX	x			x	(0.07;1.93)	0.03 ●
BPC vs. W.HAN		x	x		(-0.93;0.93)	1.0
BPC vs. W.BOX		x		x	(0.17;2.03)	0.01 ●
W.HAN vs. W.BOX			x	x	(0.17;2.03)	0.01 ●
64 emissions/estimate	7.3 (0.82)	7.8 (0.79)	7.5 (0.97)	5.5 (0.71)		
BAPES vs. BPC	x	x			(-1.34;0.35)	0.63
BAPES vs. W.HAN	x		x		(-1.04;0.64)	1.0
BAPES vs. W.BOX	x			x	(0.95;2.65)	<0.0001 ●
BPC vs. W.HAN		x	x		(-0.54;1.15)	1.0
BPC vs. W.BOX		x		x	(1.45;3.15)	<0.0001 ●
W.HAN vs. W.BOX			x	x	(1.15;2.85)	<0.0001 ●
32 emissions/estimate	8.0 (0.94)	7.7 (1.25)	3.4 (1.51)	2.3 (1.25)		
BAPES vs. BPC	x	x			(-1.24;1.84)	1.0
BAPES vs. W.HAN	x		x		(3.06;6.14)	<0.0001 ●
BAPES vs. W.BOX	x			x	(4.16;7.24)	<0.0001 ●
BPC vs. W.HAN		x	x		(2.76;5.84)	<0.0001 ●
BPC vs. W.BOX		x		x	(3.86;6.94)	<0.0001 ●
W.HAN vs. W.BOX			x	x	(-0.44;2.64)	0.31
16 emissions/estimate	7.0 (1.15)	5.0 (1.15)	0.5 (0.53)	0.5 (0.53)		
BAPES vs. BPC	x	x			(0.84;3.16)	0.0002 ●
BAPES vs. W.HAN	x		x		(5.34;7.66)	<0.0001 ●
BAPES vs. W.BOX	x			x	(5.34;7.66)	<0.0001 ●
BPC vs. W.HAN		x	x		(3.34;5.66)	<0.0001 ●
BPC vs. W.BOX		x		x	(3.34;5.66)	<0.0001 ●
W.HAN vs. W.BOX			x	x	(-1.16;1.16)	1.0
8 emissions/estimate	3.1 (1.10)	1.3 (0.94)	0 (0)	0 (0)		
BAPES vs. BPC	x	x			(0.99;2.61)	<0.0001 ●
BAPES vs. W.HAN	x		x		(2.29;3.91)	<0.0001 ●
BAPES vs. W.BOX	x			x	(2.29;3.91)	<0.0001 ●
BPC vs. W.HAN		x	x		(0.49;2.11)	0.0006 ●
BPC vs. W.BOX		x		x	(0.49;2.11)	0.0006 ●
W.HAN vs. W.BOX			x	x	(-0.81;0.81)	1.0
4 emissions/estimate	0.6 (0.84)	0.6 (0.70)	0 (0)	0 (0)		
BAPES vs. BPC	x	x			(-0.62;0.62)	1.0
BAPES vs. W.HAN	x		x		(-0.02;1.21)	0.062
BAPES vs. W.BOX	x			x	(-0.02;1.21)	0.062
BPC vs. W.HAN		x	x		(-0.02;1.21)	0.062
BPC vs. W.BOX		x		x	(-0.02;1.21)	0.062
W.HAN vs. W.BOX			x	x	(-0.62;0.62)	1.0
2 emissions/estimate	0 (0)	0(0)	0(0)	0(0)		

Table 7: The mean of scores is given on volunteer level in the range 0 to 9 (and standard deviation) for each combination method/OW indicated by "x". Each comparison test is given with 95% CI in difference of means and p-value (marked: ●=significant).

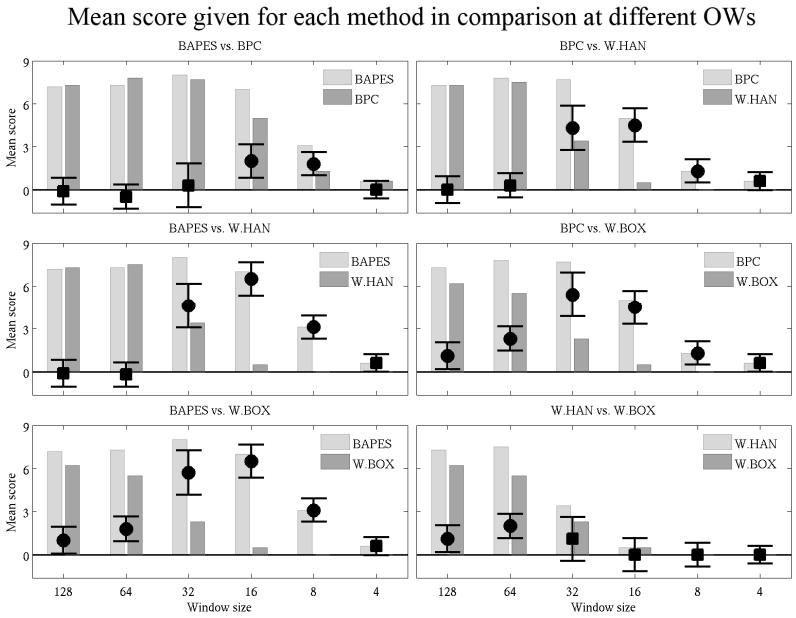

Figure 22: The mean score is with a histogram and the 95% confidence interval for the difference in means as a bar (marked: ■=insignificant and ●=significant).

For each method, tests for multiple comparisons were also used to investigate at which OWs the given scores were significantly different from the scores given at OW 128. W.BOX performed significantly worse when OW was reduced to 64 compared to W.BOX at OW 128 (p=0.03). W.HAN was not scored differently when reducing OW to 64 (p=0.55) but was scored significantly less at OW 32 (p <0.0001). BPC performed equally well at OW 32 compared to OW 128 (p=0.30) while BAPES scored significantly higher at OW 32 compared to OW 128 (p=0.02). Only BAPES performed as well for OW 16 as at OW 128 (p = 0.55). All four methods had decreased performances at OW 8, 4 and 2 compared to OW 128. The intraobserver variability for three radiologist evaluating the same 280 spectrograms with >14 days apart showed good agreement with an averaged Cohen's kappa value of 0.79 (94%, κ=0.88; 83%, κ=0.67; 93%, κ=0.81). The interobserver variability showed moderate agreement using Fleiss' kappa (78%, κ=0.57).

In conclusion study IV showed that the adaptive methods were superior to the conventional Welch's method and that BAPES was superior to BPC. The quantitative tests showed that BAPES and BPC had improved spectral resolution and BAPES had improved spectral contrast compared to Welch's method. According to the given judgments, OW can be reduced to 32 when using BPC, and 16 when using BAPES method for estimating spectrogram without losing performance. The results indicate that the adaptive methods BPC and BAPES potentially can bring improvements to spectral blood estimation as an increase of the temporal resolution of the spectrogram or as an increase of the frame rate for the interleaved B-mode images.

Discussion

New achievements

No previous studies have validated vector velocity or adaptive spectral estimators *in-vivo*, and no previous studies have obtained *in-vivo* sequences of angle independent instantaneous vector velocity images at a frame rate of 100 Hz. In study I and II it was shown that experimental vector velocity methods can produce reliable stroke volume measurements *in-vivo* when compared to magnetic resonance phase contrast angiography. In study III it was shown that a vector velocity method acquiring estimates at a high frame rate could reveal novel information of complex blood flow *in-vivo*. Finally, in study IV it was shown that spectrograms can be produced *in-vivo* with adaptive spectral methods and that these experimental methods outperform the conventional spectral estimator.

Previous studies

Experimental ultrasound methods for volumetric measurements have previously been examined by other groups. Kim et al. validated cardiac output estimates obtained *in-vivo* with a 2-D ultrasound system using color Doppler mapping of the short axis view, which showed good agreement compared with both thermo dilution (-0.16+/-0.94 l/min) and magnetic resonance (0.21+/-0.83 l/min)(99). Kripfgans et al. obtained in a flow phantom, volume flow measurements in the same manner but extended to a 3-D ultrasound system where the measured volume flow rates were within ±15% of actual values (100). An *in-vivo* validation study of volumetric flow obtained by an invasive Doppler flow wire system was published by Jenni et al. where excellent correlation was found compared to transit-time flowmeter (r=0.97) (101) and Krams reported on an experimental multigated spectral Doppler system validated in a flow phantom with an error less than 15% compared to computational fluid models (33). Two studies have reported on a technique based on multigated dual-ultrasound beam technology and it was shown that reliable volume flow in flow phantoms and *in-vivo* could be obtained when compared to conventional spectral Doppler (102;103). Shuping et al. and Forsberg et al., both validated 4-D Doppler ultrasound systems for volumetric flow *in-vivo* where Shuping et al. compared the estimates to phase contrast MRA with good agreement (r=0.92) and Forsberg et al. compared the volumetric estimates to a transit-time flowmeter also showing good agreement (r^2= 0.86 for mean volume flow and r^2= 0.62 for maximum volume flow) (104;105). It should be noted that none of the mentioned studies of experimental US methods for volumetric measurements were done with actual angle independent methods as all the experimental methods were based on conventional Doppler.

Studies of accuracy and reproducibility of experimental ultrasound methods with reduced angle dependency have also been carried out. Schank et al. examined a triangulation method for blood flow estimation in a flow phantom

and *in-vivo* by repositioning the transducer using a position locating system. The phantom experiment revealed 5% error for velocity magnitudes and error of less than 3° in Doppler angle when the angle of insonation was kept below 75° (106). Steel et al. reported maximum velocity variation of 7.6% for insonation angles between 40° to 80° obtained in a phantom study using a dual-beam ultrasound method on a split aperture system (107) and extended later this to an *in-vivo* study for inter- and intraobserver variation (intraobserver: -41.3 to 45.2 cm/s; interobserver:-29.6 to 46.8 cm/s.) (108). Likewise, Ricci et al. reported on accuracy and reproducibility for a dual-beam system based on two separate transducers. The *phantom* experiment showed a mean error of velocity magnitude of 1.9%, the reproducibility tests showed a variation of 0.8% to 10% on the estimates and the *in-vivo* experiment showed intraobserver variation of +/-9.6% (109). Though the methods have reduced angle dependency they still have impaired performances at angles close to 90° and cannot visualize complex flow.

Angle independent methods for visualizing blood flow have also been examined. Fei et al. estimated velocities in the carotid artery and bifurcation with an approach where blood velocities were reconstructed from three different scan sessions of varying insonation angles. The estimates compared to conventional spectral Doppler estimation agreed well (r = 0.94) (34;110). However, the method cannot provide instantaneous vector velocities as several cardiac cycles are used for each velocity estimation. Nyrnes et al. examined an approach called Blood Flow Imaging where speckle motion is visualized. In a setup similar to study IV, the usefulness was examined in comparison to conventional color Doppler imaging when scanning arterial septal defect *in-vivo.* The study indicated that the technique improves the visualization of interatrial blood flow in children compared to color Doppler imaging (111). Also Lovstakken et al. reported on the technique in a study concerning intraoperative assessment on blood flow patterns in coronary anastomoses (112). It should be noted that the speckle imaging technique visualizes flow with a high frame rate but without any quantitative parameters. Pastorelli et al. reported on multigated dual-beam method. Real-time angle independent vector velocity maps were validated in a flow phantom with velocity magnitude error of 23% and examples of *in-vivo* measurements were shown. The method performs with a frame rate of 6 Hz and down to a maximal scanning depth of 1 cm due to the necessary beam crossing (113).

Reference modalities

In study I and II, three vector velocity methods were validated *in-vivo* through volumetric flow measurements. In *in-vivo* setup no control of the flow is possible, which gives emphasis to the need of a reliable reference method. No reference can measure instantaneous velocity estimates to all points in the scan plane. Spectral Doppler ultrasound only interrogates the velocity distribution along a single line and several studies have shown the inaccuracy both in respect to estimated blood velocities and volumetric flow estimation (114). Magnetic resonance phase contrast angiography measure velocity

estimates as an average over several heart cycles covering the entire lumen of the vessel in through-plane setup. The accuracy, reproducibility and interobserver variability of magnetic resonance phase contrast angiography have been assessed in numerous studies and the method has been reported to be both accurate and robust (115-118). As a consequence, magnetic resonance phase contrast angiography is accepted as the gold standard for non-invasive, cerebral blood flow estimation (13-17) and was therefore chosen to be reference method in study I and II.

RASMUS (1;2) is not magnetic resonance compatible (as most other ultrasound systems) and therefore the scans were performed at different examinations. This affected the alignment of scan planes in the rotational and longitudinal direction, and the point-to-point comparison of the estimates, as the velocity profile fluctuates over time. Therefore, the comparison of the vector velocity estimates was made with respect to volume flow and more specifically stroke volume as this variable is less heart rate dependent and thus, a more reliable parameter when comparing volumetric measurements obtained at two different occasions (119).

In magnetic resonance angiography the blood flow is measured in a plane perpendicular to the longitudinal axis of the vessel using a through-plane encoding. Intuitively, it would have been a better comparison to choose an end-plane setup aligned with the two encoded directions of the corresponding vector velocity measurement to examine each voxel in pairs. Apart from difficulty of scan plane alignment, the inadequate in-plane resolution (slice thickness) in magnetic resonance angiography of 6 mm would confound the blood signal with the vessel surroundings and result in underestimated velocities. Furthermore, it has been shown that flow measurements acquired with a through-plane flow encoding are more precise than those acquired with end-plane flow encoding (118).

In study IV the reference modality was the conventional method for spectral Doppler estimation called Welch's method. The method was applied with two different window settings so both reference spectrograms with good contrast and good spectral resolution were used in the comparison with BPC and BAPES. As each acquired data set was processed by all four methods a direct comparison was feasible and no considerations of bias as a consequence of time or acquisition differences were necessary.

Assumption of rotationally symmetric flow and circular vessel geometry

In 2-D ultrasound vector velocity estimation, out-of-plane velocity data is not acquired and only a single projection through the long axis of the vessel is examined. On the contrary the data obtained with phase contrast angiography in through-plane flow encoding covers the entire short axis, i.e. lumen of the vessel. To reduce the information gap between the two methods in compare, a simple *in-vivo* model, was chosen. The normal common carotid artery is a straight vessel with an expected unidirectional flow and is parallel to skin

surface (120;121). Moreover, the vessel is assumed to have a circular geometry and an expected symmetric flow profile.

The assumptions necessary for the vector velocity derived stroke volume calculations were investigated for all 11 volunteers. 1-D lines from the phase velocity maps to every angle were integrated up to form 2-D circles from which stroke volume estimates were derived. There showed to be a remarkable difference in stroke volume estimates over all 180 degrees with a mean of 24.1% for each volunteer (Fig. 8). It underlines that the assumption of circular geometry and rotationally symmetric flow profile is a simplification. By examining the different magnetic resonance phase velocity maps, it was evident that the asymmetric flow profile contributed most to the angle dependent stroke volume difference. In Fig. 23, a phase velocity map of the common carotid artery of one volunteer is shown. The phase velocity map is taken from late systole and visualizes the marked asymmetry of the flow profile. This is consistent with Brands et al. and Tortoli el al., whom both reported asymmetry of the flow profile in the common carotid artery of healthy volunteers (25) and especially after the systolic peak (122).

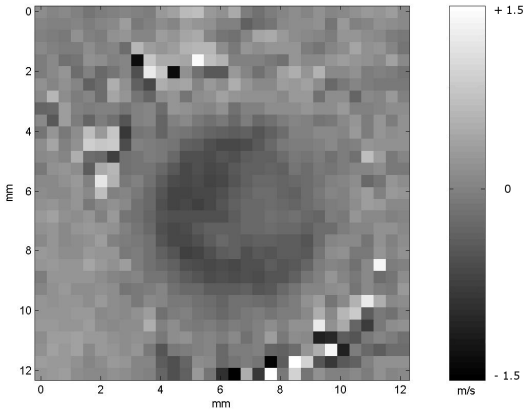

Figure 23: Phase velocity map of the common carotid artery of one volunteer taken from late systole showing marked asymmetry of the flow profile.

Thus, the placement of the longitudinal scan plane through the centre axis of the vessel in the ultrasound examination was an important confounder to study I and II. According to the magnetic resonance angiography data, the stroke volume obtained with the vector velocity methods could change up to 24.3% simply by changing the insonation window of the same vessel section.

Additionally, misplacement of the ultrasound planes away from the centre axis would add up to the bias. When performing the ultrasound examination it was crucial to scan the vessel parallel to the longitudinal axis exactly through the centre axis where the diameter of the lumen was largest, and where *intima* was most clearly delineated. Vessel *intima* was a reliable marker when positioning the scan plane through the middle of the vessel, because the layer structures were most clearly visible when the ultrasound beam direction was perpendicular to the planes of the layers. However, vessels are not perfectly

straight tubes and inevitably a part of the centre axis will be out of the scan plane due to curvature resulting in underestimation of the averaged volume flows.

Clutter filtering

The echo signal of moving blood is about 100 times weaker than the echo signal deriving from soft tissue (60;123). One of the major challenges in 2-D ultrasound velocity estimation is clutter filtering, where stationary echoes from the vessel surroundings, i.e. soft tissue, are cancelled out (124). Clutter filtering was one of the most important confounders in study I and II as blood signal representing low velocities near the vessel wall was cancelled out together with clutter signal.

The Transverse Oscillation method is the most robust method in terms of echo cancelling as a result of the lateral oscillation and the estimates in study I and II obtained with this method were done with only one filter applied. Synthetic Transmit Aperture and Directional Beamforming use the same scheme for velocity estimation. Nevertheless, the Synthetic Transmit Aperture method potentially has an advantage in terms of echo cancelling as the method uses continued data that can be echo cancelled with very long filters.

This was not reflected in the results (Table 3, Fig. 10 and Fig. 11) as only one filter was used in Synthetic Transmit Aperture while an adaptive filter approach was used in Directional Beamforming. The adaptive filter in Directional Beamforming consisted of two different filters, one for systolic flow and one diastolic flow used for all volunteers. It was employed by manually setting a threshold value for each volunteer defining systole and diastole.

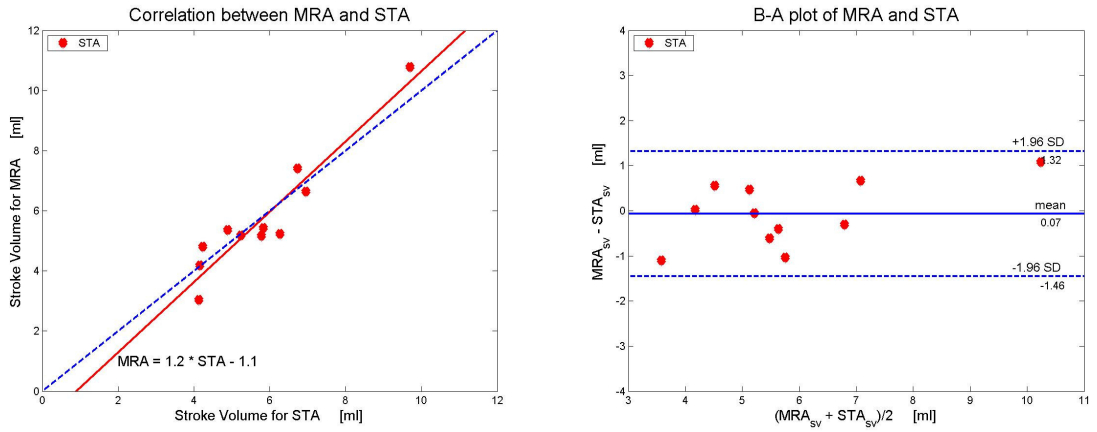

Figure 24: When applying a second filter for the three outliers a correlation plot is given for which R = 0.95 (p<0.01; 95% confidence interval: 0.82 to 0.99) and a Bland-Altman plot with a mean difference of -0.07 ml (95% confidence interval: -0.54 ml to 0.41 ml) and limits of agreement from -1.46 to 1.32 ml.

The Synthetic Transmit Aperture measurement deviated from the magnetic resonance angiography measurement for three volunteers: no.1, no.2 and no. 9 (Table 2). When inspecting the vector velocity images it was clear that vector

velocities near the vessel wall for the three volunteers were measured inaccurately: in wrong directions and with overestimated magnitudes. The three volunteers acted as outliers presumably as a consequence of a non-moving carotid artery during systole. The filter used in Synthetic Transmit Aperture was optimized to vessel movement as this was present for the majority of the samples. Thus, the mismatch in filter and vessel movement resulted in the observed overestimation of stroke volume for the three outliers. When applying another filter optimized to the reduced vessel movements of the three outliers, an improved overall result appeared for Synthetic Transmit Aperture when compared to magnetic resonance (Fig. 24).

Averaging in magnetic resonance angiography

The volume flow profile consisting of one complete heart cycle was found as a mean of measurements over 192 heart cycles in study I and II and each data acquisition was triggered by the *R*-peak of the ECG-signal. To ensure that one complete heart cycle was recorded, the data acquisition extended into the second systole. It has previously been addressed that due to fluctuations in heart rate and changing *R*-*R* interval over the averaged heart cycles, the second averaged systole will not be in phase, making it difficult to determine the correct duration of the complete heart cycle (118). In study I and II the shortest heartbeat of the 192 heart cycles defined the length of the complete averaged heart cycle, i.e. where the upstroke of the second systole initiated. Hence, it is expected that the calculated magnetic resonance angiography stroke volumes were slightly underestimated.

Complex flow patterns visualized in a high frame rate setting

In study III the vector velocity method Plane Wave Excitation was used to visualize complex flow profiles in the cardiovascular system in both simple and complex vessel geometries. This was carried out to investigate the possibilities of vector flow imaging but also in the attempt to gather new information of fluid dynamics. In total six bifurcations and two veins were examined on four healthy volunteers.

It was shown when examining the carotid bifurcations on two volunteers that a well-defined vortex was present in the carotid bulb during the entire heart cycle (Fig. 12). This is in accordance with earlier results obtained with US vector velocity examinations (36;125). No stable vortices were observed during systole in the other four bifurcations, and they did not reveal same consistency in terms of flow pattern.

Previous studies with ultrasound Doppler and magnetic resonance imaging have shown retrograde flow in femoral arteries and the brachiocephalic trunk during diastole (106). Study III is consistent with this literature. The new information obtained with Plane Wave Excitation is how the flow reverses. It was shown that the flow in the femoral only reversed in the superficial branch while remaining antegrade in the deep branch (Fig. 15) and that the flow in the brachiocephalic trunk reversed in the subclavian artery and remained antegrade in the common carotid artery (Fig. 13).

It is well known that the flow in the carotid arteries is without retrograde flow (126) and it is believed that the antegrade flow in diastole primarily is forwarded from the aorta. It is known as the windkessel effect (127). The effect describes how half of the left ventricular stroke volume during systole is stored in the aorta and due to the elastic forces of the aortic wall is forwarded in diastole to the peripheral circulation. The vector velocity sequence obtained with Plane Wave Excitation indicates that the blood reserve forwarded in diastole to the brain could derive from other arteries than the aorta.

It was shown by using Plane Wave Excitation that competent valves in the great saphenous vein were present, and that vortices were formed in the pockets behind valves (Fig. 16). This is consistent with previous studies (128;129). The internal jugular vein was also examined and the examination revealed the presence of incompetent valves and retrograde flow (Fig. 17). Incompetent valves of the internal jugular vein have been described before with prevalence of 36.8% to 38.4% in healthy persons (130-132). The findings concerning flow around valves in the great saphenous vein and the internal jugular vein obtained with Plane Wave Excitation are consistent with the literature. However, vortices on both sides of the valves created by bidirectional flow have not been reported previously.

Finally, secondary flow was seen in the common carotid artery (Fig. 17) and in the subclavian artery (Fig. 14). Secondary flow in different vessels has been predicted by computational fluid dynamics and magnetic resonance imaging in several studies but not before has it been possible to visualize secondary flow with ultrasound (29-32). The secondary flow is thought to have a protective role in the development of atherosclerosis and may be an important issue in vascular disease assessment (133).

The stable vortex of the carotid bulb and its relationship with baroreceptor controlled blood pressure regulation

The vortex is fundamental in the carotid bifurcation and has in numerous studies been linked to the development of atherosclerosis (31;134-136) as disturbed flow around vessel bifurcation has been linked more widely to atheroma deposition (137;138). The findings in study III indicate that flow patterns in the carotid bifurcation are different from flow patterns in other bifurcations of the human cardiovascular system. It appears that the stable vortex is related to the bulb and not the bifurcation. In the bulb a high concentration of blood pressure regulating baroreceptors is present, and it is therefore reasonably to speculate if the vortex of the carotid bulb is essential in blood pressure regulation (139;140).

Bernoulli's principle relates velocity and pressure,

$$\text{Const} = P + \tfrac{1}{2}\rho v^2 \qquad (3),$$

where P is the pressure, ρ is the density of blood, and v the velocity along a flow line. The increase in vessel diameter in the carotid bulb results in a loss of blood velocity, which is counterbalanced by an increase in blood pressure. The

carotid bulb can be perceived as a blood pressure amplifier creating high pressure values by slow moving vortices. Hence, the vortices are providing the necessary input for the baroreceptors of the carotid bulb in order to achieve a correct autonomic control of the blood pressure by the regulating centre in the medulla oblongata. Several authors have previously addressed Bernoulli's principle in relation to bifurcations and venous valves (129;135;141;142), and Henze showed by calculating the pressure gradients from vector velocity estimates that indeed high pressure gradients exist in the carotid bulb during peak systole (143). However, the relationship between the stable vortex, the geometry of the carotid bulb and blood pressure regulation has not previously been addressed nor investigated.

Temporal resolution

In study IV adaptive spectral Doppler estimators with improved temporal resolution performances were investigated. While the Plane Wave Excitation method achieves a high frame rate performance by manipulating the emitted signal, the adaptive spectral estimators achieve improved performances by using adaptive filtration on the received signal so fewer data is necessary per estimate. Several groups have proposed adaptive filtering techniques for blood velocity estimation and for the majority of works only simulations have been performed (144;145). Only a few studies have been extended to flow phantom validation and only Herment et al. has produced an example of adaptive spectral filtration on *in-vivo* data (69;146;147). Thus, study IV is unique as an *in-vivo* validation study of adaptive filtering methods for blood velocity estimation. The performances of BAPES and BPC were investigated quantitatively through the parameters FWHM and ratio, and qualitatively by letting radiologists score the resulting spectrograms.

FWHM given in m/s is a measure of spectral resolution and should be as low as possible, while the ratio given in dB is a measure of spectral contrast and should be as high as possible. It is seen in Table 5 and Fig. 20 that on average for all OWs above 2, W.BOX performed with better resolution than W.HAN and W.HAN performed with better contrast than W.BOX. The adaptive methods outperformed Welch's method in terms of resolution at all OWs below 128 and it is seen that BPC had a slightly better resolution than BAPES. In terms of contrast, BAPES was superior compared to both BPC and Welch's method for all OWs. The W.HAN had better contrast than BPC for all OWs above 8.

In Fig. 18 examples of acquired spectrograms obtained with the four approaches at OW 128 and 16 are shown. Spectral resolution in the spectrogram corresponds to the width of the white curve representing estimated blood velocities, while the difference between the white curve and the dark surroundings corresponds to contrast. The spectrograms underline the results of the quantitative evaluations. At OW 128 the four approaches produced spectrograms of good quality while the estimators differed in performance at OW 16. At OW 16, it is seen that W.BOX estimated with a higher spectral resolution than W.HAN and the adaptive methods with higher spectral resolution than Welch's method. Furthermore, it is seen that the

contrast decreased from BAPES to BPC and Welch's method. W.BOX performed poorest among the four methods in terms of contrast and a so-called ringing phenomenon at OW 16 can be seen.

Spectra for the methods are shown in Fig. 19. The side lobes representing leakage from the true velocity were suppressed, while the main lobe representing the true velocity was broadened for W.HAN compared to W.BOX. The pronounced side lobes for W.BOX at OW 16 correspond to the ringing phenomenon shown in Fig. 18. The adaptive methods had a narrower main lobe at OW 16 compared to Welch's method and BAPES displayed better side lobe levels compared to both BPC and Welch's method.

The overall result of the qualitative evaluation displayed in Table 6 and Fig. 21 shows that the radiologists preferred the adaptive methods over Welch's method, BAPES over BPC and W.HAN over W.BOX. The inter- and intra-observer variability were additionally tested and showed moderate and good agreement, respectively, indicating consistent scores given by each radiologist with a base-line difference among the radiologists. In Table 7 and Fig. 22 the results of the statistical analyses on the mean of scores using Bonferroni adjusted tests for multiple comparisons are displayed. It is seen that at OW 128 and 64, BAPES, BPC and W.HAN performed equally well while W.BOX scored significantly less. When reducing the OW to 32, the adaptive methods BAPES and BPC performed better than W.HAN and W.BOX. However, BAPES was superior to BPC at OW 16 and 8. According to the radiologists, at OW 16 and 8 the conventional methods failed and at OW 4 and 2, all four methods failed.

For each method, the scores given at window sizes below OW 128 were compared to the score given at OW 128 to evaluate how robust each method was to reduction of OW. At OW 64 only W.BOX scored significantly worse, while W.HAN significantly decreased in score at OW 32. At OW 32, BPC scored as at OW 128 while BAPES actually scored significantly better. At OW 16, only BAPES was scored equal to OW 128. Hence, W.HAN at OW 64, BPC at 32 and BAPES at 16 can produce spectrograms, according to the nine radiologists, which are as acceptable as if they were produced at OW 128.

Moreover, the radiologists preferred contrast to spectral resolution when comparing scores given for W.BOX and W.HAN at OW 128 and 64 and in most modern scanners the Hanning weighting scheme is accordingly implemented for spectral blood estimation. However, when comparing BPC and W.HAN the improved resolution in BPC was preferred to the improved contrast in W.HAN. This is seen in Table 7 and Fig. 22 at OW 32 and 16. It indicates that it is not only the raised side lobe level in W.BOX, which reduces the quality of the spectrogram compared to W.HAN but also the accompanying ringing phenomenon.

Finally, the radiologists significantly preferred BAPES at OW 32 compared to BAPES at OW 128 ($p = 0.01$). The reason could be that the observers were disturbed visually by the high contrast and spectral resolution of the spectrograms obtained with BAPES at OW 128 and somewhat preferred the

smoothing of details as presented in spectrograms obtained with BAPES at OW 32.

The US examination of today can potentially be improved if the conventional Welch's method for blood velocity estimation used in commercial scanners was replaced with one of adaptive spectral estimators BPC or BAPES. Consequently, either the temporal resolution of the spectrogram could be increased to obtain more information of the blood velocity profile, or the frame rate for the interleaved B-mode images could be increased to facilitate navigation under US examination. According to Gran et al. (2009), the adaptive methods are more computationally demanding than the conventional Welch's method, and BAPES is more computationally heavy than BPC. However, when reducing the OW, the computational costs decrease as well. Therefore, the BAPES method implemented with an OW 16 or the BPC method with an OW 32 may be as tractable as Welch's method with a much longer OW. It should therefore be possible to implement the methods into commercial scanners and convert the methods to an actual real-time modality.

Reproducibility of flow measurements

The storage time from the experimental scanner RASMUS to the linux cluster and the off-line processing time on the cluster were considerable for each of the US methods investigated in study I-IV. It had two consequences for the study designs. Firstly, it had an impact on the logistics and reduced the number of samples that realistically could be enrolled into the study population, thereby affecting confidence intervals and limits of agreements of the all statistical calculations. Secondly, different days were used for examinations on the same volunteer. Although the volunteers rested 15 min before each scan, the flow dynamics, e.g. cardiac output, heart rate and stroke volume, were expected to fluctuate

For none of the four studies, the velocity estimation was repeated on the same volunteer with the same method. Furthermore, in study I and II where several methods estimated blood flow on the same volunteer, the examinations on each volunteer were accomplished within three weeks.

In study IV inter- and intraobserver variability were assessed as tests for reproducibility. It was feasible as the experimental scanner RASMUS and the linux cluster already had produced the spectrograms, which were shown to the radiologists.

Therefore, tests of reproducibility of the flow measurements neither quantitative nor qualitative have been assessed. This would have required more observations along with the scans in comparison acquired simultaneously or within minutes. It will be a concern in future trials. It may be solved either by converting the methods into real-time estimation through commercial scanner implementation using dedicated processors or by implementing the methods into the new experimental scanner SARUS, which is under development in CFU and will be able to acquire data much faster than the existing RASMUS scanner (148).

Conclusion and perspectives

Based on the *in-vivo* ultrasound studies on human volunteers presented in the thesis, it can be concluded that ultrasound vector flow and adaptive filtration have a number of advantages. The potentials in angle independent vector velocity techniques were investigated in study I- III. In study I and II it was shown that *in-vivo* measurements of volume flow using the techniques Transverse Oscillation, Synthetic Transmit Aperture and Directional Beamforming were possible and that the estimates were in good agreement with magnetic resonance angiography. In study III it was shown that *in-vivo* measurements of complex flow patterns in the cardiovascular system were possible with Plane Wave Excitation bringing forth novel information on fluid dynamics. Finally it was shown that the optimization in frame rate and temporal resolution was possible. In study III, high frame rate was achieved with the vector velocity technique Plane Wave Excitation using plane wave emissions and in study IV high temporal resolution was achieved with the spectral Doppler techniques BAPES and BPC using adaptive filtration.

With vector velocity estimation, methods have been introduced to obtain quantitative blood flow measurements from the entire frame (and not only within a range gate), to estimate blood velocities in all vessels regardless of angle and to enable correct visualization of complex flow. Quantitative volume flow measurements obtained from the entire frame could be usable information when e.g. evaluating the severity of stenoses of the internal carotid artery, measuring cardiac output of a. pulmonalis/aorta or performing follow-up of transplanted organs. Additionally and perhaps mainly, vector velocity methods may uncover novel information of fluid dynamics. That is of complex flow patterns in simple and complex vessel geometries, secondary flow, vortices in bifurcations and around valves, and turbulence in the heart. Hence, vector velocity estimation could be a prognostic tool in the treatment of diseased vessels looking into altered flow patterns connected to e.g. venous insufficiency, atherosclerosis, tumor neovascularization or aneurysms.

With the adaptive spectral estimators BPC and BAPES and the vector velocity method Plane Wave Excitation is was shown that increased frame rate and temporal resolution can be achieved. The rapid temporal and spatial changes in blood flow especially in complex vessel geometries are crucial to understand and can be visualized with a high frame rate vector velocity method like Plane Wave Excitation. With the methods BPC and BAPES, solutions to increase the performance of spectral Doppler estimation were proposed. The results indicate that the adaptive methods BPC and BAPES potentially can bring improvements to spectral blood estimation as an increase of the temporal resolution of the spectrogram or as an increase of the frame rate for the interleaved B-mode image.

A number of new experiments could be interesting to follow-up on the results presented in this thesis.

- Validation of ultrasound vector velocity methods in flow phantoms with controlled complex flow patterns.

- Validation of ultrasound vector velocity methods *in-vivo* on a larger population with the experimental scanner SARUS (148)

- *In-vivo* visualization of altered flow in arterial stenoses using ultrasound vector velocity methods to test quantitative estimates as markers for stenotic severity.

- *In-vivo* visualization of altered flow around soft and hard plaques in the internal carotid artery using ultrasound vector velocity methods and evaluated as a marker for stroke incidence.

- *In-vivo* examination and characterization of the stable vortex in the carotid bulb and the connection to blood pressure control of the baroreceptors by using ultrasound vector velocity methods and MRI.

- *In-vivo* visualization of altered flow in aneurysms using ultrasound vector velocity methods and evaluated as a prognostic tool.

- *In-vivo* examination of secondary flow in simple vessels and complex flow around venous valves on a larger population using ultrasound vector velocity methods.

- *In-vivo* examination of retrograde flow patterns in greater vessels such as the brachiocephalic trunk and the femoral bifurcation using ultrasound vector velocity methods.

- Examination of adaptive filtration in spectral Doppler examination in different vessel to examine signal-to-noise ratios and performances to different scan depths and different types of flow.

- Development and validation of an improved BAPES method without gaps in the spectrogram for B-mode imaging.

Reference list

(1) Jensen JA, Holm O, Jensen LJ, Bendsen H, Pedersen HM, Salomonsen K, et al. Experimental ultrasound system for real-time synthetic imaging. IEEE Ultrason Symp 1999;1595-9.

(2) Jensen JA, Holm O, Jensen LJ, Bendsen H, Nikolov S, Tomov BG, et al. Ultrasound research scanner for real-time synthetic aperture image acquisition. IEEE Trans Ultrason Ferroelec Freq Contr 2005;52(5):881-91.

(3) Caro CG, Pedley TJ, Schroter RC, Seed WA. The mechanics of the circulation. Oxford: Oxford University Press; 1978.

(4) Griffiths PD, Hoggard N, Dannels WR, Wilkinson ID. In vivo measurement of cerebral blood flow: a review of methods and applications. Vasc Med 2001;6(1):51-60.

(5) Masood S, Yang G-Z. Blood Flow Measurement. Encyclopedia of Biomedical Engineering. John Wiley & Sons, Inc.; 2005.

(6) Headley JM. Invasive hemodynamic monitoring: physiological principles and clinical applications. Irvine: 2002.

(7) Miles KA. Perfusion imaging with computed tomography: brain and beyond. Eur Radiol 2006 Nov;16 Suppl 7:M37-M43.

(8) Ota H, Takase K, Rikimaru H, Tsuboi M, Yamada T, Sato A, et al. Quantitative vascular measurements in arterial occlusive disease. Radiographics 2005 Sep;25(5):1141-58.

(9) Zaharchuk G. Theoretical basis of hemodynamic MR imaging techniques to measure cerebral blood volume, cerebral blood flow, and permeability. AJNR Am J Neuroradiol 2007 Nov;28(10):1850-8.

(10) Turner J, Belch JJ, Khan F. Current concepts in assessment of microvascular endothelial function using laser Doppler imaging and iontophoresis. Trends Cardiovasc Med 2008 May;18(4):109-16.

(11) Joyner MJ, Dietz NM, Shepherd JT. From Belfast to Mayo and beyond: the use and future of plethysmography to study blood flow in human limbs. J Appl Physiol 2001;91:2431-41.

(12) Nair DG. About being BOLD. Brain Res Brain Res Rev 2005 Dec 15;50(2):229-43.

(13) van der Geest RJ, Rob J, Niezen AR, van der Wall EE, de Roos A, Rieber JHC. Automated Measurement of Volume flow in the Ascending Aorta using MR Velocity Maps: Evaluation of Inter- and Intraobserver Variability in Healthy Volunteers. J Comput Assist Tomogr 1998;22:904-11.

(14) Split A, Box FMA, van der Geest, Reiber RJ, Kunz P, Kamper AM, et al. Reproducibility of total Cerebral Blood Flow Measurements Using Phase Contrast Magnetic Resonance Imaging. J Magn Reson Imaging 2002;16:1-5.

(15) Oktar SO, Yucel C, Karaosmanoglu D, Akkan K, Ozdemir H, Tokgoz N, et al. Blood-flow volume quantification in internal carotid and vertebral arteries: Comparison of 3 different ultrasound techniques with phase-contrast MR imaging. AJNR Am J Neuroradiology 2006;27(2):363-9.

(16) Ho SS, Chan YL, Yeung DK. Blood flow volume quantification of cerebral ischemia: comparison of three noninvasive imaging techniques of carotid and vertebral arteries. AJR Am J Roentgenol 2002;178:551-6.

(17) Bakker CJ, Kouwenhoven M, Hartkamp MJ. Accuracy and precision of time-averaged flow as measured by non-triggered 2D phase-contrast MR angiography, a phantom evaluation. Magn Reson Imaging 1995;13:959-65.

(18) Kondo C, Caputo GR, Semelka R, Foster E, Shimakawa A, Higgins CB. Right and left ventricular stroke volume measurements with velocity-encoded cine MR imaging: in vitro and in vivo validation. AJR Am J Roentgenol 1991 Jul;157(1):9-16.

(19) Stahlberg F, Ericsson A, Nordell B, Thomsen C, Henriksen O, Persson BR. MR imaging, flow and motion. Acta Radiol 1992 May;33(3):179-200.

(20) Graves MJ. Magnetic resonance angiography. Br J Radiol 1997 Jan;70:6-28.

(21) Jensen JA. Medical ultrasound imaging. Prog Biophys Mol Biol 2007 Jan;93(1-3):153-65.

(22) Jensen JA. Estimation of Blood velocities using ultrasound: A signal processing approach. New York: Cambridge University Press; 1996.

(23) Tola M, Yurdakul M. Effect of Doppler angle in diagnosis of internal carotid artery stenosis. J Ultrasound Med 2006 Sep;25(9):1187-92.

(24) Hoskins PR. Peak velocity estimation in arterial stenosis models using colour vector Doppler. Ultrasound Med Biol 1997;23(6):889-97.

(25) Tortoli P, Michelassi V, Bambi G, Guidi F, Righi D. Interaction between secondary velocities, flow pulsation and vessel morphology in the common carotid artery. Ultrasound Med Biol 2003 Mar;29(3):407-15.

(26) Ford MD, Xie YJ, Wasserman BA, Steinman DA. Is flow in the common carotid artery fully developed? Physiol Meas 2008 Nov;29(11):1335-49.

(27) Hansen KL, Udesen J, Thomsen C, Jensen JA, Nielsen MB. In vivo validation of a blood vector velocity estimator with MR angiography. IEEE Trans Ultrason Ferroelectr Freq Control 2009 Jan;56(1):91-100.

(28) Frazin LJ, Lanza G, Vonesh M, Khasho F, Spitzzeri C, McGee S, et al. Functional chiral asymmetry in descending thoracic aorta. Circulation 1990 Dec;82(6):1985-94.

(29) Lee KL, Doorly DJ, Firmin DN. Numerical simulations of phase contrast velocity mapping of complex flows in an anatomically realistic bypass graft geometry. Med Phys 2006 Jul;33(7):2621-31.

(30) Steinman DA, Thomas JB, Ladak HM, Milner JS, Rutt BK, Spence JD. Reconstruction of carotid bifurcation hemodynamics and wall thickness using computational fluid dynamics and MRI. Magnet Reson Med 2002;47(1):149-59.

(31) Zhao SZ, Xu XY, Hughes AD, Thom SA, Stanton AV, Ariff B, et al. Blood flow and vessel mechanics in a physiologically realistic model of a human carotid arterial bifurcation. J Biomech 2000;33(8):975-84.

(32) Zhao SZ, Papathanasopoulou P, Long Q, Marshall I, Xu XY. Comparative study of magnetic resonance imaging and image-based computational fluid dynamics for quantification of pulsatile flow in a carotid bifurcation phantom. Ann Biomed Eng 2003;31(8):962-71.

(33) Krams R, Bambi G, Giudi F, Helderman F, van der Steen AFW, Tortoli P. Effect of Vessel Curvature on Doppler Derived Velocity Profiles and Fluid Flow. Ultrasound in Medicine and Biology 2005;31:663-71.

(34) Fei DY, Liu DD, Fu CT, Makhoul RG, Fisher MR. Feasibility of angle independent Doppler color imaging for in vivo application: Preliminary study on carotid arteries. Ultrasound Med Biol 1997;23(1):59-67.

(35) Phillips DJ, Beach KW, Primozich J, Strandness DE, Jr. Should results of ultrasound Doppler studies be reported in units of frequency or velocity? Ultrasound Med Biol 1989;15(3):205-12.

(36) Udesen J, Nielsen MB, Nielsen KR, Jensen JA. Examples of In Vivo Blood vector velocity Estimation. Ultrasound Med Biol 2007;33(4):541-8.

(37) Cheng C, Tempel D, van Harperen R, van der Baan A, Grosveld F, Daermen M, et al. Atherosclerotic lesion size and vulnerability are determined by patterns of fluid shear stress. Circulation 2006;113(23):2744-53.

(38) Richter Y, Edelman ER. Cardiology is flow. Circulation 2006;113(23):2679-82.

(39) Vera N, Steinman DA, Ethier CR, Johnston KW, Cobbold RS. Visualization of complex flow fields, with application to the interpretation of colour flow Doppler images. Ultrasound Med Biol 1992;18(1):1-9.

(40) Birchall D, Zaman A, Hacker J, Davies G, Mendelow D. Analysis of haemodynamic disturbance in the atherosclerotic carotid artery using computational fluid dynamics. Eur Radiol 2006;16(5):1074-83.

(41) Hoskins PR. A review of the measurement of blood velocity and related quantities using Doppler ultrasound. Proc Inst Mech Eng [H] 1999;213(5):391-400.

(42) Walker A, Olsson E, Wranne B, Ringqvist I, Ask P. Accuracy of spectral Doppler flow and tissue velocity measurements in ultrasound systems. Ultrasound Med Biol 2004 Jan;30(1):127-32.

(43) Deane CR, Markus HS. Colour velocity flow measurement: in vitro validation and application to human carotid arteries. Ultrasound Med Biol 1997;23(3):447-52.

(44) Stewart SF. Effects of transducer, velocity, Doppler angle, and instrument settings on the accuracy of color Doppler ultrasound. Ultrasound Med Biol 2001 Apr;27(4):551-64.

(45) Gaitini D, Soudack M. Diagnosing carotid stenosis by Doppler sonography: state of the art. J Ultrasound Med 2005 Aug;24(8):1127-36.

(46) Ranke C, Creutzig A, Becker H, Trappe H-J. Standardization of Carotid Ultrasound: A Hemodynamic Method to Normalize for Interindividual and Interequipment Variability. Stroke 1999;30:402-6.

(47) Honish C, Sadanand V, Fladeland D, Chow V, Pirouzmand F. The reliability of ultrasound measurements of carotid stenosis compared to MRA and DSA. Canadian Journal of Neurological Sciences 2005;32(4): 465-471:-471.

(48) Paivansalo MJ, Suramo I, Merikanto J, Lindholm EL. Interobserver, interequipment and intersubject variability of echo-Doppler examination of the common carotid and vertebral arteries. Eur J Ultrasound 1998 Apr;7(2):145-51.

(49) Henry-Feugeas M, Kilic Genauzeau I, Ayme N, Schouman-Claeys E. Variability of ultrasonography velocity assessment of the carotid arteries. J Radiol 2000 Apr;81(4):445-9.

(50) Daigle RE, Miller CW, Histand MB, McLeod FD, Hokanson DE. Nontraumatic aortic blood flow sensing by use of an ultrasonic esophageal probe. J Appl Physiol 1975;38:1153-60.

(51) Fox MD. Multiple crossed-beam ultrasound Doppler velocimetry. IEEE Trans Son Ultrason 1978;25:281-6.

(52) Trahey GE, Allison JW, Ramm OT. Angle independent ultrasonic detection of blood flow. IEEE Trans Biomed Eng 1987;34(12):965-7.

(53) Bohs LN, Geiman BJ, Anderson ME, Gebhart SC, Trahey GE. Speckle tracking for multi-dimensional flow estimation. ultrasonics 2000 Mar;38(1-8):369-75.

(54) Newhouse VL, Censor D, Vontz T, Cisneros JA, Goldberg BB. Ultrasound Doppler probing of flows transverse with respect to beam axis. IEEE Trans Biomed Eng 1987;34:779-88.

(55) Bonnefous O. Measurement of the complete (3D) velocity vector of blood flows. Proc IEEE Ultrason Symp 1988;795-9.

(56) Dunmire KW, Beach KW, Labs K-H, Plett M, Strandness DE. Cross-beam vector Doppler ultrasound for angle independent velocity measurements. Ultrasound Med Biol 2000;26:1213-35.

(57) Overbeck JR, Beach KW, Strandness DE, Jr. Vector Doppler: accurate measurement of blood velocity in two dimensions. Ultrasound Med Biol 1992;18(1):19-31.

(58) Kruskal JB, Newman PA, Sammons LG, Kane RA. Optimizing Doppler and color flow US: Application to hepatic sonography. Radiographics 2004;24(3):657-75.

(59) Pozniak MA, Zagzebski JA, Scanlan KA. Spectral and color Doppler artifacts. Radiographics 1992 Jan;12(1):35-44.

(60) Ferrara K, DeAngelis G. Color flow mapping. Ultrasound Med Biol 1997;23(3):321-45.

(61) Stoica P, Moses R. Spectral analysis of signals. Upper Saddle River, N.J.: Prentice Hall; 2005.

(62) Coats AJS, Murphy C, Conway J, Sleight P. Validation of the beat to beat measurement of blood velocity in the human ascending aorta by a new high temporal resolution Doppler ultrasound spectral analyser. Br Heart J 1992 Aug;68(8):223-9.

(63) Tanaka N, Ohtsuki S. Estimation of Doppler shift frequency using selected phase information for high frame rate color flow mapping. Journal of Medical Ultrasonics 2004;31(1):5-12.

(64) Udesen J, Gran F, Nielsen MB, Jensen JA. A Frequency Splitting Method for CFM Imaging. IEEE Ultrason Symp 2006;2019-22.

(65) Gran F, Udesen J, Nielsen MB, Jensen JA. Coded ultrasound for blood flow estimation using subband processing. IEEE Trans Ultrason Ferroelec Freq Contr 2009;55(10):2211-20.

(66) Oddershede N, Gran F, Jensen JA. Multi-frequency encoding for fast color flow or quadroplex imaging. IEEE Trans Ultrason Ferroelectr Freq Control 2008 Apr;55(4):778-86.

(67) Jensen JA. Spectral velocity estimation in ultrasound using sparse data sets. J Acoust Soc Am 2006;120(1):211-20.

(68) Li J, Stoica P. An adaptive filtering approach to spectral estimation and SAR imaging. IEEE Transactions on Signal Processing 1996;44(6):1469-84.

(69) Herment A, Giovannelli JF. An adaptive approach to computing the spectrum and mean frequency of Doppler signals. Ultrason Imaging 1995 Jan;17(1):1-26.

(70) Vaikus PJ, Cobbold RSC. A comparative study and assessment of Doppler ultrasound spectral estimation techniques, Part 1: Estimation methods. Ultrasound Med Biol 1988;14:661-72.

(71) Vaikus PJ, Cobbold RSC, Johnston KW. A comparative study and assessment of Doppler ultrasound spectral estimation techniques, Part 2: Methods and results. Ultrasound Med Biol 1988;14:673-88.

(72) Jensen JA, Munk P. A new method for estimation of velocity vectors. IEEE Trans Ultrason Ferroelec Freq Contr 1998;45:837-51.

(73) Jensen JA. A new estimator for vector velocity estimation. IEEE Trans Ultrason Ferroelec Freq Contr 2001;48:886-94.

(74) Udesen J, Jensen JA. Investigation of transverse oscillation method. IEEE Trans Ultrason Ferroelec Freq Contr 2006;53:959-71.

(75) Jensen JA, Bjerngaard R. Directional velocity estimation using focusing along the flow direction: II: Experimental investigation. IEEE Trans Ultrason Ferroelec Freq Contr 2003;873-80.

(76) Jensen JA. Directional velocity estimation using focusing along the flow direction: I: Theory and simulation. IEEE Trans Ultrason Ferroelec Freq Contr 2003;857-72.

(77) Jensen JA. Field: A program for simulating ultrasound systems. Med Biol Eng Comp, vol 10th Nordic-Baltic Conference on Biomedical Imaging 1996;4:351-3.

(78) Jensen JA, Svendsen NB. Calculation of pressure fields from arbitrarily shaped, apodized, and excited ultrasound transducers. IEEE Trans Ultrason Ferroelec Freq Contr 1992;39:262-7.

(79) Holfort IK, Kortbek J, Jensen JA. In-vivo Vector Velocity Imaging Using Directional Cross-Correlation. Proc IEEE Ultrason Symp 2006;2023-6.

(80) Jensen JA. Velocity vector estimation in synthetic aperture flow and B-mode imaging. Proc IEEE Int Symp Biomed Imaging: from nano to macro 2004;1:33-6.

(81) Jensen JA, Nikolov S. Transverse flow imaging using synthetic aperture directional beamforming. Proc IEEE Ultrason Symp 2002;2:1488-92.

(82) Jensen JA, Oddershede N. Estimation of velocity vectors in synthetic aperture ultrasound imaging. IEEE Trans Med Imag 2006;25:1637-44.

(83) Nikolov S, Jensen JA. In-Vivo Synthetic aperture flow Imaging in Medical Ultrasound. IEEE Trans Ultrason Ferroelec Freq Contr 2003;50:848-56.

(84) Oddershede N, Jensen JA. Experimental investigation of synthetic aperture flow angle estimation. Proc SPIE Med Imag 2005;5750:417-26.

(85) Oddershede N, Jensen JA. Effects influencing focusing in synthetic aperture vector flow imaging. IEEE Trans Ultrason Ferroelec Freq Contr 2007;54:1811-25.

(86) Udesen J, Gran F, Hansen KL, Jensen JA, Thomsen C, Nielsen MB. High frame-rate blood vector velocity imaging using plane waves: simulations and preliminary experiments. IEEE Trans Ultrason Ferroelec Freq Contr 2008;55(8):1729-43.

(87) Udesen J, Gran F, Hansen KL, Jensen JA, Nielsen MB. Fast blood vector velocity imaging: Simulations and preliminary in vivo results. Proc IEEE Ultrason Symp 2007;1005-8.

(88) Friemel BH, Bohs LN, Trahey GE. Relative performance of two-dimensional speckle-tracking techniques: normalized correlation, non-normalized correlation and sum-absolute-difference. Proc IEEE Ultrason Symp 1995;2:1481-4.

(89) Stoica P, Moses R. Introduction to spectral analysis. Upper Saddle River, N.J: Prentice Hall; 1997.

(90) Gran F, Jakobsson A, Jensen JA. Adaptive spectral Doppler estimation. IEEE Trans Ultrason Ferroelec Freq Contr 2009;56(4):700-14.

(91) Gran F, Jakobsson A, Jensen JA. Adaptive blood velocity estimation in medical ultrasound. Proc IEEE ICASSP 2007;1:293-6.

(92) Stoica P, Jakobsson A, Li J. Matched-filterbank interpretation of some spectral estimators. Signal Processing 1998;66:45-59.

(93) Proakis JG, Manolakis DG. Digital signal processing: Principles, algorithms and applications. 4. ed. Upper Saddle River, N.J.: Prentice Hall; 2007.

(94) Chenevert TL, Fechner KP, Gelblum DY. Improvements in MR angiography using phase-corrected data sets. Magn Reson Med 1989 Apr;10(1):38-49.

(95) Tublin ME, Bude RO, Platt JF. Review. The resistive index in renal Doppler sonography: where do we stand? AJR Am J Roentgenol 2003 Apr;180(4):885-92.

(96) Altman DG. Practical statistics for medical research. London: Chapmann & Hall/CRC; 1991.

(97) Landis JR, Koch GG. The measurement of observer agreement for categorical data. Biometrics 1977;33:159-74.

(98) Fleiss JL. Measuring nominal scale agreement among many raters. Psychol Bull 1971;76(5):378-82.

(99) Kim WY, Poulsen JK, Terp K, Staalsen NH. A new Doppler method for quantification of volumetric flow: in vivo validation using color Doppler. J Am Coll Cardiol 1996 Jan;27(1):182-92.

(100) Kripfgans OD, Rubin JM, Hall AL, Gordon MB, Fowlkes JB. Measurement of volumetric flow. J Ultrasound Med 2006 Oct;25(10):1305-11.

(101) Jenni R, Matthews F, Aschkenasy SV, Lachat M, van Der LB, Oechslin E, et al. A novel in vivo procedure for volumetric flow measurements. Ultrasound Med Biol 2004 May;30(5):633-7.

(102) Soustiel JF, Levy E, Zaaroor M, Bibi R, Lukaschuk S, Manor D. A new angle-independent Doppler ultrasonic device for assessment of blood flow volume in the extracranial internal carotid artery. J Ultrasound Med 2002 Dec;21(12):1405-12.

(103) Rothoerl RD, Schebesch KM, Woertgen C, Brawanski A. Ultrasonic blood flow volume assessment in the extracranial internal carotid artery in arteriovenous malformations. Neurol Res 2005 Mar;27(2):209-11.

(104) Shuping GE, Liping BU, Honghai Z, Schelbert E, Disterhoft M. A Real-time 3-dimensional Digital Doppler Method for Measurement for Flow Rate and Volume Thorugh Mitral Valve in Children: A Validation Study Caompared With Magnetic Resonance Imaging. J Am Soc Echocardiogr 2005;18:1-7.

(105) Forsberg F, Stein AD, Lui J, Deng X, Ackerman W, Herzog D, et al. Validating volume Flow Measurements from a Novel Semiautomated Four-dimensional Doppler Ultrasound Scanner. Acad Radiol 2006;13(10):1204-10.

(106) Schrank E, Phillips DJ, Moritz WE, Strandness DE, Jr. A triangulation method for the quantitative measurement of arterial blood velocity magnitude and direction in humans. Ultrasound Med Biol 1990;16(5):499-509.

(107) Steel R, Ramnarine KV, Davidson F, Fish PJ, Hoskins PR. Angle-independent estimation of maximum velocity through stenoses using vector Doppler ultrasound. Ultrasound Med Biol 2003 Apr;29(4):575-84.

(108) Steel R, Ramnarine KV, Criton A, Davidson F, Allan PL, Humphries N, et al. Angle-dependence and reproducibility of dual-beam vector doppler ultrasound in the common carotid arteries of normal volunteers. Ultrasound Med Biol 2004 Feb;30(2):271-6.

(109) Ricci S, Diciotti S, Francalanci L, Tortoli P. Accuracy and Reproducibility of a Novel Dual-Beam Vector Doppler Method. Ultrasound Med Biol 2008 Dec 23.

(110) Fei DY, Fu CT. New method to obtain ultrasonic angle independent Doppler color images using a sector transducer. Ann Biomed Eng 1999 Mar;27(2):187-93.

(111) Nyrnes SA, Lovstakken L, Torp H, Haugen BO. Blood flow imaging-a new angle-independent ultrasound modality for the visualization of flow in atrial septal defects in children. Echocardiography 2007 Oct;24(9):975-81.

(112) Lovstakken L, Ibrahim KS, Vitale N, Henriksen ST, Kirkeby-Garstad I, Torp H, et al. Blood flow imaging: a new two-dimensional ultrasound modality for enhanced intraoperative visualization of blood flow patterns in coronary anastomoses. J Am Soc Echocardiogr 2008 Aug;21(8):969-75.

(113) Pastorelli A, Torricelli G, Scabia M, Biagi E, Masotti L. A real-time 2-D vector Doppler system for clinical experimentation. IEEE Trans Med Imaging 2008 Oct;27(10):1515-24.

(114) Ho SS, Metreweli C. Preferred technique for blood flow volume measurement in cerebrovascular disease. Stroke 2000 Jun;31(6):1342-5.

(115) Powell AJ, Maier SE, Chung T, Geva T. Phase-velocity cine magnetic resonance imaging measurement of pulsatile blood flow in children and young adults: in vitro and in vivo validation. Pediatr Cardiol 2000 Mar;21(2):104-10.

(116) Hundley WG, Li HF, Hillis LD. Quantitation of cardiac output with velocity-encoded, phase-difference magnetic resonance imaging. Am J Cardiol 1995;75:1250-5.

(117) Rebergen SA, van der Wall EE, Doornbos J, de RA. Magnetic resonance measurement of velocity and flow: technique, validation, and cardiovascular applications. Am Heart J 1993 Dec;126(6):1439-56.

(118) Lotz J, Meier C, Leppert A, Galanski M. Cardiovascular flow measurement with phase-contrast MR imaging: basic facts and implementation. Radiographics 2002 May;22(3):651-71.

(119) Higginbotham MB, Morris KG, Williams S, McHale PA, Coleman RE, Cobb FR. Regulation of Stroke Volume during Submaximal and Maximal Upright Exercise in Normal Man. Circ Res 1986;58:281-91.

(120) Polak JF. Peripheral Vascular Sonography: A Practical Guide. 2. ed. Lippincott Williams & Wilkins; 2004.

(121) Oshinski JN, Curtin JL, Loth F. Mean-average wall shear stress measurements in the common carotid artery. J Cardiovasc Magn Reson 2006;8(5):717-22.

(122) Brands PJ, Hoeks AP, Hofstra L, Reneman RS. A noninvasive method to estimate wall shear rate using ultrasound. Ultrasound Med Biol 1995;21(2):171-85.

(123) Rubin JM. Spectral Doppler US. Radiographics 1994 Jan;14(1):139-50.

(124) Friemel BH, Bohs LN, Nightingale KR, Trahey GE. Wall filtering challenges in two-dimensional vector velocity estimation. Proc IEEE Ultrason Symp 1993;2:1031-4.

(125) Oddershede N, Hansen KL, Nielsen MB, Jensen JA. In-vivo examples of synthetic aperture vector flow imaging. Proc SPIE Med Imag 2007;8:6510-3.

(126) Marshall I, Papathanasopoulou P, Wartolowska K. Carotid flow rates and flow division at the bifurcation in healthy volunteers. Physiol Meas 2004 Jun;25(3):691-7.

(127) Belz GG. Elastic properties and Windkessel function of the human aorta. Cadiovasc Drugs Ther 1995;9(1):73-83.

(128) Qui Y, Quijano RC, Wang SK, Hwang HC. Fluid dynamics of venous valve closure. Ann Biomed Eng 1995;23(6):750-9.

(129) Lurie F, Kistner RL, Eklof B, Kessler D. Mechanism of venous valve closure and role of the valve in circulation: A new concept. J Vasc Surg 2003;38(5):955-61.

(130) Fisher J, Vaghaiwalla F, Tsitlik J, Levin H, Brinker J, Weisfleldt M, et al. Determinants and clinical significance of jugular venous valve competence. Circulation 1982;65(1):188-96.

(131) Nedelmann M, Techner D, Dieterich M. Analysis of internal jugular vein insufficiency - a comparison of two ultrasound methods. Ultrasound Med Biol 2007;33(6):857-62.

(132) Akkawi NM, Agosti C, Borroni B, Rozzini L, Magoni M, Vignolo LA, et al. Jugular valve incompetence: A study using air contrast ultrasonography on a general population. J Ultrasound Med 2002;21(7):747-51.

(133) Shipkowitz T, Rodgers VGJ, Frazin LJ, Chandran KB. Numerical study on the effect of secondary flow in the human aorta on local shear stresses in abdominal aortic branches. J Biomech 2000;33(6):717-28.

(134) Xue YJ, Gao PY, Duan Q, Lin Y, Dai CB. Preliminary study of hemodynamic distribution in patient-specific stenotic carotid bifurcation by image-based computational fluid dynamics. Acad Radiol 2008;49(5):558-65.

(135) Schuierer G, Huk WJ. Diagnostic significance of flow separation within the carotid bifurcation demonstrated by digital subtraction angiography. Stroke 1990;21(12):1674-9.

(136) Stokholm R, Oyre S, Ringgaard S, Flaagoy H, Paaske W, Pedersen EM. Determination of Wall Shear Rate in the Human Carotid Artery by Magnetic Resonance Techniques. Eur J Vasc Endovasc surg 2000;20(5):427-33.

(137) Papathanasopoulou P, Zhao SZ, Kohler U, Robertson MB, Long Q, Hoskins P, et al. MRI measurement of time-resolved wall shear stress vectors in a carotid bifurcation model, and comparison with CFD predictions. J Magn Reson Imaging 2003;17(2):153-62.

(138) Marshall I, Zhao S.Z., Papathanasopoulou P, Hoskins P, Xu XY. MRI and CDF studies of pulsatile flow in healthy and stenosed carotid bifurcation models. J Biomech 2004;37(5):679-87.

(139) Timmers M, Wieling W, Karemaker JM, Lenders JWM. Denervation of carotid baro- and chemoreceptors in humans. J Physiol 2003;553(1):3-11.

(140) Mancia G, Ferrari A, Gregorini L, Valentini R, Ludbrook J, Zanchetti A. Circulatory reflexes form carotid and extracarotid baroreceptor areas in man. Circ Res 1977;41:309-15.

(141) Conley RB, Doux JD, Lee PY, Bazar KA, Daniel SM, Yun AJ. Integrating the theories of Darwin and Bernoulli: Maladaptive baroreceptor network dysfunction may explain the pathogenesis of aortic aneurysms. Med Hypotheses 2005;65:266-72.

(142) Illig KA, Ouriel JA, Holen J, Green RM. Measurement of carotid birfurcation pressure gradients using the Bernoulli principle. J Vasc Surg 1996;4:130-4.

(143) Henze L. In-vivo Vector Velocity Estimation Using Ultrasound, Masters Thesis. Copenhagen: Tehcnical University of Denmark; 2009.

(144) Feng N, Zhang J, Wang W. An adaptive clutter rejection method based on AR model in color flow imaging. ultrasonics 2006 Dec 22;44 Suppl 1:e85-e88.

(145) Wang PD, Shen Y, Feng NZ. A novel clutter rejection scheme in color flow imaging. ultrasonics 2006 Dec 22;44 Suppl 1:e303-e305.

(146) Allam ME, Greenleaf JF. Isomorphism between pulsed-wave Doppler ultrasound and direction-of-arrival estimation - part I: Basic principles. IEEE Trans Ultrason Ferroelec Freq Contr 1996;43(5):911-22.

(147) Allam ME, Kinnick RR, Greenleaf JF. Isomorphism between pulsed-wave Doppler ultrasound and direction-of-arrival estimation - part II: Experimental results. IEEE Trans Ultrason Ferroelec Freq Contr 1996;43(5):923-35.

(148) Jensen JA, Hansen M, Tomov BG, Nikolov S, Holten-Lund H. System Architecture of an Experimental Synthetic Aperture Real-time Ultrasound System. Proc IEEE Ultrason Symp 2007;636-40.

Appendix I

In Vivo Validation of a Blood Vector Velocity Estimator with MR Angiography

Kristoffer L. Hansen, Jesper Udesen, Carsten Thomsen, Jørgen A. Jensen, *Senior Member, IEEE*, and Michael B. Nielsen

***Abstract*—Conventional Doppler methods for blood velocity estimation only estimate the velocity component along the ultrasound beam direction. This implies that a Doppler angle under examination close to 90° results in unreliable information about the true blood direction and blood velocity. The novel method transverse oscillation (TO), which combines estimates of the axial and the transverse velocity components in the scan plane, makes it possible to estimate the vector velocity of the blood regardless of the Doppler angle. The present study evaluates the TO method with magnetic resonance phase contrast angiography (MRA) by comparing *in vivo* measurements of stroke volume. Eleven healthy volunteers were included in this prospective study. From the obtained data sets recorded with the 2 modalities, vector velocity sequences were constructed and stroke volume calculated. Angle of insonation was approximately 90° for TO measurements. The correlation between the stroke volume estimated by TO and MRA was 0.91 ($p < 0.01$) with the equation for the line of regression: MRA = 1.1•TO-0.4. A Bland-Altman plot was additionally constructed where the mean difference was 0.2 ml with limits of agreement at −1.4 ml and 1.9 ml. The results indicate that reliable vector velocity estimates can be obtained *in vivo* using the presented angle-independent 2-D vector velocity method. The TO method can be a useful alternative to conventional Doppler systems by avoiding the angle artifact, thus giving quantitative velocity information.**

I. Introduction

The clinical ultrasound scanners of today perform angle-dependent blood velocity estimation where the actual velocity is a projection onto the ultrasound beam direction. The inherent limitations of the conventional Doppler system give rise to unreliable velocity estimates when the angle between the beam direction and the flow approaches 90° [1]. This can be seen from the relationship between the axial velocity v_z and the true velocity of the blood v given by

$$v = \frac{v_z}{\cos\theta} = \frac{f_p c}{2 f_0 \cos\theta} \tag{1}$$

where θ is the angle between the ultrasound beam and the blood flow, f_p is the Doppler frequency, f_0 is the center frequency of the emitted ultrasound pulse, and c is the speed of sound. All variables in (1) can be estimated if the operator manually supplies the scanner with the angle θ assuming blood flow parallel to the vessel wall.

In color flow mode (CFM), no angle correction is performed and thus no correct velocities are given unless the blood velocities are purely axial. Only in spectral Doppler examination is the angle correction scheme applied but then only at a single location.

With either method, the operator is impelled to achieve an acceptable angle of insonation (< 70°) when examining blood flow to avoid $\cos\theta \sim 0$. This is usually manageable by using a steered beam and if necessary tilting the transducer. However, when examining vessels with complex geometries, ultrasound (US) Doppler examinations fail to give the actual blood velocities, because the flow profile is multidirectional and thus impossible to angle correct. These regions are important to examine in patients with or prone to cardiovascular disease because atherosclerotic lesions have predilection for areas with lowered wall shear stress and vortices [2]–[4].

Different methods to circumvent the limitation of angle dependency in conventional US Doppler systems and extending the axial velocity estimate to a vector estimate have been suggested by several groups [5]–[9]. One promising method for vector velocity estimation, transverse oscillation (TO), has been proposed by Jensen and Munk [10]–[12]; another method, spatial quadrature, has been proposed by Anderson [13], [14]. The method introduces, along with the normal axial ultrasound oscillation, an additional oscillation in the lateral direction of the pulse-echo field. The measured signals are therefore sensitive to both an axial and a transverse motion. Using special autocorrelation estimators [11], both the axial and transverse velocity component can be determined for angle-independent 2-D blood velocity estimation. Vector velocity determination will potentially eliminate the angle dependency in US color flow mapping that will alleviate the problem of achieving a sufficient scan angle and will make it possible to quantify blood flow and to visualize complex flow patterns correctly [15].

The TO method has previously been validated in simulations and flow phantoms [16], [17], and examples of *in vivo* sequences have been produced of the carotid artery [15], [18]. However, the TO method has not yet been evaluated and validated in a clinical study, nor has its performance been compared with an independent and reliable velocity estimator.

The aim of this paper was to validate the TO method *in vivo* with respect to blood flow estimation. The artery

Manuscript received January 16, 2008; accepted July 16, 2008.

K. L. Hansen, C. Thomsen, and M. B. Nielsen are with the Department of Radiology, University Hospital of Copenhagen, Denmark (e-mail: klh@oersted.dtu.dk).

J. Udesen is with GN Resound, Ballerup, Denmark.

J. A. Jensen are with the Technical University of Denmark, Center for Fast Ultrasound Imaging, Lyngby, Denmark.

Digital Object Identifier 10.1109/TUFFC.2009.1008

of interest was chosen to be the common carotid artery from healthy volunteers to achieve an *in vivo* model with a simple geometry and a uniform, unidirectional flow. Thereby, the necessary assumptions of circular geometry of the examined vessel and rotationally symmetric blood flow used in the calculations of TO volume flow estimation were valid. The volume flow in the common carotid artery of 11 healthy volunteers was determined with the TO method when the beam-to-flow-angle was approximately 90°, that is, when the conventional Doppler method fails to estimate any blood velocities. The results were compared with measurements from the same volunteers obtained with magnetic resonance phase contrast angiography (MRA).

TO has been evaluated previously in flow rig and simulations with respect to instantaneous velocity estimates, where there was full control of the applied flow to measure.

In the *in vivo* setup, no control of the flow is possible, which emphasizes the need for a reliable reference method. No reference can measure instantaneous velocity estimates to all points in the scan plane. MRA can measure velocity estimates as an average over several heart cycles and is accepted as the gold standard for cerebral blood flow estimation [19]–[23].

TO is not MR compatible (as are all other US systems), and therefore the scans were performed at 2 different examinations. This affected the alignment of scan planes in the rotational and longitudinal direction and the point-to-point comparison of the estimates because the velocity profile fluctuates over time.

In this paper, MRA and TO are compared by evaluating the volume flow estimates. The vector velocity estimates found with the TO method have been converted into stroke volume estimates and compared with stroke volume estimates obtained with MRA. Obviously this is only an indirect validation of the vector velocity estimator. However, it should be noted that the true strength of TO and clinical value are expected to be in visualization of the nonlaminar nature of blood flow.

Furthermore, the assumptions of circular geometry of the examined vessel and rotationally symmetric blood flow were tested.

The structure of the paper is as follows: First, a brief introduction to the TO method is given followed by an outline of the calculations used to estimate the volume flow. The *in vivo* results and the different plots are then presented. Finally, the perspectives of the TO method are discussed.

II. Materials and Methods

A. Volunteers

This prospective study was performed after approval by the Danish National Committee on Biomedical Research Ethics (Date: 30–05–06, J.nr:(KF)07307579). Eleven healthy volunteers (7 males and 4 females, 24 to 44 years old, mean age: 32 years) entered the study after informed consent. The right common carotid artery was examined in all volunteers using US and MRA at 2 separate occasions with no more than a week in between. The volunteer rested supine on the examination table 15 min before both examinations. All scans were carried out by an experienced radiologist.

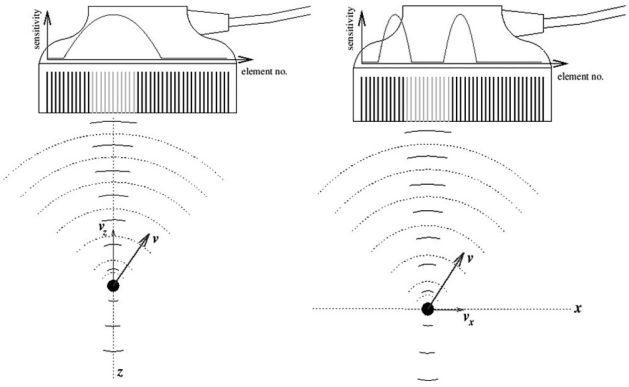

Fig. 1. The received signal from a moving scatterer moving along vector arrow v is processed in 2. The axial velocity component v_z is found by using a bell-shaped apodization function identical to conventional velocity estimation system (left figure). The transverse velocity component v_x is estimated from the same recorded data by manipulating the apodization function so it resembles a 2-point source (right figure). The active elements in transmit are light gray, the emitted signal is represented with solid lines, and the scattered signal with dotted lines. The apodization functions for the 2 approaches are shown as curves superimposed on the transducer.

B. TO Method

The basis for estimating the vector velocity with the TO method has been described previously [10]–[12], [17]. In brief, the motion in the transverse direction is found by creating a double oscillation (an axial oscillation and a transverse oscillation) in the pulse-echo field from which 2 different frequencies can be found. The double oscillation is founded on the theory of Fraunhofer diffraction, which states that the lateral field component at the focal point scales with the Fourier transform of the apodization function. Manipulation of the apodization function is only done in receive beamforming. The 2 frequencies can be manipulated to give the transverse vector velocity. The axial vector velocity is found as in conventional Doppler systems from an axial oscillation. The 2 vector velocities are found from the same data set by changing the receive beamforming (Fig. 1).

A special estimator different from the autocorrelation estimator used in conventional CFM [24] is used, and the 2 vector estimates are combined to yield the 2-D vector velocity of the moving scatterer. The emitted pulse used in estimating the 2 vector velocity components is identical to the pulse used in conventional ultrasound Doppler system. Details about the measurement setup are described

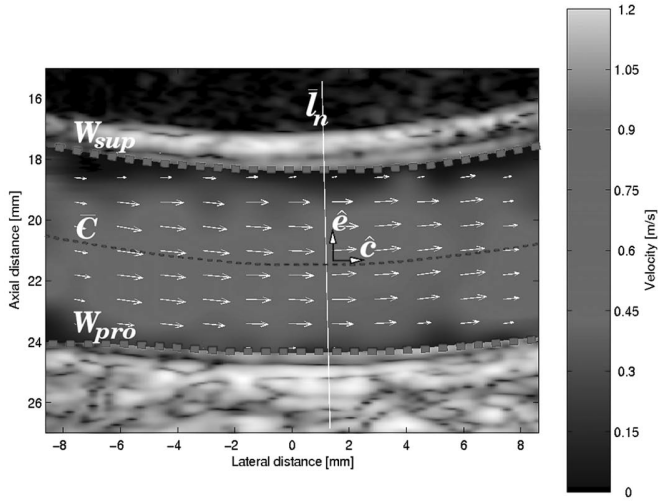

Fig. 2. Example of VVI obtained with TO. The vessel boundaries W_{sup} and W_{pro} (thick dashed line), the center curve $\bar{C}$ (thin dashed line) and a line $\bar{l}_n$ (solid line) orthogonal to center line $\bar{C}$ are delineated. The unit vectors $\hat{e}$ and $\hat{c}$ are shown as black vector arrows. Notice that VVI is superimposed on the B-mode image.

TABLE I. Scanner and Transducer Setup.

Transducer	Linear array, BK 8812
Center frequency	5 MHz
Number of cycles per pulse	8 cycles/pulse
fprf	6 kHz
Sampling frequency	40 MHz
Lateral wavelength	1.0 mm
Apodization in transmit	Hanning
Apodization in receive	Two Hannings
Focus in transmit	18 mm
Focus in receive	Dynamic
F-number in transmit	3.3
F-number in receive	0.8
Number of firings per vel. est.	64 firings/vel. est.
Lateral distance between vel. est.	4 pitch
Ispta	293 mW/cm^2
MI	1.07
TIS	1.65

by Udesen *et al.* [15], and the estimators are described by Jensen [11]. The volume flow is found as described in the next section.

1) TO Setup: The recorded sequences for vector velocity images (VVI) were obtained with the experimental scanner RASMUS [25], [26] and a 5 MHz linear array transducer as described by the parameters depicted in Table I.

The post processing was done with MATLAB 6.5 (MathWorks, Natick, MA). All sequences of VVI were obtained from the right common carotid arteries of the volunteers with angles of insonation of approximately 90° as shown in Fig. 2. The vessel of interest was scanned approximately 2 cm upstream of the bifurcation to prevent confounding turbulence. For data analysis, the stored 3 s sequence was processed by an algorithm that automatically identified the vessel region in each frame from the B-mode image [15].

M_{ul} and N_{ul} represent the number of pixels along the horizontal and vertical axes, respectively, in each frame i. The volume flow [ml/s] q for each frame i with dimensions $M_{\mathrm{ul}} \times N_{\mathrm{ul}}$, was estimated in the following way. Let $W_{\mathrm{sup},i}(n)$, $n = 1, 2, \ldots, N_{\mathrm{ul}}$, be the pixel position of the superficial vessel wall and let $W_{\mathrm{pro},i}(n)$, $n = 1, 2, \ldots, N_{\mathrm{ul}}$, be the pixel position of the profound vessel wall for image i (Fig. 2). The center curve $\bar{C}_i(n)$ of the vessel was defined as a 3rd order polynomial fit over n with the pixel positions given by

$$\bar{C}_i(n) = \left({}^{n}_{\left(W_{\mathrm{sup},i}(n) + W_{\mathrm{pro},i}(n)\right) / 2} \right). \tag{2}$$

The polynomial was for each individual frame found in a least-square sense using MATLAB 6.5. The order of the polynomial was set to 3, which showed the best approximation to the vessel wall when inspected visually.

For each lateral pixel position $n = 1, 2, \ldots, N_{\mathrm{ul}}$, a line $\bar{l}_{n,i}(k)$ normal to $\bar{C}_i(n)$ was defined as

$$\bar{l}_{n,i}(k) = \bar{C}_i(n) + k\hat{e}, k \in Z \tag{3}$$

where $\hat{e}$ is a unit vector satisfying that the dot product $\hat{e} \bullet \hat{c} = 0$ and $\hat{c}$ defined as a unit vector along the center curve $\bar{C}_i(n)$.

The volume flow [ml/s] $q_i(n)$ through the cross section defined by $\bar{l}_{n,i}(k)$ assuming circular vessel geometry and a rotationally symmetric blood flow profile was calculated from

$$q_i(n) = \sum_{k=-L_{ul}}^{L_{ul}} \bar{V}(\bar{l}_{n,i}(k)) \bullet \hat{c}\pi \left| \bar{l}_{n,i}(k) - \bar{C}_i(n) \right| \Delta r \tag{4}$$

where $\bar{V}(\bar{l}_{n,i})$ is the vector velocity to any given spatial position on $\bar{l}_{n,i}(k)$, Δr the pixel spacing, assumed to be equal in both image directions, pixel values equal to zero outside the vessel and $L_{\mathrm{ul}} = \sqrt{M_{\mathrm{ul}}{}^2 + N_{\mathrm{ul}}{}^2}$.

The mean volume flow [ml/s] $\bar{q}$ for each frame i was found by averaging the estimated volume flow at all lateral positions

$$\bar{q}_i = \frac{1}{N_{ul}} \sum_{n=1}^{N_{ul}} q_i(n) \tag{5}$$

yielding a volume flow profile for the examined artery.

2) MRA Setup: MRA examinations were performed with a 1.5 T whole body scanner (Magnetom Vision, Siemens AG, Munich, Germany). A prospective ECG-triggered phase contrast sequence using a cervical coil was employed. Phase interval was 29 ms, echo time 7 ms, flip angle 30°, pixel resolution 0.52 × 0.39 mm in a matrix of

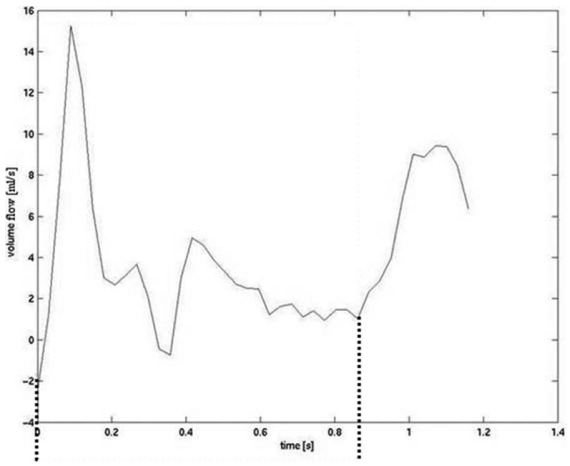

Fig. 3. Graph showing the MRA-derived volume flow profile for one volunteer. The dashed lines encompass the first averaged heart cycle used for calculating the mean stroke volume. The second systole has a broader and flatter profile due to dephasing.

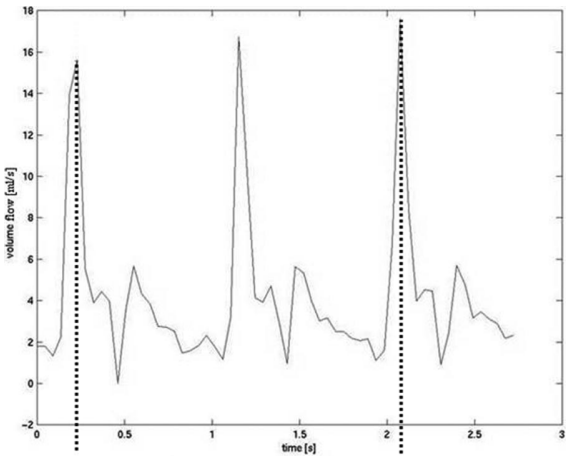

Fig. 4. Graph showing the TO-derived volume flow profile for one volunteer. The dashed lines encompass 2 full heart cycles used for calculating the mean stroke volume.

192 × 256 pixels interpolated up to 256 × 256 pixels, FOV 100 mm, slice thickness 6 mm, and maximum velocity encoding V_{ENC} ±1.5 m/s.

The scan plane for the volume flow measurements was selected to be perpendicular to the right common carotid artery and placed 2 cm upstream of the bifurcation as in TO. The volume flow estimation of the resulting MRA scanning was carried out in MATLAB 6.5 using MR DICOM images. The MR flow images were recorded interleaved with anatomic images.

The region of interest (ROI) was defined as pixel values above a certain threshold. The threshold pixel value defining the ROI was manually set so that the vessel boundaries visually appeared as smooth as possible with the ROI as large as possible.

The ROI encompassing the lumen of the vessel was then used as a window on the phase velocity maps to ensure that pixel values from the vessel surroundings representing, e.g., vena jugularis were ignored in the volume flow measurement. Another region near the vessel on the flow sequence was selected to correct the phase offset [27]. The volume flow [ml/s] for each frame j was found by adding the pixel values, i.e., the velocity values, in the ROI and multiplying with pixel area.

3) Comparison: As a result of the low signal-to-noise ratio in MRA, the MRA-derived volume flow profile was calculated as an average of ECG-triggered measurements obtained over 192 heart cycles. Due to fluctuations in heart rate and changing R-R interval over the 192 heart cycles, the second averaged systole was not well defined (Fig. 3).

Only the first averaged heart cycle of the volume flow profile was perfectly ECG-triggered and in phase, and therefore used for calculating the mean volume flow. Hence, it was the shortest heartbeat of the 192 heart cycles that defined the time where volume flow was found. It must thus be expected that the MRA stroke volume was slightly underestimated.

The TO volume flow profile was determined from an averaged heart cycle consisting of all complete heart cycles recorded in the VVI sequence. A characteristic point in each VVI sequence, e.g., the systolic peak was tracked to define the number of complete heart cycles used in the averaged TO volume flow profile (Fig. 4).

The comparison of the achieved volume flow profiles was made with respect to stroke volume. This variable is less heart rate dependent and thus a more reliable parameter when comparing measurements obtained at 2 different occasions [28].

The stroke volume Q for TO was found with

$$Q_{\mathrm{TO}} = \sum_{i=1}^{I} \overline{q}_i \Delta t \tag{6}$$

where $\overline{q}_i$ is the mean volume flow [ml/s] for each frame i, Δt is time between each frame, and I is the number of frames encompassing the averaged heart cycle.

The stroke volume Q for MRA was analogous found with

$$Q_{\mathrm{MRA}} = \sum_{j=1}^{J} q_j \Delta t \tag{7}$$

where q_j is the volume flow [ml/s] for each frame j and J is the number of frames encompassing the averaged heart cycle.

4) Assumption: To examine the assumption of circular geometry and rotationally symmetric flow in the TO volume flow estimation, an algorithm was designed to compute the volume flow from the MRA sequences in a similar manner.

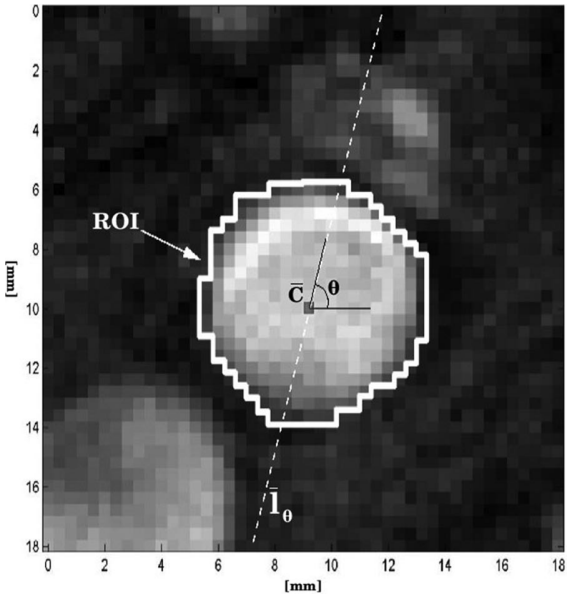

Fig. 5. Example of a frame from the anatomic sequence obtained with MR where vessel boundaries (solid line) encompassing ROI and a line $\overline{l}_\theta$ (dashed line) going through the center point $\overline{C}$ for the angle θ are shown. The white area at the bottom left represents a part of the right jugular vein.

The center point $\overline{C}_j = (C_{x,j}, C_{y,j})$ of the ROI_j of each MRA frame j with the dimensions $M_{\mathrm{MRA}} \times N_{\mathrm{MRA}}$ was found by

$$C_{x,j} = \frac{1}{P_j}\sum_{p=1}^{P_j} c_{x,j} \tag{8}$$

$$C_{y,j} = \frac{1}{P_j}\sum_{p=1}^{P_j} c_{y,j} \tag{9}$$

where $c_{x,j}$ and $c_{y,j}$ are the sets of pixel positions within ROI_j to each frame j of, respectively, x- and y-coordinates and P_j the total amount of pixels constituting the inner lumen of the vessel to each frame j.

Lines $\overline{l}_{\theta,j}$ for every angle θ going through the center point $\overline{C}_j$ were calculated for each frame according to the parametric representation

$$\overline{l}_{\theta,j}(k) = \overline{C}_j + \overline{r}_\theta k \Delta l, k \in Z \tag{10}$$

where $\overline{r}_\theta = \begin{pmatrix}\cos\theta \\ \sin\theta\end{pmatrix}$, Δl denotes the step length equal to pixel size in mm and pixel values equal to zero outside the ROI (Fig. 5) .

Assuming circular vessel geometry and rotationally symmetric blood flow, the volume flow $q_{\theta,j}$ for each angle θ in every frame j was calculated by multiplying the velocity $V_j(\overline{l}_{\theta,j}(k))$ along the line $\overline{l}_{\theta,j}$ with the corresponding area segment $\pi\left|\overline{l}_{\theta,j}(k) - \overline{C}_j\right|$ and summing over the vessel diameter. Setting $V_j(\overline{l}_{\theta,j}(k))$ to zero outside the ROI_j, $q_{\theta,j}$ can be written as

$$q_{\theta,j} = \sum_{k=-L_{\mathrm{MRA}}}^{L_{\mathrm{MRA}}} V_j(\overline{l}_{\theta,i}(k))\pi\left|\overline{l}_{\theta,j}(k) - \overline{C}_j\right|\Delta l \tag{11}$$

where $\left|\overline{l}_{\theta,j}(k) - \overline{C}_j\right|$ is the distance from a pixel on the line $\overline{l}_{\theta,j}(k)$ to the center point $\overline{C}_j$ and $L_{\mathrm{MRA}} = \sqrt{{M_{\mathrm{MRA}}}^2 + {N_{\mathrm{MRA}}}^2}$.

Analogous to (6) and (7), the volume flow per stroke at angle θ was found from

$$Q_\theta = \sum_{j=1}^{J} q_{\theta,j}\Delta t \tag{12}$$

where $q_{\theta,j}$ is the volume flow [ml/s] for each frame j at angle θ and J the number of frames encompassing the heart cycle, which produces a stroke volume range to every volunteer.

C. Statistics

A descriptive statistical analysis was computed on the stroke volume data for the 2 modalities finding mean value, standard deviation, and stroke volume range. The stroke volume data obtained with TO were then compared with stroke volume data obtained with MRA using linear regression analysis with 2-tailed significance value given and $p < 0.05$ considered significant. The correlation coefficient, regression equation, and confidence interval (CI) using Fisher's r-to-z-transformation were calculated. Finally a Bland-Altman plot was made to illustrate the difference of stroke volume estimated by TO and MRA along with confidence intervals [29]. All statistical analyses were performed within the MATLAB 6.5 environment.

III. Results

The study population consisted of 11 volunteers; and the mean volume flow obtained by TO and MRA was recorded. The overall results of the stroke volume measurements are summarized in Table II. Mean, standard deviation, and range reflect the biological variability among the 11 volunteers found with either TO or MRA.

The correlation between the stroke volume estimated by TO and MRA is illustrated in Fig. 6 as a scatterplot. R was 0.91 ($p < 0.01$; 95% CI: 0.69 to 0.98) and the linear regression line, MRA = 1.1 • TO − 0.4, was found to be close to unity. The full range for the averaged MRA stroke volume calculated for every angle assuming rotationally symmetric flow and circular vessel geometry is shown as a bar for every volunteer in the scatterplot.

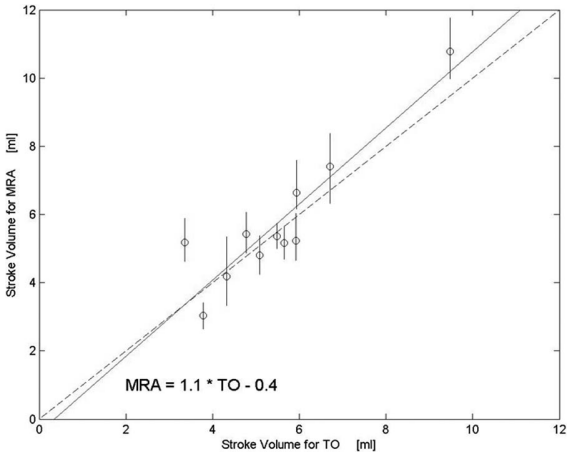

Fig. 6. Graph showing the regression line (solid line) between MRA and TO. The full range of MRA measured stroke volume over all angles when assuming circular geometry and rotationally symmetric flow is for every volunteer shown as a bar. Line of perfect fit is drawn as a dashed line.

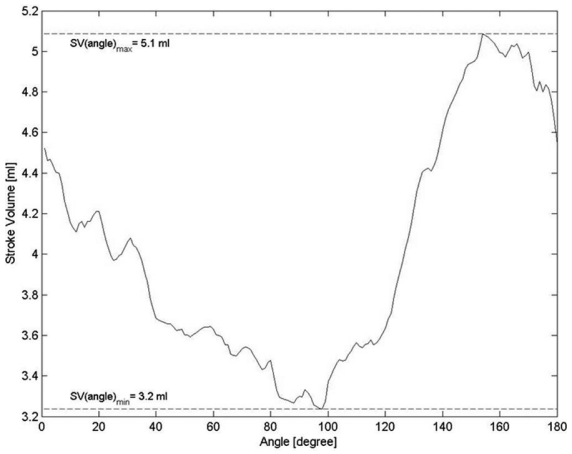

Fig. 7. Graph showing the calculated stroke volume for every line of angle for MRA data of one volunteer when assuming circular vessel geometry and rotationally symmetric blood flow. The maximum ($SV(angle)_{max}$) and minimum ($SV(angle)_{min}$) stroke volumes are marked by dashed lines.

In Fig. 7, the angle-dependent stroke volume for one volunteer (no. 7) is depicted with a volume flow range of 3.2 ml to 5.1 ml and in Fig. 8 the full ranges of angle-dependent stroke volume as percentages of the actual MRA stroke volumes for all volunteers are plotted giving a mean ratio of 24.1%. One volunteer (no. 7) presented a ratio between angle-dependent MRA stroke volume and actual MRA stroke volume of 45.3%. By examining the phase velocity maps of this particular volunteer, it was seen that a substantial asymmetric flow was present while the vessel had approximately circular geometry.

In Fig. 9, a Bland-Altman plot is constructed, where the difference between the methods is plotted against their mean. The mean difference was 0.24 ml with limits of agreement (LoA) at −1.41 ml and 1.90 ml (95% CI for mean difference: −0.32 ml to 0.81 ml; 95% CI for lower limit: −2.39 ml to −0.43 ml; 95% CI for upper limit: 0.92 ml to 2.88 ml).

TABLE II. STROKE VOLUME MEASUREMENTS FOR ALL VOLUNTEERS, STROKE VOLUME AVERAGE ± ONE STANDARD DEVIATION AND STROKE VOLUME RANGE OBTAINED WITH TO AND MRA.

	TO [ml/heartbeat]	MRA [ml/heartbeat]
Volunteer 1	3.78	3.03
Volunteer 2	5.65	5.17
Volunteer 3	5.93	6.64
Volunteer 4	6.71	7.41
Volunteer 5	4.78	5.42
Volunteer 6	9.48	10.78
Volunteer 7	4.32	4.18
Volunteer 8	5.09	4.80
Volunteer 9	5.92	5.23
Volunteer 10	3.36	5.18
Volunteer 11	5.49	5.36
Volume flow ± std	5.50 ± 1.65	5.75 ± 2.02
Range	3.78–9.48	3.03–10.78

IV. DISCUSSION

The paper describes results of a comparison study between TO and MRA in an *in vivo* setup. The correlation of variables TO and MRA, when determining the stroke volume in the right common carotid artery of 11 healthy volunteers, was significant ($R = 0.91$, $p < 0.01$); the linear regression line as shown in the Fig. 6 was found to be near unity.

The TO method underestimated the stroke volume compared with MRA. This was illustrated by the equation of the linear regression line and by the estimated mean difference of 0.24 ml/stroke according to the Bland-Altman plot. This is consistent with earlier results, which showed an underestimation of less than 10% for all angles between 50° to 90° [17].

Presumably one of the major reasons for the underestimation of stroke volume obtained with TO is the stationary echo-cancelling filter, which cancels out echoes from stationary tissue. The blood scattterers with lowest vector velocities near the vessel boundaries are confounded with the stationary tissue and filtered out. Even though these vector velocities are negligible, they correspond to a large cross-sectional area and thus add up to a significant blood volume.

This is a known problem in 2-D vector velocity estimation because the frequency content of the signal to be stationary-echo-cancelled is strongly dependent on the angle of flow. Therefore, it is not, in general, possible to choose a cut-off frequency that precisely discriminates between clutter and blood [30].

Two other common problems in US blood estimation are the overestimation of low velocities relative to $V_{nyquist}$ when doing stationary echo cancelling where $V_{nyquist}$ is defined by

$$V_{\text{nyquist}} = \frac{f_p c}{4 f_0} \tag{13}$$

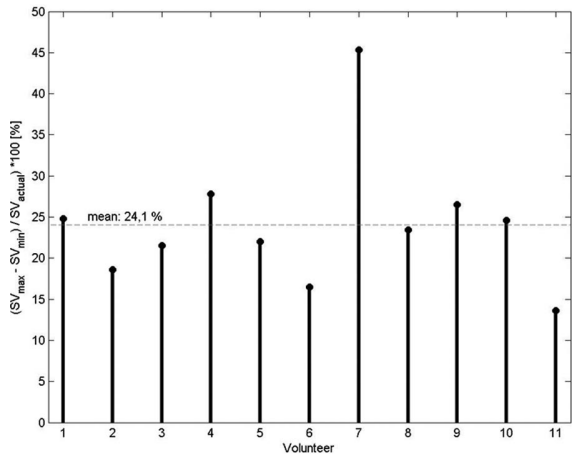

Fig. 8. Graph showing the ratio between angle-dependent MRA stroke volume and actual MRA stroke volume. The mean ratio for the whole population is shown as a dashed line.

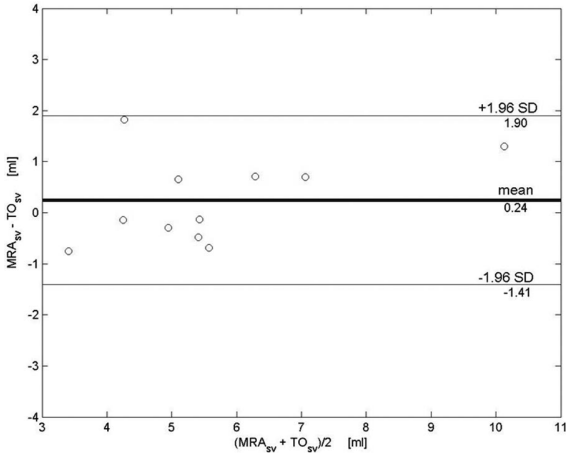

Fig. 9. Bland-Altman plot of stroke volumes measured with MRA and TO showing mean (thick solid line) ± 2SD (thin solid line).

and the dependency on local acceleration because of finite resolution of the velocity estimate [31]–[34]. Because these are general problems for Doppler velocity estimation, it is foreseen to influence the result and add up to the estimated bias for TO compared with MRA.

In the TO method, the V_{nyquist} can be found for both the axial and the transverse velocity component. The axial velocity $V_{z,\text{nyquist}}$ and the transverse velocity $V_{x,\text{nyquist}}$ have previously been estimated to be $V_{z,\text{nyquist}} = 0.46$ m/s and the $V_{x,\text{nyquist}} = 3$ m/s for a setup identical to the setup used in the present study [15]. According to the Nyquist sampling theorem, the axial estimate is therefore more liable to be aliased than the lateral estimate.

The length of the emitted pulse is proportionally related to the axial resolution in the velocity estimate and inversely proportionally related to the variance of the velocity estimate when obtained with the autocorrelation estimator. Hence, if a short pulse is used to improve the axial resolution, the performance of the estimator inevitable will degrade [1]. The setup in the TO method is taken from a commercial system and uses 8 cycles/pulse as a compromise between the 2 parameters; thus, this pulse is identical to the transmitted pulse used in conventional systems.

In MRA, the blood flow is measured in a plane perpendicular to the longitudinal axis of the vessel. Intuitively it would have been a better comparison to choose an end-plane setup aligned with the 2 encoded directions of the corresponding TO measurement to examine each voxel in pairs. Unfortunately, the inadequate in-plane resolution of 6 mm in MRA would confound the blood signal with the vessel surroundings and result in underestimated velocities.

Conversely, when measuring 2-D vector velocity with the TO method there is an unavoidable lack of out-of-plane information. Therefore, a simple model was chosen to minimize the impact of the information gap. The normal common carotid artery is a straight vessel with expected unidirectional flow and parallel-to-skin surface that consequently favors an angle of insonation of 90°. Moreover, the vessel generally has a circular geometry and, thus, an expected symmetric flow profile.

The assumptions necessary for the TO derived stroke volume calculations were investigated for all 11 volunteers. When inspecting the MRA data, there appeared to be a remarkable difference in stroke volume over 180 degrees with a mean of 24.1% (Fig. 8), which underlines that the assumption of circular geometry and rotationally symmetric flow profile is a simplification. By examining the different MRA phase velocity maps, it was evident that the asymmetric flow profile contributed by far the greatest angle-dependent stroke volume difference. In Fig. 10, a phase velocity map of the common carotid artery of one volunteer is shown. The phase velocity map is taken from the late systole and visualizes the marked asymmetry of the flow profile. This is consistent with Brands *et al.,* which reported asymmetry of the flow profile in the common carotid artery of healthy volunteers and especially after the systolic peak [35].

Udesen found that TO systematically underestimated vector velocities in an experimental flowrig [17]. The estimates in this study found below the line of perfect fit in the scatterplot (Fig. 6) could be explained as an effect of the employed assumption, which clearly gives rise to both under- and overestimation of the blood volume flow. For 2 volunteers, the full range did not overlap the line of perfect fit while the estimates were found below the line. It indicates that the simplifying assumption of circular geometry and rotationally symmetric flow profile cannot entirely explain the differences between stroke volumes measured with TO and MRA.

To obtain reliable volume flow measurements by TO, it was crucial to scan the vessel parallel to the longitudinal axis exactly through the middle of the vessel. According to the B-mode image where the diameter of the lumen was greatest and where *intima* most clearly was delineated, it is obvious that vessel *intima* is a reliable marker

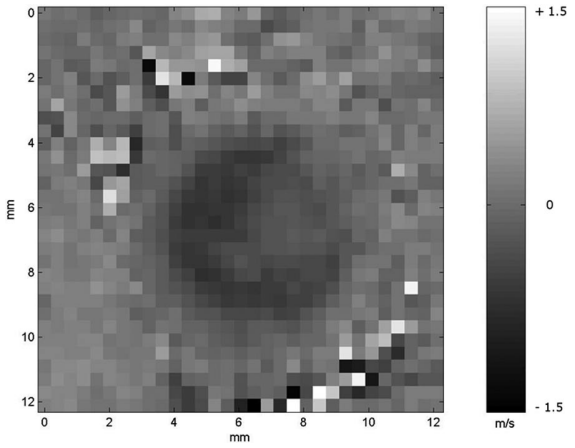

Fig. 10. Phase velocity map of the common carotid artery of one volunteer taken from late systole showing marked asymmetry of the flow profile.

for positioning the scan plane through the middle of the vessel, because the layer structures only clearly are visible when the ultrasound beam direction is perpendicular to the planes of the layers. Vessels are not perfectly straight tubes, so when scanning parallel to axis, inevitably a part of the artery will be out of the scan plane due to curvature, resulting in slightly lower averaged volume flow.

Also it has to be taken into account that the heart rate, cardiac output, and stroke volume alter between 2 consecutive scans. In this study, up to one week occurred between compared with and MRA scans. The stroke volume is a more stable parameter to measure than cardiac output, but still it fluctuates and is to a certain point proportional to heart rate [28].

In this study, MRA was used as the reference. Studies have shown that even this modality is subject to artifacts limiting the accuracy of velocity measurements [36], [37]. It underlines the need for an alternative, reliable, noninvasive modality as well as the problem of achieving a reliable *in vivo* reference.

The LoA of the Bland-Altman plot corresponded to 28% of the TO and 30% of MRA mean values. The LoA depend on variation of differences and, in this study, suffer from measurements on volunteer no. 10, who is considered an outlier. This obviously reduces the significance of the results.

The major limitation of this study is the small number of samples in the study population. This affects the correlation coefficient, LoA, and CI of all the statistical calculations. The examinations with the TO method were performed with the experimental scanner RASMUS [25], [26] and calculated using MATLAB 6.5 on a 100 CPU Linux cluster. The cluster gave the most flexible environment for processing the data from an experimental point of view, but the processing time was considerable. One VVI sequence took 3 s to acquire, 10 h to store, and 48 h to process. Obviously this affected the logistics and reduced the number of samples that realistically could be enrolled into the study population. However, TO is not a heavy method in terms of processing because it is based on an autocorrelation estimator [1], [10]. The number of calculations for each velocity estimate is approximately 3 times higher than for conventional velocity estimation [15]. It should therefore be possible to implement the method into a commercial scanner and convert the method to an actual real-time modality.

V. Conclusion

Volume flow measurements were obtained *in vivo* with the angle-independent blood vector velocity method TO. The results validated against volume flow measurements obtained by MRA were found to be comparable for stroke volume using correlation, regression, and Bland-Altman analyses. With TO, a method has been introduced to obtain quantitative blood flow measurements from the entire frame, to facilitate the examination of simple flow, and to enable correct visualization of complex flow.

This study gives reason to believe that the TO method can be a useful alternative to conventional Doppler systems bringing forth new and relevant information to the US examination of the blood flow. However, it remains to evaluate TO on a larger population using different transducers on different vessels, at different depths, and with variable angles of insonation.

Further studies of the TO method are needed to conclude the usability of the method in clinical practice examining diseased vessels where flow patterns are likely to be multidirectional, the vessel geometry irregular, and the blood flow asymmetric.

References

[1] J. A. Jensen, *Estimation of Blood Velocities Using Ultrasound: A Signal Processing Approach*. New York: Cambridge University Press, 1996.

[2] D. Birchall, A. Zaman, J. Hacker, G. Davies, and D. Mendelow, "Analysis of haemodynamic disturbance in the atherosclerotic carotid artery using computational fluid dynamics," *Eur. Radiol.*, vol. 16, no. 5, pp. 1074–1083, May 2006.

[3] C. Cheng, D. Tempel, R. van Harperen, A. van der Baan, F. Grosveld, M. Daermen, R. Krams, and R. de Crom, "Atherosclerotic lesion size and vulnerability are determined by patterns of fluid shear stress," *Circulation*, vol. 113, no. 23, pp. 2744–2753, Jun. 2006.

[4] Y. Richter and E. R. Edelman, "Cardiology is flow," *Circulation*, vol. 113, no. 23, pp. 2679–2682, 2006.

[5] G. E. Trahey, J. W. Allison, and O. T. Ramm, "Angle independent ultrasonic detection of blood flow," *IEEE Trans. Biomed. Eng.*, vol. 34, pp. 965–967, Dec. 1987.

[6] J. A. Jensen, "Directional velocity estimation using focusing along the flow direction: I: Theory and simulation," *IEEE Trans. Ultrason. Ferroelectr. Freq. Control*, vol. 50, no. 7, pp. 857–872, Jul. 2003.

[7] M. D. Fox, "Multiple crossed-beam ultrasound Doppler velocimetry," *IEEE Trans. Sonics Ultrason.*, vol. 25, no. 5, pp. 281–286, 1978.

[8] V. L. Newhouse, D. Censor, T. Vontz, J. A. Cisneros, and B. B. Goldberg, "Ultrasound Doppler probing of flows transverse with respect to beam axis," *IEEE Trans. Biomed. Eng.*, vol. 34, no. 10, pp. 779–788, Oct. 1987.

[9] O. Bonnefous, "Measurement of the complete (3D) velocity vector of blood flows," in *Proc. IEEE Ultrasonics Symp.*, 1988, pp. 795–799.

[10] J. A. Jensen and P. Munk, "A new method for estimation of velocity vectors," *IEEE Trans. Ultrason. Ferroelectr. Freq. Control*, vol. 45, no. 3, pp. 837–851, May 1998.

[11] J. A. Jensen, "A new estimator for vector velocity estimation," *IEEE Trans. Ultrason. Ferroelectr. Freq. Control*, vol. 48, no. 4, pp. 886–894, Jul. 2001.
[12] P. Munk, "Estimation of the 2-D flow vector in ultrasonic imaging: A new approach," M.S. thesis, Tech. Univ. Denmark, Copenhagen, 1996.
[13] M. E. Anderson, "Spatial quadrature: A novel technique for multidimensional velocity estimation," in *Proc. IEEE Ultrasonics Symp.*, 1997, pp. 1233–1238.
[14] M. E. Anderson, "A heterodyning demodulation technique for spatial quadrature," in *Proc. SPIE Medical Imaging*, 2000, vol. 2, pp. 1487–1490.
[15] J. Udesen, M. B. Nielsen, K. R. Nielsen, and J. A. Jensen, "Examples of *in vivo* blood vector velocity estimation," *Ultrasound Med. Biol.*, vol. 33, no. 4, pp. 541–548, Apr. 2007.
[16] J. Udesen and J. A. Jensen, "Experimantal investigation of transverse flow estimation using transverse oscillation," in *Proc. IEEE Ultrasonics Symp.*, 2003, pp. 1586–1589.
[17] J. Udesen and J. A. Jensen, "Investigation of transverse oscillation method," *IEEE Trans. Ultrason. Ferroelectr. Freq. Control*, vol. 53, no. 5, pp. 959–971, May 2006.
[18] J. Udesen and J. A. Jensen, "An *in vivo* investigation of transverse flow estimation," in *Proc. SPIE—Progress in biomedical optics and imaging*, 2004, vol. 5373, pp. 307–314.
[19] R. J. van der Geest, R. A. Niezen, E. E. van der Wall, A. de Roos, and J. H. Rieber, "Automated measurement of volume flow in the ascending aorta using MR velocity maps: Evaluation of inter- and intraobserver variability in healthy volunteers," *J. Comput. Assist. Tomogr.*, vol. 22, no. 6, pp. 904–911, Nov.–Dec. 1998.
[20] A. Spilt, F. M. Box, R. J. van der Geest, J. H. Reiber, P. Kunz, A. M. Kamper, G. J. Blauw, and M. A. van Buchem, "Reproducibility of total cerebral blood flow measurements using phase contrast magnetic resonance imaging," *J. Magn. Reson. Imaging*, vol. 16, no. 1, pp. 1–5, Jul. 2002.
[21] S. O. Oktar, C. Yucel, D. Karaosmanoglu, K. Akkan, H. Ozdemir, N. Tokgoz, and T. Tali, "Blood-flow volume quantification in internal carotid and vertebral arteries: Comparison of 3 different ultrasound techniques with phase-contrast MR imaging," *AJNR Am. J. Neuroradiol.*, vol. 27, no. 2, pp. 363–369, 2006.
[22] S. S. Ho, Y. L. Chan, and D. K. Yeung, "Blood flow volume quantification of cerebral ischemia: Comparison of three noninvasive imaging techniques of carotid and vertebral arteries," *AJR Am. J. Roentgenol.*, vol. 178, no. 3, pp. 551–556, Mar. 2002.
[23] C. J. Bakker, M. Kouwenhoven, and M. J. Hartkamp, "Accuracy and precision of time-averaged flow as measured by non-triggered 2D phase-contrast MR angiography, a phantom evaluation," *Magn. Reson. Imaging*, vol. 13, no. 7, pp. 959–965, 1995.
[24] C. Kasai, K. Namekawa, A. Koyano, and R. Omoto, "Real-time two-dimensional blood flow imaging using an autocorrelation technique," *IEEE Trans. Sonics Ultrason.*, vol. 32, no. 3, pp. 458–463, 1985.
[25] J. A. Jensen, O. Holm, L. J. Jensen, H. Bendsen, H. M. Pedersen, K. Salomonsen, J. Hansen, and S. Nikolov, "Experimental ultrasound system for real-time synthetic imaging," in *Proc. IEEE Ultrasonics Symp.*, 1999, pp. 1595–1599.
[26] J. A. Jensen, O. Holm, L. J. Jensen, H. Bendsen, S. Nikolov, B. G. Tomov, P. Munk, M. Hansen, K. Salomonsen, J. Hansen, K. Gormsen, H. M. Pedersen, and K. L. Gammelmark, "Ultrasound research scanner for realtime synthetic aperture image acquisition," *IEEE Trans. Ultrason. Ferroelectr. Freq. Control*, vol. 52, no. 5, pp. 881–891, May 2005.
[27] T. L. Chenevert, K. P. Fechner, and D. Y. Gelblum, "Improvements in MR angiography using phase-corrected data sets," *Magn. Reson. Med.*, vol. 10, no. 1, pp. 38–49, Apr. 1989.
[28] M. B. Higginbotham, K. G. Morris, S. Williams, P. A. McHale, R. E. Coleman, and F. R. Cobb, "Regulation of stroke volume during submaximal and maximal upright exercise in normal man," *Circ. Res.*, vol. 58, no. 2, pp. 281–291, Feb. 1986.
[29] J. M. Bland and D. G. Altman, "Statistical methods for assessing agreement between two methods of clinical measurement," *Lancet*, vol. 1, no. 8476, pp. 307–310, Feb. 1986.
[30] B. H. Friemel, L. N. Bohs, K. R. Nightingale, and G. E. Trahey, "Wall filtering challenges in two-dimensional vector velocity estimation," in *Proc. IEEE Ultrasonics Symp.*, 1993, vol. 2, pp. 1031–1034.
[31] P. M. Vandervoort, D. S. Aghassi, and J. D. Thomas, "Impact of wall filtration on the accuracy of quantitative CD velocity measurements: Numerical and in vitro study," *Adv. Bioeng.*, vol. 22, pp. 367–370, 1992.
[32] P. M. Vandervoort, D. H. Thoreau, J. M. Rivera, R. A. Levine, A. E. Weyman, and J. D. Thomas, "Automated flow rate calculations based on digital analysis of flow convergence proximal to regurgitant orifices," *J. Am. Coll. Cardiol.*, vol. 22, no. 2, pp. 535–541, Aug. 1993.
[33] G. J. Perry, A. S. Anayiotos, D. W. Green, J. G. Myers, P. H. Fan, and N. C. Nanda, "Accuracy of color Doppler velocity in the flow field proximal to a regurgitant orifice: Implications for color Doppler quantitation of valvular incompetence," *Ultrasound Med. Biol.*, vol. 22, no. 5, pp. 605–621, 1996.
[34] J. G. Myers, J. F. Fox, A. M. Elmahdi, G. J. Perry, and A. S. Anayiotos, "Evaluation of the proximal flow field to circular and noncircular orifices of different aspect ratios," *J. Biomech. Eng.*, vol. 119, no. 3, pp. 349–356, Aug. 1997.
[35] P. J. Brands, A. P. Hoeks, L. Hofstra, and R. S. Reneman, "A noninvasive method to estimate wall shear rate using ultrasound," *Ultrasound Med. Biol.*, vol. 21, no. 2, pp. 171–185, 1995.
[36] I. Marshall, P. Papathanasopoulou, and K. Wartolowska, "Carotid flow rates and flow division at the bifurcation in healthy volunteers," *Physiol. Meas.*, vol. 25, no. 3, pp. 691–697, Jun. 2004.
[37] K. L. Lee, D. J. Doorly, and D. N. Firmin, "Numerical simulations of phase contrast velocity mapping of complex flows in an anatomically realistic bypass graft geometry," *Med. Phys.*, vol. 33, no. 7, pp. 2621–2631, Jul. 2006.

Kristoffer Lindskov Hansen was born in Copenhagen, Denmark, in 1974. He earned his M.D. degree in 2003 from Copenhagen University, and he is currently with the Department of Radiology at the University Hospital of Denmark, working on his Ph.D. thesis, "Validation of new ultrasound techniques." The focus of his work is mainly in the field of blood flow estimation.

Jesper Udesen was born in 1971 and earned his M.S. degree in mathematics and physics from Roskilde University Center, Denmark, in 2002. He received his Ph.D. degree in 2006 from the Technical University of Denmark for work on blood vector velocity estimation. From 2006 to 2007 he was employed as a postdoctoral researcher at the University Hospital of Copenhagen. Since 2007, he has been employed at the Technical University of Denmark as an assistant professor. His research interests include blood vector velocity estimation and beamforming techniques.

Carsten Thomsen was born in Copenhagen Denmark, in 1955. He earned his M.D. degree in 1981 from Copenhagen University and his Ph.D. degree in 1996 from the University of Copenhagen, Marts, with the thesis "Quantitative magnetic resonance methods for *in vivo* investigation of the human liver and spleen. Technical aspects and preliminary clinical results." He has been the chief consultant and head of neuroradiology since 1995 and full professor in radiology at Rigshospitalet Copenhagen University since 1997. His current research activities include work on quantitative magnetic resonance imaging and spectroscopy of the brain.

Jørgen Arendt Jensen earned his M.S. degree in electrical engineering in 1985 and the Ph.D. degree in 1989, both from the Technical University of Denmark. He received the Dr.Techn. degree from the same university in 1996.

He has published more than 160 journal and conference papers on signal processing and medical ultrasound and the book *Estimation of Blood Velocities Using Ultrasound* with Cambridge University Press in 1996. He is also developer of the Field II simulation program. He has been a visiting scientist at Duke University, Stanford University, and the University of Illinois at Urbana-Champaign. He is currently full professor of biomedical signal processing at the Technical University of Denmark, Department of Electrical Engineering and head of the Center for Fast Ultrasound Imaging. He is also adjunct full professor at the Faculty of Health Sciences at the University of Copenhagen. He has given courses on blood velocity estimation at both Duke University and the University of Illinois and teaches biomedical signal processing and medical imaging at the Technical University of Denmark. He has given several short courses on simulation, synthetic aperture imaging, and flow estimation at international scientific conferences.

He has received several awards for his research. He is also the co-organizer of the biomedical engineering education offered by the Technical University of Denmark and the University of Copenhagen. His research is centered on simulation of ultrasound imaging, synthetic aperture imaging, and vector blood velocity estimation and constructing systems for ultrasound imaging.

Michael B. Nielsen was born in Copenhagen in 1959. He received his M.D. degree from Copenhagen University in 1985. He served a consultancy with the Department of Radiology of Rigshospitalet in 1998 and earned a full professorship in 2008. He is chair of the imaging research group at the Department of Radiology, Rigshospitalet (National Danish University hospital) and editor of *Ultraschall in der Medicine/European Journal of Ultrasound*. He serves as chairman of the European Federation of Societies for Ultrasound in Medicine and Biology (EFSUMB) publication committee.

Appendix II

In-vivo comparison of three ultrasound vector velocity techniques to MR phase contrast angiography

Hansen KL(1), Udesen J(2), Oddershede N(2), Henze L(3), Thomsen C(1), Jensen JA(3), Nielsen MB(1)

(1) Department of Radiology, Section of Ultrasound, Rigshospitalet. Blegdamsvej 9, DK-2100 Kbh. Ø, Denmark.
(2) GN Resound, Lautrupsbjerg 9, DK-2750 Ballerup, Denmark
(3) Center for Fast Ultrasound Imaging, DTU Elektro, Bldg. 349, Technical University of Denmark, DK-2800 Lyngby, Denmark

Abstract: The objective of this paper is to validate angle in-dependent vector velocity methods for blood velocity estimation. Conventional Doppler ultrasound (US) only estimates the blood velocity along the US beam direction where the estimate is angle corrected assuming laminar flow parallel to vessel boundaries. This results in incorrect blood velocity estimates, when angle of insonation approaches 90 º or when blood flow is non-laminar. Three angle independent vector velocity methods are evaluated in this paper: directional beamforming (DB), synthetic aperture flow imaging (STA) and transverse oscillation (TO). The performances of the three methods were investigated by measuring the stroke volume in the right common carotid artery of eleven healthy volunteers with magnetic resonance phase contrast angiography (MRA) as reference. The correlation with confidence intervals (CI) between the three vector velocity methods and MRA were: DB vs. MRA: R=0.84 (p<0.01, 95% CI: 0.49 to 0.96); STA vs. MRA: R=0.71 (p<0.05, 95% CI: 0.19 to 0.92) and TO vs. MRA: R=0.91 (p<0.01, 95% CI: 0.69 to 0.98). No significant differences were observed for any of the three comparisons (DB vs. MRA: p=0.65; STA vs. MRA: p=0.24; TO vs. MRA: p=0.36). Bland-Altman plots were additionally constructed, and mean differences with limits of agreements (LoA) for the three comparisons were: DB vs. MRA = 0.17 ml (95% CI: -0.61 to 0.95) with LoA = -2.11 ml to 2.44 ml; STA vs. MRA =-0.55 ml (95% CI: -1.54 to 0.43) with LoA = -3.42 ml to 2.32 ml; TO vs. MRA = 0.24 ml (95% CI: -0.32 to 0.81) with LoA = -1.41 ml to 1.90 ml. According to the results, reliable volume flow estimates can be obtained with all three methods. The three US vector velocity techniques can yield quantitative insight into flow dynamics and visualize complex flow patterns, which potentially can give the clinician a novel tool for cardiovascular disease assessment.

INTRODUCTION

Non-invasive techniques for flow measurement in blood vessels are limited to three different modalities: plethysmography, magnetic resonance phase contrast angiography (MRA), and Doppler ultrasound (US). While plethysmography can be used for investigating limb blood flow, yielding a global blood arterial inflow for the investigated limb [1], the selective evaluation of small vessels, sections of vessels, blood flow in the major vessels and cerebral blood flow are only feasible non-invasively with MRA and Doppler techniques [2]. The assessment of blood flow with MRA is time-consuming, the equipment is expensive and non-mobile, and the evaluation is not performed in real time. Conversely, Doppler US, which is the clinical method of choice for real time assessment of blood velocities, is an easily manageable and fast technique, and the equipment is mobile and relatively inexpensive.

However, one of the main limitations of the current Doppler systems is angle dependency. The velocity estimate in conventional Doppler is only found along the US beam direction i.e. in the axial direction [3]. In color flow mapping (CFM) no angle correction is performed and thus, no correct velocities are given. Consequently, CFM is only used as a qualitative method for visualizing flow. In spectral Doppler examination angle correction is applied on blood velocities estimated within the range gate. The spectral Doppler method is used quantitatively as actual velocities of the blood scatterers are displayed after angle correction. However, the correction scheme only provides satisfactory results when laminar flow parallel to the vessel is present. Human vessels are branching, curving and highly elastic, and complex flow profiles are created though out the cardiovascular system. Thus, it is in general difficult to predict the direction of a blood scatterer based on the B-mode image [4,5] albeit this is exactly what the operator does when angle correcting. Incorrect blood velocities are therefore often given with the conventional Doppler methods, and information on the complexity of the blood flow is kept unrevealed. This information is important as especially the regions of complex geometries with turbulence and vortices have predilection for atherosclerotic lesions [6-8]. The limitation has been reflected in several papers concerning the validity of Doppler US estimations, where velocity estimates using commercial systems have been reported to be in error by 10 to 100 percent [9,10]. Further, it has been shown that the flow angle in the cardiovascular system changes as a function of space and time [11]. At bifurcation, branching, valves or any kind of constriction the pulsative nature of human blood flow will give rise to disturbed or even turbulent flow, where flow direction changes within the heart cycle and as a function of spatial location. Correcting for the angle would, thus, entail finding the direction in any location for any images, which is practically impossible to perform manually.

Several authors have tried to bypass the angle dependency in conventional Doppler systems. Fox applied two beams [12], Trahey et al. used speckle tracking [13], Newhouse et al. used the total bandwidth of the received signal [14] and Bonnefous worked with several beamformers in parallel [15]. However, these techniques have neither been evaluated in clinical trials nor have they made it into commercial US systems.

Three different vector velocity estimators have been designed to address the problems of Doppler angle dependency and are evaluated in this paper: directional beamforming (DB) proposed by Jensen and Bjerngaard [16,17], synthetic transmit aperture flow imaging (STA) proposed by Jensen and Nikolov [18] and transverse oscillation (TO) proposed by Jensen and Munk [19]. Anderson introduced an approach similar to TO called Spatial Quadrature [20].

The purpose of this paper is to determine the accuracy of these new vector velocity techniques and to determine whether they can yield quantitative velocity magnitudes for *in-vivo* scans. To validate the vector methods *in-vivo* under conditions where a reliable and independent reference can be assessed, the vessel of interest was chosen to be the common carotid artery of healthy individuals, because this vessel generally has a circular geometry with an expected uniform, unidirectional flow [21,22] and moreover has a superficial location, which means that it can readily be evaluated by ultrasound. The study was performed with a straight vessel without branching as no valid references are available in measuring complex flow patterns. However, the true strength of the vector velocity techniques is expected to be in the visualization of the non-laminar nature of blood flow.

The three vector velocity methods were validated *in-vivo* with MRA comparing volume flow in the right common carotid artery. MRA was chosen to be the reference as it is considered the gold standard for non-invasive cerebral blood flow measurement [23], and because conventional US Doppler is rather imprecise under *in-vivo* settings [9,10,24,25]. However, it should be noted that conventional US Doppler under controlled *in-vitro* settings with string phantoms has shown an improved performance with estimation errors below 2.2% [26].

The three vector velocity methods are implemented on an US system which is not MR compatible. Therefore the scans were performed at four different examinations. Blood motion measured with US and MRA at different examinations can be compared with respect to either blood velocities or volume flow. When comparing blood velocities, difficulties arise (i) due to mismatch in alignment of the scan planes in the rotational and longitudinal direction and (ii) due to mismatch in the point-to-point comparison of the estimates, as the velocity profile fluctuates over time. When comparing volume flow obtained by the two modalities, the mentioned difficulties are less prominent because of averaging but on the expense of spatial and temporal details.

Along with validation of the vector velocity methods, the assumptions of circular geometry of the examined vessel and rotationally symmetric blood flow necessary for volume flow calculation were tested.

MATERIALS AND METHODS

This prospective study was performed after approval by The Danish National Committee on Biomedical Research Ethics. Eleven healthy volunteers (seven males and four females, mean age: 32 years, range: 24 – 44 years) entered the study after informed consent. The right common carotid artery was examined in all volunteers using US and MRA. The four examinations were carried out on four different days due to storage and processing limitations as each ultrasound sequence took 3 sec. to acquire, 10 hours to store and up to 48 hours to process. The volunteer rested supine on the examination table for 15 minutes before all examinations. All scans were carried out by a medical doctor (KLH).

The conventional US Doppler method along with the three different vector velocity methods are presented in this section. The three vector velocity methods are all characterized by the ability to estimate the instantaneous 2-D velocity of the blood scatterers in every point at every time in order to obtain quantitative velocity data.

Conventional Doppler US

Conventional Doppler US estimates real-time velocities of blood scatterers *in-vivo*, using an autocorrelation estimator for CFM [27] and the Welch's method for spectral Doppler estimation [28]. The estimated velocities are projections onto the beam direction. An emitted focused pulse is reflected by blood scatterers, and the echoes are received by the transducer and focused along the image line by the scanner. Identical echo lines are created from consecutive pulses and the axial movement of the blood scatterer is determined by the phase shift of the received signal. Knowing the phase shift and the time between consecutive received lines yields the axial velocity estimate, which is presented by the scanner as a color map in CFM and as a spectrogram in spectral Doppler [3].

Directional beamforming

A focused pulse is emitted with the focal point placed below the depth of interest. Hence, the acoustic energy around the scatterer is sufficient for beamforming echo lines in a star-shaped pattern with the scatterer as the centre. Lines are compared through a normalized cross-correlation across matching angles for consecutive pulses [16,17]. The highest normalized cross-correlation is ideally found for the correct angle. When the correct angle is known, the magnitude of the motion along the correct echo line is found by cross-correlation for consecutive pulses.

Synthetic transmit aperture flow imaging

A STA image is acquired by emitting a spherical unfocused wave from a few elements and receiving the scattered signal with all elements. Since the position for the emission is known, the

precise origin of the received scattered signal can be calculated from time-of-flight for all elements and used in focusing. The STA approach generates one low-resolution image for every emitted pulse. A high-resolution image is constructed by adding a number of consecutive low-resolution images. For every emission, a high-resolution image can be created by applying a recursive approach, where the oldest transmission event is replaced by the newest. The STA method can therefore yield a frame rate equal to pulse repetition frequency with dynamic transmit and receive foci in all image points.

An approach to estimate vector velocities, identical to DB is computed. Echo lines in a star-shaped pattern are created to every point of interest and compared between emission-identical high-resolution images for every angle. The normalized cross-correlation peaks for the right angle. The magnitude is found through cross-correlation across echo-lines of the right angle [29,30].

Transverse oscillation

The TO method tracks scatterer motion along two orthogonal axes by emitting a pulse identical to conventional Doppler. The motion in the axial direction is found exactly as in conventional Doppler US. An oscillation in the transverse direction is created by changing the sensitivity of the receiving elements and the transverse velocity component is found from the frequency content of this oscillation [31]. By combining the velocity components along the two axes, vector velocities are achieved.

US setup

The vector velocity images obtained with the three US methods were recorded with the experimental scanner RASMUS [32]. The parameters for the three setups are delineated in Table 1. In Fig. 1 three frames, one from each method, are depicted. The examples are taken from three different carotid arteries and to three different moments in the heart cycle.

	DB	**STA**	**TO**
Transducer (linear array)	BK 8812	BK 8812	BK 8812
Center frequency	6.2 MHz	6.2 MHz	5 MHz
Cycles/pulse	2 cycles/pulse	2 cycles/pulse	8 cycles/pulse
Fprf	6 kHz	21 kHz (or 21kHz / 9 between xcorr)	6 kHz
Sampling frequency	40 MHz	40 MHz	40 MHz
Lateral wave length	NA	NA	1.0 mm
Apodization in transmit	Hanning	Tukey	Hanning
Apodization in receive	Rectangular	Rectangular	Two Hannings
Focus in transmit	36 mm	None	18 mm
Focus in receive	Dynamic	Dynamic	Dynamic
F-number in transmit	2.7	-0,75	3.3
F-number in receive	NA	NA	0.8
Firings/velocity estimate	32/64 firings/vel.est.	y(n) = (1-a)*x(n) + a*y(n-1), a = 0.98	64 firings/vel.est.

Table 1: Scanner and transducer setup

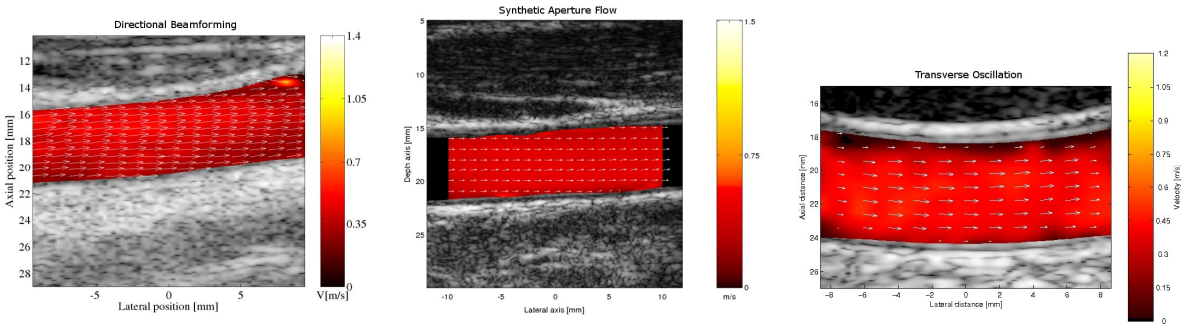

Figure 1: The frames obtained with the three methods are recorded on different volunteers and to different time. The vector arrows, superimposed onto color flow maps, delineate magnitude and direction of the moving blood scatterers.

The estimates obtained with the TO method were obtained with only one clutter filter applied. In DB an adaptive filter was used consisting of two different filters for all volunteers, one for systolic flow and one diastolic flow. It was employed by manually setting a threshold value for each volunteer defining the systole and diastole. Estimates obtained with STA were obtained with both a single clutter filter approach and an adaptive clutter filter approach. In the adaptive filter approach two different clutter filters were designed, one optimized to flow data obtained from moving arteries and another optimized to flow data from non-moving arteries. The chosen filters were employed after visually inspecting the B-mode sequences. The post processing was done offline with MATLAB (Mathworks, Natick, MA, USA) on a 100 CPU Linux cluster.

All US sequences were recorded from the right common carotid artery two cm from the bifurcation to prevent confounding disturbed flow. An identical approach was used for the three methods to calculate the volume flow from the recorded flow data. The sequences were processed by an algorithm that automatically identified the vessel boundaries in each frame from the B-mode images [11] so the change in diameter from systole to diastole which is up to 10% in normal conditions [33] was taken into the calculations. By knowing the vessel geometry in every frame the vector velocity profiles could be calculated from the vector velocity images by setting the surroundings to zero and integrating the 2-D vessel up to form a 3-D vessel. This was only possible by assuming (i) circular vessel geometry, (ii) rotationally symmetric blood flow and (iii) a correctly placed window of insonation parallel to the longitudinal axis of the vessel, going exactly through the middle of the vessel. The volume flow to every frame was found by averaging over the whole image, thus, yielding a volume flow profile to every sequence. Details about the calculations are described by Hansen et al. [34].

MR setup

MRA examinations were performed with a 1.5 T whole body scanner (Magnetom Vision, Siemens AG). A prospective ECG triggered phase contrast sequence using a cervical coil was employed. (Phase interval: 29 ms, echo time: 7 ms, flip angle: 30°, FOV: 100 mm, slice thickness: 6 mm, VENC: +/-1.5 m/s, pixel resolution: 0.52 x 0.39 mm^2 in a matrix of 192 x 256 pixels interpolated up to 256 x 256 pixels).

The scan plane for the volume flow measurements was selected to be perpendicular to the right common carotid artery and placed two cm from the bifurcation as in the US examinations. Through-plane setup was chosen instead of end-plane setup. Firstly, to alleviate the problems of scan plane alignment and fluctuations of the velocity profile between heart beats. Secondly as a consequence of the slice thickness in MRA measurements considering that the common carotid artery normally has a diameter of approx. 1 cm.

The MR volume flow estimations were carried out in MATLAB 6.5 (Mathworks, Natick, MA, USA) using MR DICOM images. For each velocity map an anatomic image was calculated. A threshold pixel value defined the ROI on the anatomic images in order to discriminate between the pixel values of blood and vessel boundaries. For each examination the value was set manually by the operator so the delineation of the vessel boundaries visually appeared as smooth as possible with the ROI as large as possible. The ROI encompassing the lumen of the vessel was used as a window on the phase velocity maps to ensure that velocity values from the vessel surroundings representing e.g. vena jugularis were ignored in the volume flow measurement. A region near the common carotid artery was selected to correct the phase off-set [35]. The volume flow to each frame was found by multiplying the velocity with the area it occupied i.e. the pixel area and then adding up all the pixel derived volume flows encompassing the ROI. The volume flow profile was given by the estimated volume flows of the full sequence of frames.

The four different methods to estimate volume flow were performed for every volunteer within 3 weeks. To circumvent the inevitable fluctuations in heart rate over this period the comparisons were done with respect to stroke volume, which is shown to be a more stable parameter [36].

Test of assumptions

The consequence of using the assumptions in US derived volume flow calculations has been investigated in this paper. Stroke volumes were calculated from MRA velocity data as if they were obtained in the longitudinal plane. A line of the phase velocity map going through the centre of the carotid artery was taken out and integrated up to form a cross section of a whole vessel. Hereby, a volume flow estimated solely form this line could be found. For the same angle in consecutive velocity maps the calculations were repeated and summed up to a stroke volume. Stroke volumes for all angles were found in order to derive a stroke volume range for every volunteer, and the range was compared to the stroke volume estimate found by the ROI approach described above where all pixels covering the vessel lumen were used. Details about the calculations used for the stroke volume estimation and the MR derived stroke volume range are previously described by Hansen et al. [34].

Statistics

A descriptive statistical analysis was computed on the stroke volume data of the four modalities finding mean value, standard deviation, and stroke volume range. The stroke volume data obtained with STA, DB, and TO were each compared to stroke volume data obtained with MRA by using linear regression analysis with two-tailed significance value given and $p<0.05$ considered significant. The correlation coefficients, regression equations, and confidence intervals (CI) using Fisher's r-to-z-transformation were calculated for each comparison. Paired two-tailed t-test was performed on each comparison. Finally Bland-Altman plots along with confidence intervals were computed to illustrate the differences of estimated stroke volumes between each of the three US modalities and MRA [37].

RESULTS

The stroke volume in the right common carotid artery was measured for the 11 volunteers with the three US methods and MRA. The results are displayed in Table 2 along with mean, standard deviation, and range for each modality.

Volunteer no.	DB [ml/heartbeat]	STA [ml/heartbeat]	TO [ml/heartbeat]	MRA [ml/heartbeat]
Volunteer 1	4.81	5.58	3.78	3.03
Volunteer 2	5.02	7.45	5.65	5.17
Volunteer 3	6.48	6.95	5.93	6.64
Volunteer 4	9.31	6.74	6.71	7.41
Volunteer 5	6.00	5.83	4.78	5.43
Volunteer 6	9.52	9.70	9.48	10.78
Volunteer 7	3.92	4.16	4.32	4.18
Volunteer 8	3.66	4.24	5.09	4.80
Volunteer 9	4.08	8.50	5.92	5.23
Volunteer 10	3.72	5.25	3.36	5.18
Volunteer 11	4.85	4.89	5.49	5.36
mean SV +/- SD	5.58 +/- 2.10	6.30 +/- 1.76	5.30 +/- 1.65	5.75 +/- 2.02
SV range	3.72 - 9.53	4.16 - 9.70	3.78 - 9.48	3.03 - 10.78

Table 2: Stroke volume (SV) measurements for all volunteers, mean SV +/- one standard deviation (SD) and SV range obtained with DB, STA, TO and MRA.

In Fig. 2 the scatter plots are given, showing the correlation between the each of the three US techniques and MRA, with DB vs. MRA: R=0.84 (p<0.01, 95% CI: 0.49 to 0.96); STA vs. MRA: R=0.71 (p<0.05, 95% CI: 0.19 to 0.92) and TO vs. MRA: R=0.91 (p<0.01, 95% CI: 0.69 to 0.98). No significant differences were observed for any of the three comparisons (DB vs. MRA: p=0.65; STA vs. MRA: p=0.24; TO vs. MRA: p=0.36). The MR derived stroke volume range assuming rotationally symmetric flow and circular vessel geometry is shown as a bar for every volunteer in the three scatter plots.

In Fig. 3, the angle dependent stroke volume for one volunteer (no.7) is depicted with a volume flow range of 3.2 ml to 5.1 ml and in Fig. 4, the full range of angle dependent stroke volume as percentage of the ROI derived actual MRA stroke volumes is plotted for all volunteers giving a mean ratio of 24.3%. One volunteer (no.7) presented a ratio between angle dependent MRA stroke volume and actual MRA stroke volume of 45.3%.

The resultant Bland-Altman plots are shown in Fig. 5. The mean difference, with confidence intervals and limits of agreement is for all plots given in Table 3. The CI for the mean differences overlapped zero for all three methods and was narrowest for TO and broadest for STA (TO: 1.13 ml; DB: 1.56 ml; STA: 1.97 ml). This also applied to the limits of agreement (TO: 3.31 ml; DB: 4.55 ml; STA: 5.74 ml). In terms of mean differences in the Bland-Altman plots, DB was the most precise method followed by TO and STA (DB: 0.17 ml; TO: 0.24 ml; STA: -0.55 ml).

The STA measurement deviated from the MRA measurement for three volunteers (no.1, no.2, no. 9). This is shown in Table 2 and illustrated in Fig. 2 and 5. The three outliers all displayed a non-moving artery during data acquisition and as the filter used in STA was optimized to vessel movement, this resulted in an overestimation. When applying another filter optimized to a reduced vessel movement, an improved overall result appeared for the STA method when compared to MRA with R value of 0.95, mean difference of 0.07 ml, CI of the mean difference of 0.95 ml and limits of agreement of 2.78 ml. This is illustrated in Fig. 6.

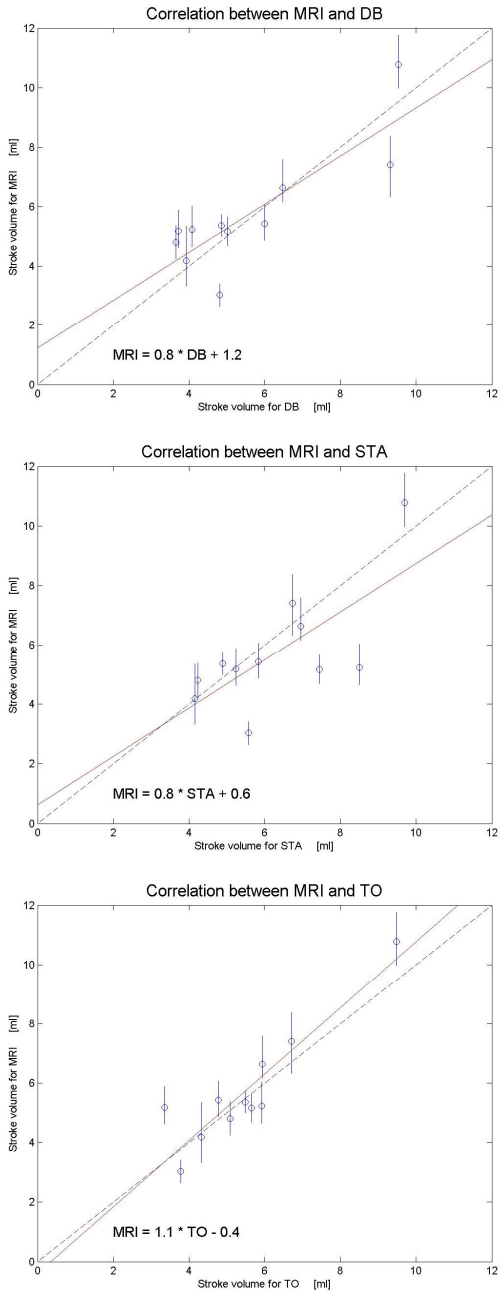

Figure 2: Graph showing the correlation between MRA and the three vector methods. Line of best fit (solid line) and line of perfect fit (dashed line) are drawn for each scatter plot. The MR derived stroke volume range when assuming circular geometry and rotationally symmetric flow is for every volunteer shown as a bar.

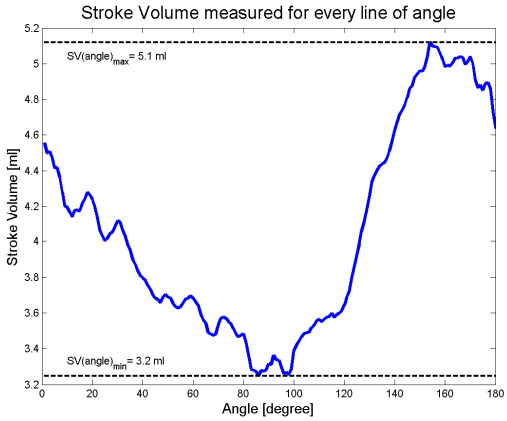

Figure 3: Graph showing the calculated stroke volume for every line of angle for MRA data of one volunteer when assuming circular vessel geometry and rotationally symmetric blood flow. The maximum ($SV(angle)_{max}$) and minimum ($SV(angle)_{min}$) stroke volumes are marked by dashed lines.

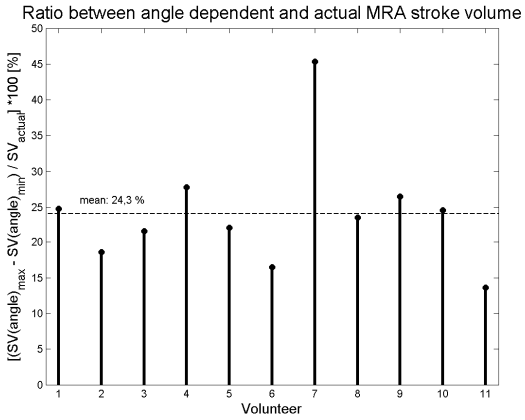

Figure 4: Graph showing the ratio between angle dependent and actual MRA stroke volume. The mean ratio for the whole population is shown as a dashed line.

Method	Mean [ml] (95% CI)	Lower limit [ml]	Upper limit [ml]
DB vs. MRA	0.17 (-0.61 to 0.95)	-2.11	2.44
STA vs. MRA	-0.55 (-1.54 to 0.43)	-3.42	2.32
TO vs. MRA	0.24 (-0.32 to 0.81)	-1.41	1.90

Table 3: Mean of differences with confidence intervals (CI), lower and upper limits of agreement for Bland-Altman plots.

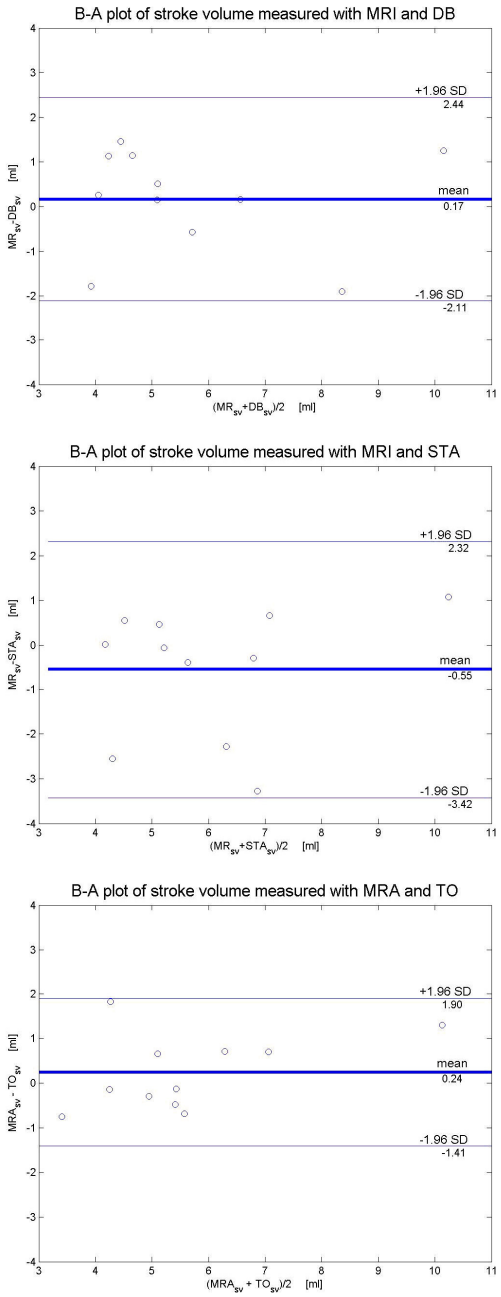

Figure 5: Bland-Altman plot of stroke volumes comparing MRA with each of the three vector velocity methods showing for each plot mean +/- 2 SD as thick solid and thin solid lines, respectively.

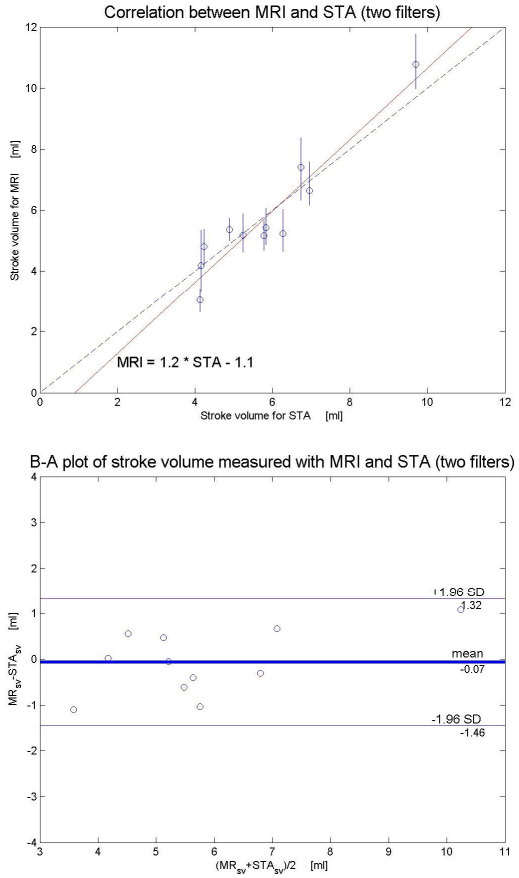

Figure 6: When applying a second filter for the three outliers a correlation plot is given for which R=0.95 (p<0.01; 95% CI: 0.82 to 0.99) and a Bland-Altman plot with a mean difference of -0.07 ml (95% CI: -0.54 ml to 0.41 ml) and limits of agreement from -1.46 to 1.32 ml.

DISCUSSION

The correlations of variables DB, STA and TO compared to MRA, when determining the stroke volume in the right common carotid artery of 11 healthy volunteers, were all significant and correlated well. According to the scatter plots (Fig. 2) and the Bland-Altman plots (Fig. 5), the velocities were underestimated with the TO and DB method while overestimated with the STA method compared to MRA, and the TO method performed best among the three vector velocity methods. But when examining the CI for the *R*-values and CI for the mean differences it is clear that the differences in performance between the three methods are not significant. This is due to the sample size of 11 volunteers.

The considerable storage and processing time used for each US methods had two consequences for the study design. Firstly, it affected the logistics and reduced the number of samples that realistically could be enrolled into the study population. Secondly, different days were used for examinations on the same volunteer. In the ideal situation, compared results from examinations on the same volunteer with different methods should be accomplished simultaneously and moreover, enough volunteers should be enrolled to avoid ambiguous results according to CI and LoA. The vector velocity US methods realized with the experimental scanner RASMUS dictated an unfavorable study design where the four measurements on each of the ten volunteers were accomplished within three weeks. Although the volunteers rested 15 min before each measurement,

the flow dynamics were expected to fluctuate. This increased the variability of the results as heart rate, cardiac output, and stroke volume altered between the scans in comparison.

DB has previously been evaluated in Field II simulations [38] by Kortbek and Jensen [39] with angle deviations below 2º for flow angles at 60º to 90º and magnitude deviations between 0.7% and 7.7% for flow angles between 45º and 90º. Flow rig and *in-vivo* measurements of the common carotid artery and the femoral bifurcation have also been performed [40]. STA has previously been evaluated in simulations, in flow rig and *in-vivo* [29,30]. The velocities were estimated in a flow rig for flow angles of 60º, 75º and 90º, with standard deviation no higher than 6.5% [41].The TO method has previously been evaluated in simulations and flow rig [42]. The standard deviation of the transverse velocity estimate in flow rig experiments was less than 10% for beam-to-flow angles between 50º and 90º. Examples of *in-vivo* sequences have also been produced of the carotid artery [11] and compared with MRA as in this paper [34]. However, TO has not yet been evaluated against other vector velocity estimators and is included as a reference vector velocity US method.

Experimental ultrasound methods for volumetric measurements have previously been examined by other groups. Kim et al. validated cardiac output estimates obtained *in-vivo* with a 2-D ultrasound system using a color Doppler mapping of the short axis view and showed good agreement compared with both thermodilution and MRI [43]. Kripfgans et al. obtained in a phantom study volume flow measurements in the same manner but extended to a 3-D ultrasound system where the measured volume flow rates were within ±15% of actual values for the tested angles of insonation [44]. An *in-vivo* validation study of volumetric flow obtained by an invasive Doppler flow wire system was published by Jenni et al. where good correlation was found compared to transit-time flowmeter [45] and Krams reported on an experimental multigated spectral Doppler system validated in a flow phantom with error lower than 15% obtained [46]. Two studies have reported on a technique based on multigated dual-ultrasound beam technology and it was shown that reliable volume flow *in-vitro* and *in-vivo* could be obtained when compared to conventional spectral Doppler [47,48]. Shuping et al. and Forsberg et al. validated both 4-D Doppler ultrasound systems for volumetric flow *in-vivo* where Shuping et al. compared the estimates to phase contrast MRA with good agreement (r=0.92) and Forsberg et al. compared the volumetric estimates to a transit-time flowmeter also showing good agreement (r^2= 0.86 for mean volume flow and r^2= 0.62 for maximum volume flow) [49,50]. It should be noted that none of the previous studies of experimental US methods for volumetric measurements were done with actual angle independent methods as all the mentioned experimental methods were based on conventional Doppler.

One of the major challenges in 2-D US velocity estimation is the clutter filtering which cancels out stationary echoes from vessel surroundings [51]. In this study it was an important confounder. Blood signal representing low velocities near the vessel wall were cancelled out together with clutter signal and added up to a significant stroke volume loss. The TO method is the most robust method in terms of echo cancelling as a result of the lateral oscillation. STA and DB use the same scheme for velocity estimation; nevertheless, the STA method potentially has an advantage in terms of echo cancelling. This relies on the fact that the STA method uses continued data that can be echo cancelled with very long filters. This was not reflected in the results when only one filter was used in STA. However, the performance of STA improved when an adaptive filter approach somewhat similar to DB was used. The R value improved from 0.71 to 0.95, mean difference from 0.55 ml to 0.07 ml, the CI range of the mean difference from 1.97 ml to 0.95 ml and the LoA range from 5.74 ml to 2.78 ml.

The validity of assumptions of circular geometry of the examined vessel and rotationally symmetric blood flow necessary for volume flow calculation were tested by calculating a ratio between angle dependent and actual MRA stroke volume. For every volunteer a stroke volume

range was calculated from MRA data assuming rotationally symmetric flow and circular vessel geometry. The ranges of angle dependent stroke volume as percentages of the ROI derived MRA stroke volumes had a mean ratio for all volunteer of 24.3%. In Fig. 2 and Fig. 4 it is clearly seen that none of the volunteers had an identical stroke volume for all angles. One volunteer even had a ratio of 45.3% (Fig. 3 and 4). By examining the phase velocity maps for all volunteers, it became clear that stroke volume angle dependency was caused by asymmetric flow, which is consistent with the literature [52,53]. According to the MRA data, the stroke volume could on average change up to 24.3% simply by changing the insonation window of the same vessel section. Thus, the placing of the longitudinal scan plane through the centre axis of the vessel in US examination was an important confounder to the study and the assumption of symmetric flow necessary for the US derived volume flow estimation was shown to be a simplification.

Even though the measured stroke volumes changed with insonation window this cannot entirely explain the differences between each vector velocity method and MRA. This is seen by inspecting Fig. 2 as several ranges did not overlap the lines of perfect fit (DB: 7 volunteers; STA: 5 volunteers; TO: 4 volunteers). One reason could be misplacing of the US planes. In the US examinations it was crucial to scan the vessels parallel to the longitudinal axis exactly through the centre axis of the vessel where the diameter of the lumen was greatest, and where *intima* was most clearly delineated. Vessel *intima* was a reliable marker when positioning the scan plane through the middle of the vessel, because the layer structures were visible when the US beam direction was perpendicular to the planes of the layers. But as vessels are not perfectly straight tubes, inevitably a part of the centre axis will be out of scan plane due to curvature, resulting in slightly lowered averaged volume flow. Another reason could be the averaging employed in MRA. The conventional MRA volume flow profile consisting of one complete heart cycle is found as a mean of measurements over several heart cycles (in this study: 192) where the end of the complete heart cycle is defined by the beginning of the second averaged systole. Due to fluctuations in heart rate and changing *R-R* interval over the 192 heart cycles, the second averaged systole is not in phase. It was obviously the shortest heartbeat of the 192 heart cycles which defined the length of the averaged complete heart cycle. Hence, it is expected that the calculated MRA stroke volumes were slightly underestimated [54].

The Linux cluster gave the most flexible environment for processing the data from an experimental point of view, but the processing time was considerable. However, all three methods can potentially be converted into real-time methods by implementation into commercial scanners which will make it possible to design studies with larger sample size to produce unambiguous results. The three methods open the possibility of estimating blood velocities in all vessels regardless of angle. Quantitative volume flow measurements could be usable information when evaluating the severity of stenoses of e.g. the internal carotid artery. Novel information about vortices in bifurcations, turbulence in the heart, flow in tumor vessels and flow in greater vessels can be obtained and could be an aid to the clinician when examining patients with cardiovascular diseases, transplanted organs or malignancies. Furthermore, from the vector velocity estimates wall shear stress can be derived, which is known to influence the build up of plaques at the vessel wall [55]. This measurement could be used in risk assessment of patients prone to plaque formation in order to initiate correctly prophylactic treatment.

CONCLUSION

In this study it was shown that reliable quantitative measurements can be obtained *in-vivo* with three different angle-independent 2-D vector velocity methods DB, STA, and TO. The three US vector velocity techniques can yield quantitative insight into flow dynamics and visualize complex flow patterns, which may give the clinician a novel tool for cardiovascular disease assessment. On-

going studies are investigating the potential in US vector velocity methods to visualize non-laminar blood flows in complex vessel geometries.

ACKNOWLEDGEMENT

This work was supported by grant 26-04-0024 from the Danish Science Foundation and by B-K Medical A/S, Herlev, Denmark.

REFERENCE LIST

[1] M. J. Joyner, N. M. Dietz, and J. T. Shepherd, From Belfast to Mayo and beyond: the use and future of plethysmography to study blood flow in human limbs, J Appl Physiol, 91 (2001) 2431-2441.

[2] S. Masood and G.-Z. Yang, Blood Flow Measurement, Encyclopedia of Biomedical Engineering, John Wiley & Sons, Inc., 2005.

[3] J. A. Jensen, Estimation of Blood velocities using ultrasound: A signal processing approach, Cambridge University Press, New York 1996.

[4] D. J. Phillips, K. W. Beach, J. Primozich, and D. E. Strandness, Jr., Should results of ultrasound Doppler studies be reported in units of frequency or velocity?, Ultrasound Med Biol, 15 (1989) 205-212.

[5] P. R. Hoskins, Peak velocity estimation in arterial stenosis models using colour vector Doppler, Ultrasound Med Biol, 23 (1997) 889-897.

[6] D. Birchall, A. Zaman, J. Hacker, G. Davies, and D. Mendelow, Analysis of haemodynamic disturbance in the atherosclerotic carotid artery using computational fluid dynamics, Eur Radiol, 16 (2006) 1074-1083.

[7] C. Cheng, D. Tempel, R. van Harperen, A. van der Baan, F. Grosveld, M. Daermen, R. Krams, and R. de Crom, Atherosclerotic lesion size and vulnerability are determined by patterns of fluid shear stress, Circulation, 113 (2006) 2744-2753.

[8] Y. Richter and E. R. Edelman, Cardiology is flow, Circulation, 113(23) (2006) 2679-2682.

[9] P. R. Hoskins, A review of the measurement of blood velocity and related quantities using Doppler ultrasound, Proc Inst. Mech. Eng [H.], 213 (1999) 391-400.

[10] S. F. Stewart, Effects of transducer, velocity, Doppler angle, and instrument settings on the accuracy of color Doppler ultrasound, Ultrasound Med Biol, 27 (2001) 551-564.

[11] J. Udesen, M. B. Nielsen, K. R. Nielsen, and J. A. Jensen, Examples of In Vivo Blood vector velocity Estimation, Ultrasound Med Biol, 33 (2007) 541-548.

[12] M. D. Fox, Multiple crossed-beam ultrasound Doppler velocimetry, IEEE Trans Son Ultrason, 25 (1978) 281-286.

[13] G. E. Trahey, J. W. Allison, and O. T. Ramm, Angle independent ultrasonic detection of blood flow, IEEE Trans Biomed Eng, 34 (1987) 965-967.

[14] V. L. Newhouse, D. Censor, T. Vontz, J. A. Cisneros, and B. B. Goldberg, Ultrasound Doppler probing of flows transverse with respect to beam axis, IEEE Trans Biomed Eng, 34 (1987) 779-788.

[15] O. Bonnefous, Measurement of the complete (3D) velocity vector of blood flows, Proc IEEE Ultrason Symp, (1988) 795-799.

[16] J. A. Jensen, Directional velocity estimation using focusing along the flow direction: I: Theory and simulation, IEEE Trans Ultrason Ferroelec Freq Contr, (2003) 857-872.

[17] J. A. Jensen and R. Bjerngaard, Directional velocity estimation using focusing along the flow direction: II: Experimental investigation, IEEE Trans Ultrason Ferroelec Freq Contr, (2003) 873-880.

[18] J. A. Jensen and S. Nikolov, Transverse flow imaging using synthetic aperture directional beamforming, Proc IEEE Ultrason Symp, 2 (2002) 1488-1492.
[19] J. A. Jensen and P. Munk, A new method for estimation of velocity vectors, IEEE Trans Ultrason Ferroelec Freq Contr, 45 (1998) 837-851.
[20] M. E. Anderson, Multi-dimensional velociy estimation with ultrasound using spatial quadrature, IEEE Trans Ultrason Ferroelec Freq Contr, 45 (1998) 852-861.
[21] J. F. Polak, Peripheral Vascular Sonography: A Practical Guide, Lippincott Williams & Wilkins, 2004.
[22] J. N. Oshinski, J. L. Curtin, and F. Loth, Mean-average wall shear stress measurements in the common carotid artery, J Cardiovasc. Magn Reson, 8 (2006) 717-722.
[23] S. O. Oktar, C. Yucel, D. Karaosmanoglu, K. Akkan, H. Ozdemir, N. Tokgoz, and T. Tali, Blood-flow volume quantification in internal carotid and vertebral arteries: Comparison of 3 different ultrasound techniques with phase-contrast MR imaging, AJNR Am J Neuroradiology, 27(2) (2006) 363-369.
[24] M. Henry-Feugeas, I. Kilic Genauzeau, N. Ayme, and E. Schouman-Claeys, Variability of ultrasonography velocity assessment of the carotid arteries, J Radiol, 81 (2000) 445-449.
[25] M. J. Paivansalo, I. Suramo, J. Merikanto, and E. L. Lindholm, Interobserver, interequipment and intersubject variability of echo-Doppler examination of the common carotid and vertebral arteries, Eur J Ultrasound, 7 (1998) 145-151.
[26] A. Walker, E. Olsson, B. Wranne, I. Ringqvist, and P. Ask, Accuracy of spectral Doppler flow and tissue velocity measurements in ultrasound systems, Ultrasound Med Biol, 30 (2004) 127-132.
[27] C. Kasai, K. Namekawa, A. Koyano, and R. Omoto, Real-time two-dimensional blood flow imaging using an autocorrelation technique, IEEE Trans Son Ultrason, 32 (1985) 458-463.
[28] P. D. Welch, The use of fast Fourier transform for the estimation of power spectra: A method based on time averaging over short, modified periodograms, IEEE Trans Audio Electroacoust., AU-15 (1967) 70-73.
[29] S. Nikolov and J. A. Jensen, In-Vivo Synthetic aperture flow Imaging in Medical Ultrasound, IEEE Trans Ultrason Ferroelec Freq Contr, 50 (2003) 848-856.
[30] J. A. Jensen and N. Oddershede, Estimation of velocity vectors in synthetic aperture ultrasound imaging, IEEE Trans Med Imag, 25 (2006) 1637-1644.
[31] J. A. Jensen, A new estimator for vector velocity estimation, IEEE Trans Ultrason Ferroelec Freq Contr, 48 (2001) 886-894.
[32] J. A. Jensen, O. Holm, L. J. Jensen, H. Bendsen, S. Nikolov, B. G. Tomov, P. Munk, M. Hansen, K. Salomonsen, J. Hansen, K. Gormsen, H. M. Pedersen, and K. L. Gammelmark, Ultrasound research scanner for real-time synthetic aperture image acquisition, IEEE Trans Ultrason Ferroelec Freq Contr, 52 (2005) 881-891.
[33] A. Blizhevsky, H. Azhari, D. Gaitini, and U. Dinnar, Pattern analysis of temporal changes in the carotid artery diameter under normal and pathological conditions, Med Eng Phys., 19 (1997) 352-358.
[34] K. L. Hansen, J. Udesen, C. Thomsen, J. A. Jensen, and M. B. Nielsen, In vivo validation of a blood vector velocity estimator with MR angiography, IEEE Trans Ultrason Ferroelectr. Freq Control, 56 (2009) 91-100.
[35] T. L. Chenevert, K. P. Fechner, and D. Y. Gelblum, Improvements in MR angiography using phase-corrected data sets, Magn Reson Med, 10 (1989) 38-49.
[36] M. B. Higginbotham, K. G. Morris, S. Williams, P. A. McHale, R. E. Coleman, and F. R. Cobb, Regulation of Stroke Volume during Submaximal and Maximal Upright Exercise in Normal Man, Circ Res, 58 (1986) 281-291.

[37] J. M. Bland and D. G. Altman, Statistical methods for assessing agreement between two methods of clinical measurement, Lancet, 1 (1986) 307-310.
[38] J. A. Jensen and N. B. Svendsen, Calculation of pressure fields from arbitrarily shaped, apodized, and excited ultrasound transducers, IEEE Trans Ultrason Ferroelec Freq Contr, 39 (1992) 262-267.
[39] J. Kortbek and J. A. Jensen, Estimation of Velocity Vector Angles Using the Directional Cross-Correlation Method, IEEE Trans Ultrason Ferroelec Freq Contr, 53 (2007) 2036-2049.
[40] I. K. Holfort, J. Kortbek, and J. A. Jensen, In-vivo Vector Velocity Imaging Using Directional Cross-Correlation, Proc IEEE Ultrason Symp, (2006) 2023-2026.
[41] N. Oddershede and J. A. Jensen, Effects influencing focusing in synthetic aperture vector flow imaging, IEEE Trans Ultrason Ferroelec Freq Contr, 54 (2007) 1811-1825.
[42] J. Udesen and J. A. Jensen, Investigation of transverse oscillation method, IEEE Trans Ultrason Ferroelec Freq Contr, 53 (2006) 959-971.
[43] W. Y. Kim, J. K. Poulsen, K. Terp, and N. H. Staalsen, A new Doppler method for quantification of volumetric flow: in vivo validation using color Doppler, J Am Coll Cardiol, 27 (1996) 182-192.
[44] O. D. Kripfgans, J. M. Rubin, A. L. Hall, M. B. Gordon, and J. B. Fowlkes, Measurement of volumetric flow, J Ultrasound Med, 25 (2006) 1305-1311.
[45] R. Jenni, F. Matthews, S. V. Aschkenasy, M. Lachat, L. B. van Der, E. Oechslin, M. Namdar, Z. Jiang, and P. A. Kaufmann, A novel in vivo procedure for volumetric flow measurements, Ultrasound Med Biol, 30 (2004) 633-637.
[46] R. Krams, G. Bambi, F. Giudi, F. Helderman, A. F. W. van der Steen, and P. Tortoli, Effect of Vessel Curvature on Doppler Derived Velocity Profiles and Fluid Flow, Ultrasound in Medicine and Biology., 31 (2005) 663-671.
[47] J. F. Soustiel, E. Levy, M. Zaaroor, R. Bibi, S. Lukaschuk, and D. Manor, A new angle-independent Doppler ultrasonic device for assessment of blood flow volume in the extracranial internal carotid artery, J Ultrasound Med, 21 (2002) 1405-1412.
[48] R. D. Rothoerl, K. M. Schebesch, C. Woertgen, and A. Brawanski, Ultrasonic blood flow volume assessment in the extracranial internal carotid artery in arteriovenous malformations, Neurol. Res, 27 (2005) 209-211.
[49] G. E. Shuping, B. U. Liping, Z. Honghai, E. Schelbert, and M. Disterhoft, A Real-time 3-dimensional Digital Doppler Method for Measurement for Flow Rate and Volume Thorugh Mitral Valve in Children: A Validation Study Caompared With Magnetic Resonance Imaging, J Am Soc Echocardiogr, 18 (2005) 1-7.
[50] F. Forsberg, A. D. Stein, J. Lui, X. Deng, W. Ackerman, D. Herzog, K. Abend, and L. Needlerman, Validating volume Flow Measurements from a Novel Semiautomated Four-dimensional Doppler Ultrasound Scanner, Acad Radiol, 13 (2006) 1204-1210.
[51] B. H. Friemel, L. N. Bohs, K. R. Nightingale, and G. E. Trahey, Wall filtering challenges in two-dimensional vector velocity estimation, Proc. IEEE Ultrason. Symp, 2 (1993) 1031-1034.
[52] P. J. Brands, A. P. Hoeks, L. Hofstra, and R. S. Reneman, A noninvasive method to estimate wall shear rate using ultrasound, Ultrasound Med Biol, 21 (1995) 171-185.
[53] P. Tortoli, V. Michelassi, G. Bambi, F. Guidi, and D. Righi, Interaction between secondary velocities, flow pulsation and vessel morphology in the common carotid artery, Ultrasound Med Biol, 29 (2003) 407-415.
[54] J. Lotz, C. Meier, A. Leppert, and M. Galanski, Cardiovascular flow measurement with phase-contrast MR imaging: basic facts and implementation, Radiographics, 22 (2002) 651-671.
[55] P. Tortoli, Noninvasive simultaneous assesment of wall shear rate and wall distension in carotid arteries, Ultrasound Med Biol, 32 (2006) 1661-1670.

Appendix III

In-vivo examples of flow patterns with a fast vector velocity ultrasound method

Hansen K.L.[(1)], Udesen J. [(2)], Gran F. [(2)], Jensen J.A. [(3)], Nielsen M.B. [(1)]

1) Department of Radiology, Section of Ultrasound, Rigshospitalet, Blegdamsvej 9, DK-2100 Cph. Ø, Denmark.
2) GN Resound, Lautrupsbjerg 9, DK-2750 Ballerup, Denmark
3) Center for Fast Ultrasound Imaging, DTU Elektro, Bldg. 349, Technical University of Denmark, DK-2800 Lyngby, Denmark.

ABSTRACT

Aim: Conventional ultrasound methods for acquiring colour flow images of the blood motion are limited by a relatively low frame rate and are restricted to only giving velocity estimates along the ultrasound beam direction. To circumvent these limitations, the Plane Wave Excitation (PWE) method has been proposed.

Material and method: The PWE method can estimate the 2D vector velocity of the blood with a high frame rate. Vector velocity estimates are acquired by using the following approach: The ultrasound is not focused during the ultrasound transmission, and a full speckle image of the blood can be acquired for each pulse emission. The pulse is a 13 bit Barker code transmitted simultaneously from each transducer element. The 2D vector velocity of the blood is found using 2D speckle tracking between segments in consecutive speckle images. Implemented on the experimental scanner RASMUS and using a 100 CPU linux cluster for post processing PWE can achieve a frame of 100 Hz where one vector velocity sequence of approximately 3 seconds, takes 10 hours to store and 48 hours to process. In this paper a case study is presented of *in-vivo* vector velocity estimates in different complex vessel geometries.

Results: The flow patterns of six bifurcations and two veins were investigated. It was shown: 1) that a stable vortex in the carotid bulb was present opposed to other examined bifurcations, 2) that retrograde flow was present in the superficial branch of the femoral artery during diastole, 3) that retrograde flow was present in the subclavian artery and antegrade in the common carotid artery during diastole, 4) that vortices were formed in the sinus pockets behind the venous valves in both antegrade and retrograde flow, and 5) that secondary flow was present in various vessels.

Conclusion: Using a fast vector velocity ultrasound method, *in-vivo* scans have been recorded where complex flow patterns were visualized in greater detail than previously visualised by conventional colour flow imaging techniques.

INTRODUCTION

Colour flow mapping (CFM) is used in almost every field of the ultrasound (US) examination. The modality displays the motion in the scan plane encoded as a colour delineated by a colour box and superimposed on a B-mode image. The method is especially used in visualizing blood flow in the cardiovascular system. However, CFM in conventional US has two major limitations. Low frame rate, and angle dependent velocity estimation.

The frame rate in CFM is mainly governed by the number of pulses used per frame and by the distance each pulse has to travel between transducer and target. The colour box and the entire frame are built up of lines, where each line is found from received echoes of several consecutive pulses. Thus, the wider and the deeper the colour box (and frame), the lower the frame rate will be (1;2). 2D duplex mode (B-mode combined with CFM) in commercial scanners is performed at frame rates down to 8-10 Hz, which is unsuitable for visualizing rapid temporal changes in the blood flow. The

problem is aggravated in 2D triplex mode (B-mode image, CFM and spectral Doppler (SD)) and will be a major hurdle in 3D duplex/triplex scanning.

The velocity estimate in conventional CFM is only found as a mean velocity along the US beam direction in the axial direction (3). In CFM no angle correction is performed and consequently, CFM is only used as a qualitative method for visualizing flow. In SD examination angle correction is applied on the estimates. The SD method is therefore used quantitatively as it is believed that true velocities after angle correction are displayed. However, the correction scheme only provides satisfactory results when laminar flow parallel to the vessel is present. Human vessels are branching, curving and highly elastic, and complex flow profiles are created throughout the cardiovascular system, creating skewed velocity profiles (4-6) and secondary flow patterns (7-11). Thus, it is in general difficult to predict the scatterer movement based on the B-mode image (12-14) albeit this is exactly what the operator does when angle correcting. Therefore, an error will always be associated with conventional SD measurements due to angle dependency, and information on the complex flow patterns kept unrevealed (15;16).

A novel method for estimating blood motion with ultrasound has been proposed by Udesen et al. (17;18). The method called Plane Wave Excitation (PWE) acquires with a high frame rate, 2D vector velocities of the blood using 1D linear transducer. Implemented on the experimental scanner RASMUS (19;20) and using a 100 CPU linux cluster for post processing, PWE can achieve a frame of 100 Hz where one vector velocity sequence of approximately 3 seconds, takes 10 hours to store and 48 hours to process.

The PWE method has previously been validated in simulations and flow-phantoms with promising results. Examples of *in-vivo* sequences have been produced of the carotid artery, and results have been compared to MR angiography measurements with mean deviation of volume flow of 9 %.

This paper presents an *in-vivo* case study of the PWE method. The aim of the study is to show that it is possible to obtain instantaneous vector velocity estimates *in-vivo* and to produce reliable CFM sequences using the PWE method. The locations of interest for the scan sequences were primarily complex geometries: bifurcations and venous valves. Also scan sequences have been obtained of the common carotid artery and the subclavian artery in a cross-sectional scan plane visualizing secondary flow patterns.

MATERIALS AND METHODS

Volunteers

This study was performed after approval by The Danish National Committee on Biomedical Research Ethics. Four healthy volunteers with no history of cardiovascular disease (three males and one female, 26 – 45 y, mean age: 34 y) entered the study after informed consent. Scan sequences were acquired of two carotid bifurcations, two femoral bifurcations, the bifurcation at the brachiocephalic trunk, the bifurcation of the subclavian artery as well as the internal jugular vein and the great saphenous vein, both with venous valves. The scans were all recorded with the volunteers in supine position except the scan of the great saphenous vein, where the volunteer was in standing position while performing dorsal and plantar flexion to simulate walking. All scans were carried out by an experienced radiologist.

The PWE method

The PWE method is based on a number of well described techniques, which have all been validated previously. A thorough introduction to the PWE method is given in (17) based on a method previously suggested for elastography (21).

In PWE all elements of the transducer are excited at the same time thereby creating a pressure wave with a nearly plane front. The unfocused pulse covers the entire imaging plane with acoustic energy, and a full speckle image is obtained for every emission. The unfocused pulse thereby yields a frame rate equal to the pulse repetition frequency of the ultrasound, which at a depth of 30 mm is 25 kHz. The drawback of using this method is degradation in image contrast due to the lack of focusing and a relatively low signal-to-noise ratio (SNR), which results in low penetration depth. To compensate for the decrease in SNR, a 13 bit Barker code is used instead of a conventional pulse (22).

Intensity measurements of the PWE method using a Barker code was carried out prior to the study (17). It was found that both the Mechanical Index (MI), maximal intensity (I_m) as well as the spatial peak pulse average intensity ($I_{sppa,is}$) were below the values proposed by the Food and Drug Administration (FDA) (23). The only concern was the spatial peak temporal average intensity ($I_{spta,is}$), which scales with the pulse repetition frequency (f_{prf}). The maximum allowed $I_{spta,is}$ of 1500 mW/cm^2 for vascular imaging is obtained when using a f_{prf} of 8.6 kHz. Thermal index was not possible to measure with the experimental setup. Intensities of the PWE method using a Barker code with a f_{prf} of 8.6 kHz are given in Table 1.

Table 1:

	Barker 13 bit	Limits set by FDA	Unit
MI	0.02	1.9	N/A
I_m	139	600	W/cm^2
$I_{sppa,is}$	111	240	W/cm^2
$I_{spta,is}$	1500	1500	mW/cm^2

The angle independent vector velocity estimates are found when tracking speckle motion between consecutive speckle images. Each speckle image is divided into small search kernels with a size of 1x1 mm^2. For a given frame and kernel, an algorithm called sum of squared differences (24;25) searches for the best fit of the kernel speckle pattern in the next image and calculates the corresponding movement and direction. When the movement of the kernel speckle pattern is divided by the time between the two frames an estimate of the blood velocity in the kernel is obtained and the direction of the movement gives the angle of the blood flow in the kernel. To reduce calculation errors this procedure can be averaged a number of times to achieve better performance. Using this approach no assumptions of laminar flow parallel to vessel boundaries are necessary for velocity estimation as no angle correction scheme is performed.

The setup

The experimental scanner RASMUS (19;20) and a 5 MHz linear array transducer were used to acquire data. The post processing was done offline with MATLAB (Mathworks, Natick, MA, USA) on a 100 CPU Linux cluster. One vector velocity sequence of approximately 3 seconds, took 10 hours to store and 48 hours to process. A description of the setup is given in Table 2.

Table 2:

Transducer	linear array, BK-8804
No. of Elements	128 elements
Transmit focus	Infinity
US pulse	5 MHz, 13 bit Barker code
US pulses pr. vector image	80 pulses/image
Pulse Repetition Frequency	8 kHz
Receive beamforming	Delay-and-sum
Wall filter	39 taps high-pass FIR filter
Time between vector images	10 ms
Resolution in vector image	1 x1 mm^2

In the PWE sequences presented in this paper, two pulse emissions are used to create one speckle image. This is necessary as the RASMUS scanner has 128 transmitting channels but only 64 in receive with 2:1 multiplexing. To calculate one vector velocity image, 40 speckle images are used. Furthermore, 65 conventional focused pulses are used to generate the interleaved conventional B-mode image. The frame rate on the vector velocity images in this study is 100 Hz. However, matching receive and transmit channels in RASMUS would give a frame rate of 200 Hz without degrading the quality of the velocity estimates.

RESULTS

Two volunteers (volunteer 1 and 2) were scanned on the carotid bifurcation and for both volunteers a vortex with low velocities in the carotid bulb was present during the entire heart cycle. Apart from the vortical recirculation in the bulb no retrograde flow was present. An example of the vortex formation in the carotid bulb is shown in Fig. 1.

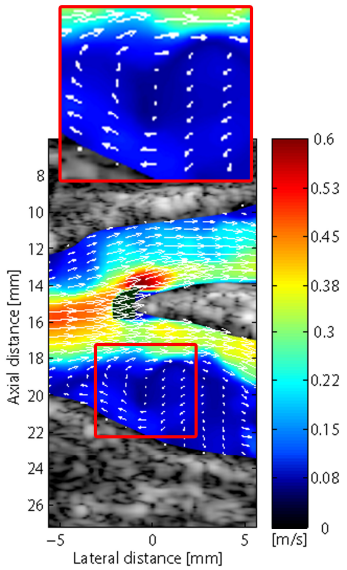

Fig.1: In the carotid bulb of the internal carotid artery a vortex was present during the entire heart cycle. The internal carotid artery is seen as the deep vessel.

In Fig. 2 the bifurcation of the brachiocephalic trunk is shown (volunteer 3). In diastole the flow was filling the common carotid artery (superficial vessel) from the subclavian artery (deep vessel). Thus, the diastolic flow was retrograde in the subclavian artery and antegrade in the common

carotid artery. No vortex was present in systole but disturbed flow with vortices was seen in the subclavian artery when flow reversed at end-systole and end-diastole.

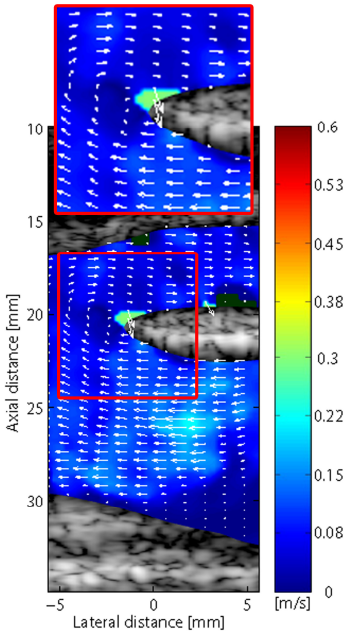

*Fig. 2: The diastolic flow was going from the subclavian artery (*deep *vessel) to the common carotid artery (superficial vessel).*

The same volunteer (volunteer 3) was scanned on the right side bifurcation of the thyrocervical trunk and the vertebral artery. During peak systole the flow propagated without disturbance from the subclavian artery to the vertebral artery and the thyrocervical trunk. Vortices in the subclavian artery scanned cross-sectionally were visible right after peak systole and throughout diastole as shown in Fig 3. The secondary flow swept from the superficial part of the subclavian artery and downwards in an s-shaped pattern creating two vortices.

Two femoral bifurcations were scanned (volunteer 1 and 4) and it was seen for both examinations that no disturbed flow was seen during the heart cycle but marked reversed flow was seen in the superficial branch during the beginning of diastole. One example of the reversed flow is given in Fig. 4. Similar to the brachiocephalic trunk depicted in Fig. 2 disturbed flow was present with vortices when flow reversed.

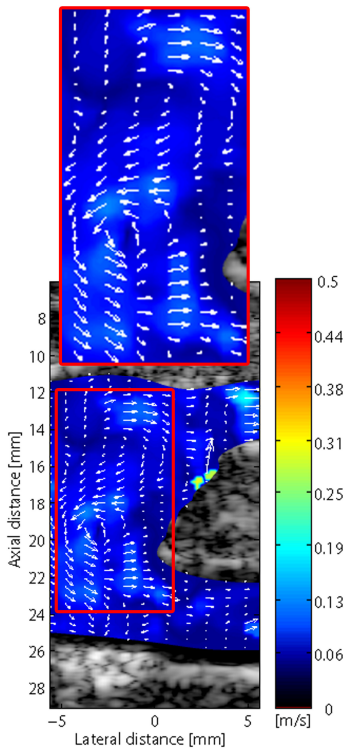

Fig. 3: In the subclavian artery (scanned cross-sectionally) vortices were present after peak systole and throughout diastole. The vertebral artery is seen as the superficial vessel and the thyrocervical trunk is seen as the deep *vessel. The frame is taken from the beginning of diastole.*

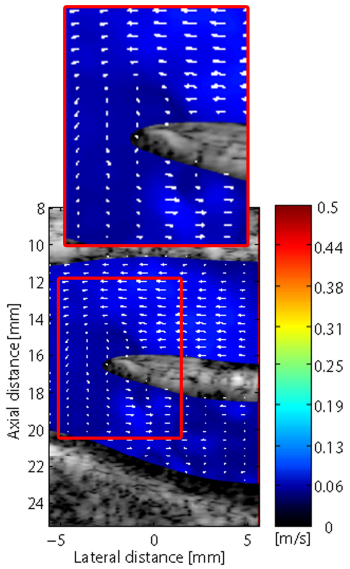

Fig. 4: During diastole retrograde flow in the superficial branch of the femoral artery was seen. The reversed flow filled the deep branch of the femoral artery in which the flow remained antegrade.

The venous valves of the great saphenous vein (volunteer 1) and internal jugular vein (volunteer 3) were scanned. In Fig. 5, a venous bulb of the saphenous vein is shown. Although the valves were not visible, the effect of the valves on the flow was obvious. During opening of the valves the flow was squeezed to form a jet and vortices were formed in the sinus pockets behind the valves. No retrograde flow was present and during the closed phase bidirectional blood motion was seen with the competent valves as a separator.

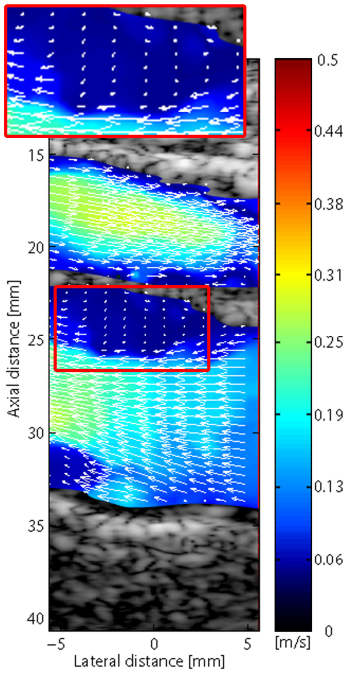

*Fig. 5: In the great saphenous vein (*deep *vessel) a jet between the valves was formed during antegrade flow and vortices were formed behind the valves. The femoral artery is seen as the superficial vessel.*

A bulb of the jugular vein was examined. During the opened phase the flow pattern was similar to the flow pattern observed in the bulb of the great saphenous vein with vortices formed in the sinus pockets behind the valves and a jet formed between the valves (Fig. 6). However, the flow patterns in the two veins were not alike during the closed phase as retrograde flow was observed in the jugular vein. Due to incompetent valves a retrograde jet was formed between the valves and vortices were formed upstream of the valves (Fig. 7). Additionally, the common carotid artery scanned cross-sectionally showed a marked secondary flow during systole (Fig. 6).

Table 3 provides an overview of the findings with data given on gender, age and scan location.

Table 3:

Volunteer no.	Gender	age	Location	Findings
Volunteer 1	male	34	carotid bifurcation	stable vortex in the carotid bulb
-	-	-	femoral bifurcation	retrograde flow in the superficial branch, antegrade flow in the deep branch
-	-	-	saphenous vein	vortices in the pockets, competent valves
Volunteer 2	female	45	carotid bifurcation	stable vortex in the carotid bulb
Volunteer 3	male	26	jugular vein	vortices in the pockets and upstream of the incompetent valves, secondary flow in the carotid artery
-	-	-	brachiocephalic trunk	retrograde flow in the subclavian artery, antegrade flow in the carotid artery
-	-	-	subclavian bifurcation	S-shaped secondary flow in the subclavian artery
Volunteer 4	male	31	femoral bifurcation	retrograde flow in the superficial branch, antegrade flow in the deep branch

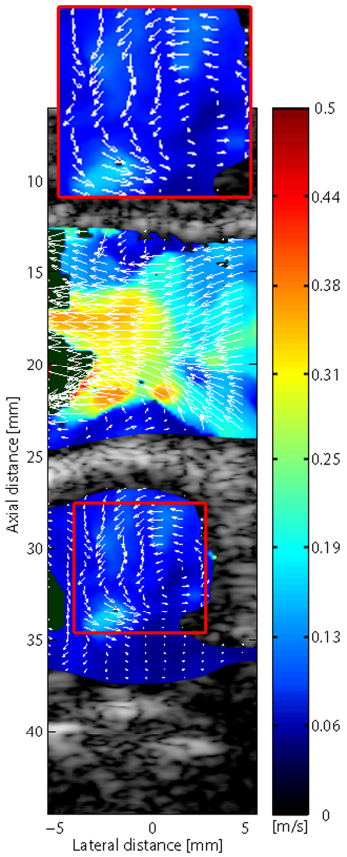

*Fig. 6: Vortices were formed in the sinus pockets of the jugular vein (superficial vessel) behind the valves during antegrade flow. In the carotid artery (*deep *vessel) secondary flow was seen during systole when scanned cross-sectionally.*

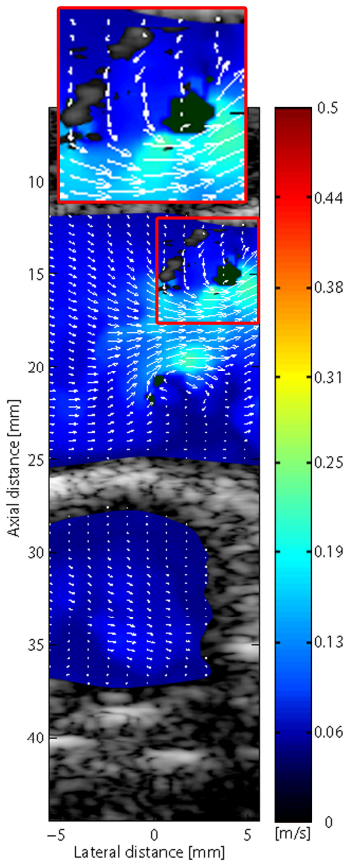

Fig. 7: In the jugular vein (superficial vessel) the reversed flow was squeezed by the incompetent venous valves forming a jet and vortices were formed upstream of the valves.

DISCUSSION

In this study new information on the complex flow profiles in the human cardiovascular system in both simple and complex vessel geometries was obtained using the PWE method. In total six arterial bifurcations and two venous bulbs were examined on four healthy volunteers.

It was shown when examining the carotid bifurcations on two volunteers that a well-defined vortex was present in the carotid bulb during the entire heart cycle. This is in accordance with earlier results obtained with US vector velocity examinations (26;27). No stable vortices were observed during systole in the other four bifurcations, and they did not reveal same consistency in terms of flow patterns. However, in the two femoral bifurcations and the brachiocephalic trunk reversed flow was observed in diastole. During diastole flow reversed in the superficial branches of the femoral artery with antegrade flow in the deep branches. In the brachiocephalic trunk the flow reversed in the subclavian artery and filled the common carotid artery. It is well known that the flow in the carotid arteries is biphasic without retrograde flow and it is believed that antegrade flow in diastole primarily is forwarded from the aorta. In literature it is known as the windkessel effect (28). The effect describes how half of the left ventricular stroke volume during systole is stored in the aorta and due to the elastic forces of the aortic wall is forwarded in diastole to the peripheral circulation. The PWE results indicate that the blood reserve forwarded in diastole to the brain, derive from other arteries than the aorta. For neither the femoral bifurcation nor the brachiocephalic trunk, have the reversed flow patterns previously been visualized in such detail as presented in this study using the PWE method.

The vortex is fundamental in the carotid bifurcation and has in numerous studies been linked to the development of atherosclerosis (10;29-32) as disturbed flow around vessel bifurcation has been linked more widely to atheroma deposition (33;34). The findings indicate that the flow pattern in the carotid bifurcation is different from flow patterns in other bifurcations of the human cardiovascular system. It appears that the stable vortex is related to the bulb and not the bifurcation.

It was shown using the PWE method that competent valves in the great saphenous vein were present, and that vortices were formed in the sinus pockets behind valves. This is in concordance with previous studies (35;36). The internal jugular vein was examined as well and the examination revealed the presence of incompetent valves and retrograde flow. Incompetent valves of the internal jugular vein have been described before with prevalence of 36.8% to 38.4% in healthy persons (37-39). The findings with the PWE method concerning valves in the great saphenous vein and the internal jugular vein are consistent with the literature. However, vortices on either side of the valves created by bidirectional flow have not been reported previously.

Secondary flow was seen in the subclavian artery (Fig. 3) and in the common carotid artery (Fig. 6). Secondary flow has been predicted by computational fluid dynamics and magnetic resonance imaging in several studies and for different vessels but it has not been possible before to visualize secondary flow with US (7-11). The secondary flow is thought to have a protective role in the development of atherosclerosis and may be an important issue in vascular disease assessment (40).

CONCLUSION

With the PWE method different vessel geometries have been examined and flow patterns described. The fast, angle independent, non-invasive, blood vector velocity method is unique compared to conventional imaging modalities in the ability to visualize complex flow patterns and has revealed new information in the field of blood dynamics.

Future studies with PWE method will be realized to follow up on discoveries described in this paper. Especially important are the studies: 1) of the stable vortex in the carotid bulb and the relation to the baroreceptors, 2) of the venous valves and the pressure dynamics around the valves, 3) of retrograde flow patterns in the brachiocephalic trunk and femoral bifurcation, and 4) of secondary flow in different vessel geometries and the relation to atheroma deposition. Other studies with the PWE method will concern flow dynamics of the heart and its valves and altered flow patterns in diseased vessels with e.g. aneurysms and stenoses.

The promising preliminary *in-vivo* results presented in this paper indicate that the PWE method has great potential. However, the PWE method requires a big effort for data acquisition and processing and is, in consequence, not ready yet for clinical routine.

REFERENCE LIST

(1) Ferrara K, DeAngelis G. Color flow mapping. Ultrasound Med Biol 1997;23(3):321-45.

(2) Kruskal JB, Newman PA, Sammons LG, Kane RA. Optimizing Doppler and color flow US: Application to hepatic sonography. Radiographics 2004;24(3):657-75.

(3) Jensen JA. Estimation of Blood velocities using ultrasound: A signal processing approach. New York: Cambridge University Press; 1996.

(4) Tortoli P, Michelassi V, Bambi G, Guidi F, Righi D. Interaction between secondary velocities, flow pulsation and vessel morphology in the common carotid artery. Ultrasound Med Biol 2003 Mar;29(3):407-15.

(5) Ford MD, Xie YJ, Wasserman BA, Steinman DA. Is flow in the common carotid artery fully developed? Physiol Meas 2008 Nov;29(11):1335-49.

(6) Hansen KL, Udesen J, Thomsen C, Jensen JA, Nielsen MB. In vivo validation of a blood vector velocity estimator with MR angiography. IEEE Trans Ultrason Ferroelectr Freq Control 2009 Jan;56(1):91-100.
(7) Frazin LJ, Lanza G, Vonesh M, Khasho F, Spitzzeri C, McGee S, et al. Functional chiral asymmetry in descending thoracic aorta. Circulation 1990 Dec;82(6):1985-94.
(8) Lee KL, Doorly DJ, Firmin DN. Numerical simulations of phase contrast velocity mapping of complex flows in an anatomically realistic bypass graft geometry. Med Phys 2006 Jul;33(7):2621-31.
(9) Steinman DA, Thomas JB, Ladak HM, Milner JS, Rutt BK, Spence JD. Reconstruction of carotid bifurcation hemodynamics and wall thickness using computational fluid dynamics and MRI. Magnet Reson Med 2002;47(1):149-59.
(10) Zhao SZ, Xu XY, Hughes AD, Thom SA, Stanton AV, Ariff B, et al. Blood flow and vessel mechanics in a physiologically realistic model of a human carotid arterial bifurcation. J Biomech 2000;33(8):975-84.
(11) Zhao SZ, Papathanasopoulou P, Long Q, Marshall I, Xu XY. Comparative study of magnetic resonance imaging and image-based computational fluid dynamics for quantification of pulsatile flow in a carotid bifurcation phantom. Ann Biomed Eng 2003;31(8):962-71.
(12) Phillips DJ, Beach KW, Primozich J, Strandness DE, Jr. Should results of ultrasound Doppler studies be reported in units of frequency or velocity? Ultrasound Med Biol 1989;15(3):205-12.
(13) Hoskins PR. Peak velocity estimation in arterial stenosis models using colour vector Doppler. Ultrasound Med Biol 1997;23(6):889-97.
(14) Fei DY, Liu DD, Fu CT, Makhoul RG, Fisher MR. Feasibility of angle independent Doppler color imaging for in vivo application: Preliminary study on carotid arteries. Ultrasound in Medicine and Biology 1997;23(1):59-67.
(15) Cheng C, Tempel D, van Harperen R, van der Baan A, Grosveld F, Daermen M, et al. Atherosclerotic lesion size and vulnerability are determined by patterns of fluid shear stress. Circulation 2006;113(23):2744-53.
(16) Richter Y, Edelman ER. Cardiology is flow. Circulation 2006;113(23):2679-82.
(17) Udesen J, Gran F, Hansen KL, Jensen JA, Thomsen C, Nielsen MB. High frame-rate blood vector velocity imaging using plane waves: simulations and preliminary experiments. IEEE Trans Ultrason Ferroelec Freq Contr 2008;55(8):1729-43.
(18) Udesen J, Gran F, Hansen KL, Jensen JA, Nielsen MB. Fast blood vector velocity imaging: Simulations and preliminary in vivo results. Proc IEEE Ultrason Symp 2007;1005-8.
(19) Jensen JA, Holm O, Jensen LJ, Bendsen H, Pedersen HM, Salomonsen K, et al. Experimental ultrasound system for real-time synthetic imaging. IEEE Ultrason Symp 1999;1595-9.
(20) Jensen JA, Holm O, Jensen LJ, Bendsen H, Nikolov S, Tomov BG, et al. Ultrasound research scanner for real-time synthetic aperture image acquisition. IEEE Trans Ultrason Ferroelec Freq Contr 2005;52(5):881-91.
(21) Tanter M, Bercoff J, Sandrin L, Fink M. Ultrafast compound imaging for 2-d motion vector estimation: application to transient elastography. IEEE Trans Ultrason Ferroelec Freq Contr 2002;49(10):1363-74.
(22) Gran F, Udesen J, Nielsen MB, Jensen JA. Coded ultrasound for blood flow estimation using subband processing. IEEE Trans Ultrason Ferroelec Freq Contr 2009;55(10):2211-20.
(23) 510 (k) guide for measuring and reporting acoustic output of diagnostic medical devices. FDA, Tech Rep, Center for Devices and Radiological Health 1985.

(24) Trahey GE, Allison JW, Ramm OT. Angle independent ultrasonic detection of blood flow. IEEE Trans Biomed Eng 1987;34(12):965-7.
(25) Friemel BH, Bohs LN, Trahey GE. Relative performance of two-dimensional speckle-tracking techniques: normalized correlation, non-normalized correlation and sum-absolute-difference. Proc IEEE Ultrason Symp 1995;2:1481-4.
(26) Oddershede N, Hansen KL, Nielsen MB, Jensen JA. In-vivo examples of synthetic aperture vector flow imaging. Proc SPIE Med Imag 2007;8:6510-3.
(27) Udesen J, Nielsen MB, Nielsen KR, Jensen JA. Examples of In Vivo Blood vector velocity Estimation. Ultrasound Med Biol 2007;33(4):541-8.
(28) Belz GG. Elastic properties and Windkessel function of the human aorta. Cadiovasc Drugs Ther 1995;9(1):73-83.
(29) Birchall D, Zaman A, Hacker J, Davies G, Mendelow D. Analysis of haemodynamic disturbance in the atherosclerotic carotid artery using computational fluid dynamics. Eur Radiol 2006;16(5):1074-83.
(30) Xue YJ, Gao PY, Duan Q, Lin Y, Dai CB. Preliminary study of hemodynamic distribution in patient-specific stenotic carotid bifurcation by image-based computational fluid dynamics. Acad Radiol 2008;49(5):558-65.
(31) Schuierer G, Huk WJ. Diagnostic significance of flow separation within the carotid bifurcation demonstrated by digital subtraction angiography. Stroke 1990;21(12):1674-9.
(32) Stokholm R, Oyre S, Ringgaard S, Flaagoy H, Paaske W, Pedersen EM. Determination of Wall Shear Rate in the Human Carotid Artery by Magnetic Resonance Techniques. Eur J Vasc Endovasc surg 2000;20(5):427-33.
(33) Papathanasopoulou P, Zhao SZ, Kohler U, Robertson MB, Long Q, Hoskins P, et al. MRI measurement of time-resolved wall shear stress vectors in a carotid bifurcation model, and comparison with CFD predictions. J Magn Reson Imaging 2003;17(2):153-62.
(34) Marshall I, Zhao S.Z., Papathanasopoulou P, Hoskins P, Xu XY. MRI and CDF studies of pulsatile flow in healthy and stenosed carotid bifurcation models. J Biomech 2004;37(5):679-87.
(35) Qui Y, Quijano RC, Wang SK, Hwang HC. Fluid dynamics of venous valve closure. Ann Biomed Eng 1995;23(6):750-9.
(36) Lurie F, Kistner RL, Eklof B, Kessler D. Mechanism of venous valve closure and role of the valve in circulation: A new concept. J Vasc Surg 2003;38(5):955-61.
(37) Fisher J, Vaghaiwalla F, Tsitlik J, Levin H, Brinker J, Weisfleldt M, et al. Determinants and clinical significance of jugular venous valve competence. Circulation 1982;65(1):188-96.
(38) Nedelmann M, Techner D, Dieterich M. Analysis of internal jugular vein insufficiency - a comparison of two ultrasound methods. Ultrasound Med Biol 2007;33(6):857-62.
(39) Akkawi NM, Agosti C, Borroni B, Rozzini L, Magoni M, Vignolo LA, et al. Jugular valve incompetence: A study using air contrast ultrasonography on a general population. J Ultrasound Med 2002;21(7):747-51.
(40) Shipkowitz T, Rodgers VGJ, Frazin LJ, Chandran KB. Numerical study on the effect of secondary flow in the human aorta on local shear stresses in abdominal aortic branches. J Biomech 2000;33(6):717-28.

Appendix IV

In-vivo validation of fast spectral velocity estimation techniques

K.L.Hansen(1,3), F.Gran(2,3), M.M.Pedersen(1,3), I.K.Holfort(3), J.A.Jensen(3), M.B.Nielsen(1)

(1) Section of Ultrasound, Department of Radiology, Rigshospitalet. Blegdamsvej 9, DK-2100 Kbh. Ø, Denmark.
(2) GN Resound, Lautrupbjerg 9, DK-2750 Ballerup, Denmark
(3) Center for Fast Ultrasound Imaging, DTU Elektro, Bldg. 349, Technical University of Denmark, DK-2800 Lyngby, Denmark

Abstract – Spectral Doppler is a common way to estimate blood velocities in medical ultrasound (US). The standard way of estimating spectrograms is Welch's method (WM), which is dependent on an observation window (OW) of up to 256 emissions per estimate to produce spectrograms of sufficient spectral resolution and contrast. Two adaptive filterbank methods have been suggested to reduce the OW: Blood spectral Power Capon (BPC) and the Blood Amplitude and Phase EStimation method (BAPES). Previous simulations and phantom studies have indicated that the two adaptive methods displayed sufficient spectral resolution for much shorter OW than WM. The purpose of this paper is to investigate the methods *in-vivo*. Ten volunteers were scanned over the carotid artery using the experimental ultrasound scanner RASMUS and a B-K Medical 7 MHz linear array transducer. Four approaches (WM with a Hanning window (W.HAN), WM with a boxcar window (W.BOX), BPC and BAPES) and seven OWs (128, 64, 32, 16, 8, 4 and 2) were combined. Thus, from each data set, 28 spectrograms were produced. To investigate the methods quantitatively, a spectrum at end-diastole was found for each spectrogram from which two parameters were calculated: the full-width-at-half-maximum (FWHM) and the ratio between main and side lobe levels. To investigate the estimates qualitatively, all 280 spectrograms were randomised and presented to nine radiologists blinded to method and OW for visual evaluation: useful or not useful. Descriptive statistic analyses, tests for multiple comparisons and kappa-statistics were performed. BAPES and BPC compared to WM showed better resolution i.e. lower FWHM for all OW below 128 while only BAPES compared to WM had improved contrast i.e. higher ratio. According to the scores given by the radiologists, BAPES, BPC and W.HAN performed equally well ($p>0.05$) at OW 128 and 64, while W.BOX scored less ($p<0.05$). At OW 32, BAPES and BPC performed better than WM ($p<0.0001$) and BAPES was significantly superior to BPC at OW 16 ($p=0.0002$) and 8 ($p<0.0001$). BPC at OW 32 performed as well at BPC at OW 128 ($p=0.29$) and BAPES at OW 16 performed as well as BAPES at OW 128 ($p=0.55$). WM at OW 16 and 8 failed as all four methods at OW 4 and 2. The intra-observer variability tested for three radiologist showed on average good agreement (90%, $\kappa=0.79$) and inter-observer variability showed moderate agreement (78%, $\kappa=0.56$) displaying consistency in given scores for each radiologist with differences in base-line among the radiologists. The results indicated that BPC and BAPES had better resolution than WM while only BAPES had better contrast than WM and that OW can be reduced to 32 using BPC and 16 using BAPES without reducing the usefulness of the resulting spectrogram. The fast spectral velocity estimation using adaptive filterbank methods could potentially increase the temporal resolution of the spectrogram or the frame rate of the interleaved B-mode images.

INTRODUCTION

In ultrasound (US) imaging visualization of blood motion can be achieved with color flow mapping, power Doppler imaging, and spectral Doppler. The three methods estimate the blood motion along the beam direction. Color flow mapping and power Doppler display the blood motion qualitatively using color coding delineated by a color box on top of a B-mode image. The spectral Doppler method is a quantitative technique providing estimates of blood flow within a range gate on a single image line. Spectral Doppler is displayed with the B-mode modality in the duplex mode where the latter is used for navigation of the range gate and flow angle correction. Alternatively, spectral Doppler is displayed in the triplex mode with a B-mode image and color flow mapping.

A typical B-mode image consists of about 100 image lines. Whether the technique is color flow mapping, power Doppler or spectral Doppler, the axial velocity of the blood is found by imaging the same image line repeatedly. In spectral Doppler, the estimates are angle-corrected by the operator and presented as blood velocities plotted against time, denoted a spectrogram. In most commercial scanners Welch's method (WM) is used for estimation of the spectrogram [1,2]. To obtain an acceptable spectral resolution with WM, an observation window (OW) of up to 256 consecutive emissions for each velocity estimate is used [3]. This affects the temporal resolution in the spectrogram and the frame rate of the interleaved B-mode image. The temporal resolution of the spectrogram in conventional spectral Doppler can be impaired to the point where the rapid changes of blood velocities in the systole are difficult to measure. The events of upstroke, peak velocity and downstroke lie temporally so close that the different phases are merged together due to the long OW [4]. Likewise, the frame rate of the interleaved B-mode images can be decreased to the point where the examination is difficult to perform [3,5]. The operator can experience difficulties in placing the range gate in the vessel of interest as respiratory movements by the patient or involuntary transducer movements by the operator are not realized and corrected.

Alternative methods for fast velocity estimation have been proposed by several groups. Coats et al. used offline computation combined with a recursive spectral estimation approach [4], Tanaka et al. used selected phase information [6], Gran et al. proposed a method with frequency splitting using Barker and Golay code excitation [7], Oddershede et al. used multi-frequency encoding [8] and Jensen used sparse data sequences [9]. Another approach is adaptive filtering, which has previously been tested in simulations [10-12] and in phantom validation studies [13,14]. Only Herment et al. has produced examples of adaptive spectral filtration on *in-vivo* data [15].

In this paper two adaptive spectral filtering methods are validated *in-vivo* against the conventional WM for blood velocity estimation. The Blood spectral Power Capon method (BPC) based on a minimum variance estimator has been proposed by Stoica et al. [2,16], and the Blood spectral Amplitude and Phase Estimation the Blood spectral Amplitude and Phase Estimation method (BAPES) has been proposed by Gran et al. [17,18]. The algorithm used in BPC has previously been compared to the averaged periodogram used in the WM [19,20] and both BPC and BAPES have been evaluated in simulations using Field II [21], in a flow rig with steady laminar flow and in a single *in-vivo* experiment [18].

The purpose of this paper is to investigate the *in-vivo* performances of BPC and BAPES compared to WM. Ten volunteers were scanned on the common carotid artery. From each data set, spectrograms were found by using BPC, BAPES and WM on a series of different OWs. To investigate the methods quantitatively, a spectrum at end-diastole was taken out for each spectrogram from which two parameters were calculated: the full-width-at-half-maximum (FWHM) and the ratio between main and side lobe levels. To investigate the estimates qualitatively, a prospective trial was conducted where all the spectrograms were randomized and presented to nine radiologists blinded to method and OW for visual evaluation.

MATERIALS AND METHODS

Volunteers

This prospective study was performed after approval by The Danish National Committee on Biomedical Research Ethics. Ten healthy volunteers (nine males and one female, mean age: 29.1 years, range: 24-36 years) entered the study after informed consent. The right common carotid artery was examined in all volunteers using US. All scans were carried out by an experienced radiologist.

Spectral estimators

WM is applied on data using two different weighting schemes to control contrast and resolution in the resulting spectrogram: WM with a Hanning window (W.HAN) and WM with a boxcar window (W.BOX) (Fig. 1). W.HAN is the preferred conventional spectral estimator. It is well known in digital signal processing [22] that due to Hanning weighting of data the resulting spectrogram has improved contrast at the expense of spectral resolution. On the contrary, spectrograms generated with the W.BOX approach have improved spectral resolution but decreased contrast compared to W.HAN.

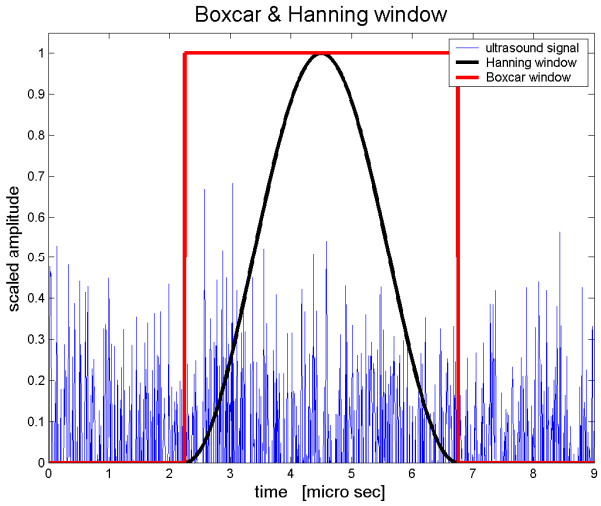

Figure 1: The scattered signal is multiplied in the time domain with a bell-shaped Hanning window or with a rectangular boxcar window. Thus, the blood signal used for velocity estimation is found under the curve corresponding to the chosen window.

BPC and BAPES are alternative methods using data-dependent adaptive filtering techniques based on a matched filterbank framework [2,23]. Unique filters are generated for each spectral velocity component and designed so the individual spectral velocity component is not distorted. Thereby, a unique filterbank is generated to each data set. In BPC the filters are designed to minimize the total power of the filtered data, while in BAPES the filters are designed to minimize the power of the filtered noise; including interfering signals, such as contributions from additional velocity components.

Setup

Ten healthy volunteers were scanned on the right common carotid artery using the experimental scanner RASMUS [24] and a B-K Medical 8804, 7 MHz linear array transducer. The setup is given in Table 1. One data set of approximately 2.5 seconds was recorded for each volunteer where the sequential data acquisition alternated between a sequence for flow estimation of 3800 consecutive emissions and a sequence for B-mode imaging of 65 consecutive emissions. The recorded data was

post processed using the four different methods: W.HAN, W.BOX, BPC and BAPES. For each method, spectrograms were estimated using different OWs: 128, 64, 32, 16, 8, 4 and 2 emissions/estimate. Hence, 28 spectrograms were calculated from every data set giving in total 280 spectrograms for all volunteers. Post processing was done offline with MATLAB (Mathworks, Natick, MA, USA) on a 100 CPU Linux cluster.

Parameter	Value	Unit
Sampling frequency	40	MHz
Center frequency	7	MHz
Pulse repetition frequency	9.3	kHz
Number of transmitting elements	64	elements
Apodization in transmit	Uniform	N/A
Number of receiving elements	64	elements
Apodization in receive	Hanning	N/A

Table 1: Scanner and transducer setup

Quantitative evaluation

To investigate the methods quantitatively, a spectrum at end-diastole was found for each spectrogram. For each data set, the time instant was chosen by visually examining the spectrogram obtained with W.HAN at OW 128. To the chosen time, spectra to all 28 spectrograms of the same data set were found. End-diastole was chosen to be the time of interest as it is easy to identify and used clinically for calculating e.g. resistive index [25]. From each spectrum, two parameters were calculated: the FWHM and the ratio between main and side lobe levels. The FWHM was found as the width of the velocity distribution of the main lobe at half of the maximum amplitude given in m/s. Thus, the FWHM is a measure of spectral resolution. The ratio was found as the relative difference between the side-lobe level and the peak amplitude. The side-lobe level was found as the median value of the distributed amplitudes outside the main-lobe, outlined by the FWHM. The ratio, given in decibel (dB), is a measure of contrast in the spectrogram.

Qualitative evaluation

To investigate the methods qualitatively, nine experienced radiologists evaluated in a blinded trial the 280 randomized spectrograms by scoring each spectrogram useful or not useful. Intra- and inter-observer variations were additionally found. The intra-observer variability was assessed by comparing the scores given twice by three radiologists with >14 days between each session. The sequence of spectrograms was randomized to each session so judgement bias was minimized.

Statistics

A descriptive statistical analysis was computed on FWHM and ratio data of the 280 spectra finding mean value and standard deviation for each combination of method and window. The scores given by the radiologists were pooled by method and window. Useful and not useful were coded with the dummy variables 1 and 0, respectively. Before data analysis, Kolmogorov-Smirnov normality test and the Levene variance homogeneity test were applied to the data. No data transformation was needed. Bonferroni adjusted tests for multiple comparisons paired on volunteer level with $p<0.05$ considered significant were performed [26]. The intra- and inter-observer variability were investigated using Cohen's and Fleiss' kappa, respectively [27,28]. Statistical analyses were performed using SAS (SAS Institute, Cary, NC, USA) and MATLAB (Mathworks, Natick, MA, USA).

RESULTS

From the same data set with three systoles recorded, examples of spectrograms, which were obtained with the four methods at OW 128 and 16, are presented (Fig. 2). The gaps in the

spectrograms represent the necessary pulse emissions used for generating the interleaved B-mode images. Examples of spectra obtained from the spectrograms shown in Fig. 2 at end-diastole to time 2.2 s are presented in Fig. 3. Mean and standard deviation of FWHM and ratio for the 280 spectra pooled by method and window are displayed in Table 2 and plotted in Fig. 4. The overall result of the scores given for each combination of method and window is displayed in Table 3 and illustrated in Fig. 5. The result of the Bonferroni adjusted tests for multiple comparisons paired on volunteer level is shown in Table 4 and illustrated in Fig. 6.

For each method, tests for multiple comparisons were also used to investigate at which OWs the given scores were significantly different from the score given at OW 128. W.BOX performed significantly worse when OW was reduced to 64 compared to W.BOX at OW 128 (p=0.03). W.HAN was not scored differently when reducing OW to 64 (p=0.55) but was scored significantly less at OW 32 (p <0.0001). BPC performed equally well at OW 32 compared to OW 128 (p=0.30) while BAPES scored significantly higher at OW 32 compared to OW 128 (p=0.02). Only BAPES performed as well for OW 16 as at OW 128 (p = 0.55). All four methods had decreased performances at OW 8, 4 and 2 compared to OW 128. The intra-observer variability for three radiologist evaluating the same 280 spectrograms with >14 days apart showed good agreement with an averaged Cohen's kappa value of 0.79 (94%, κ=0.88; 83%, κ=0.67; 93%, κ=0.81). The inter-observer variability showed moderate agreement using Fleiss' kappa (78%, κ=0.57).

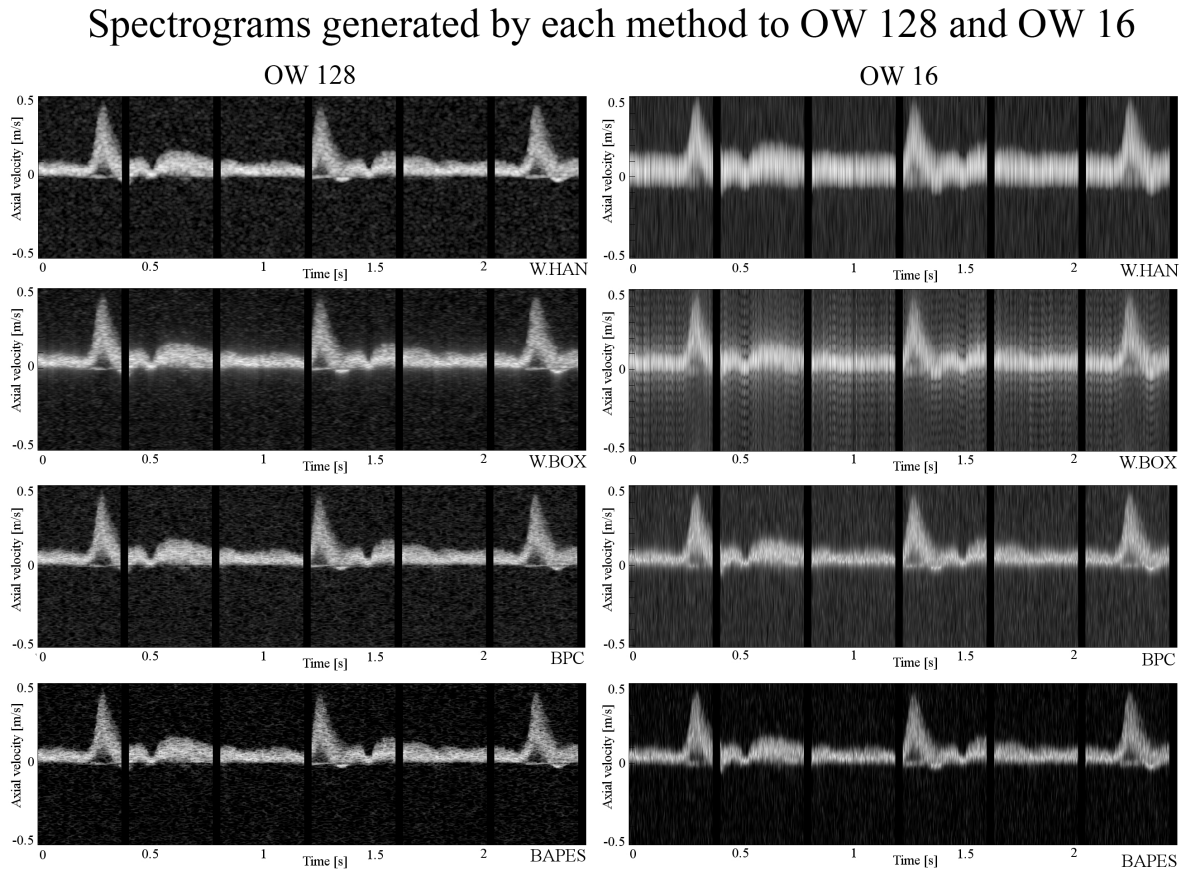

Figure 2: Spectrograms were found using the four methods with an OW 128 (left frames) and 16 (right frames). At OW 128 all methods displayed good performances. At OW 16, W.HAN and W.BOX estimated spectrograms with decreased quality compared to BPC and BAPES.

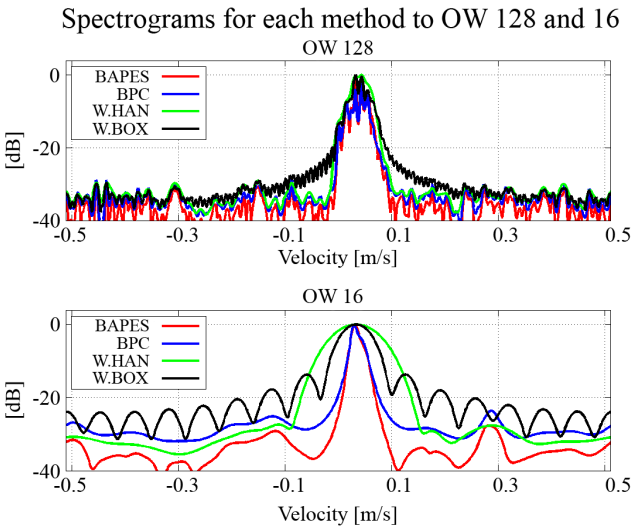

Figure 3: From the same volunteer at one time instant, spectra were generated using the four methods with an OW 128 and 16.

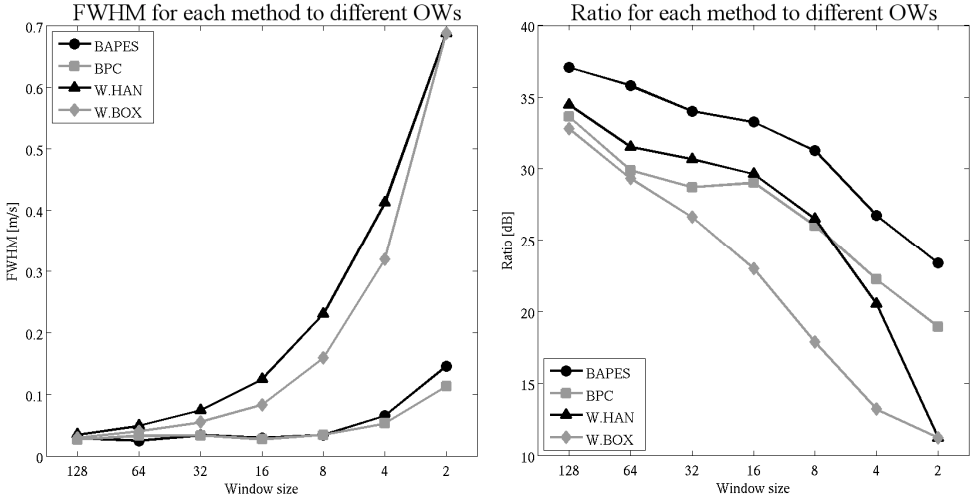

Figure 4: FWHM (left frame) and ratio (right frame) are plotted against OW for each method.

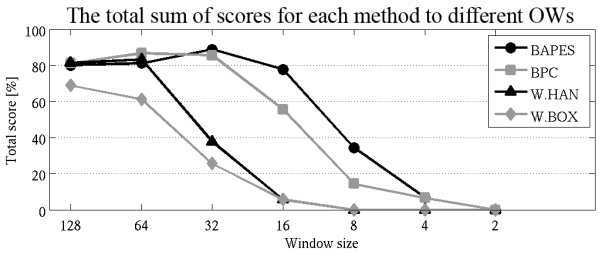

Figure 5: The total sum of scores in percentage for each method to different OWs

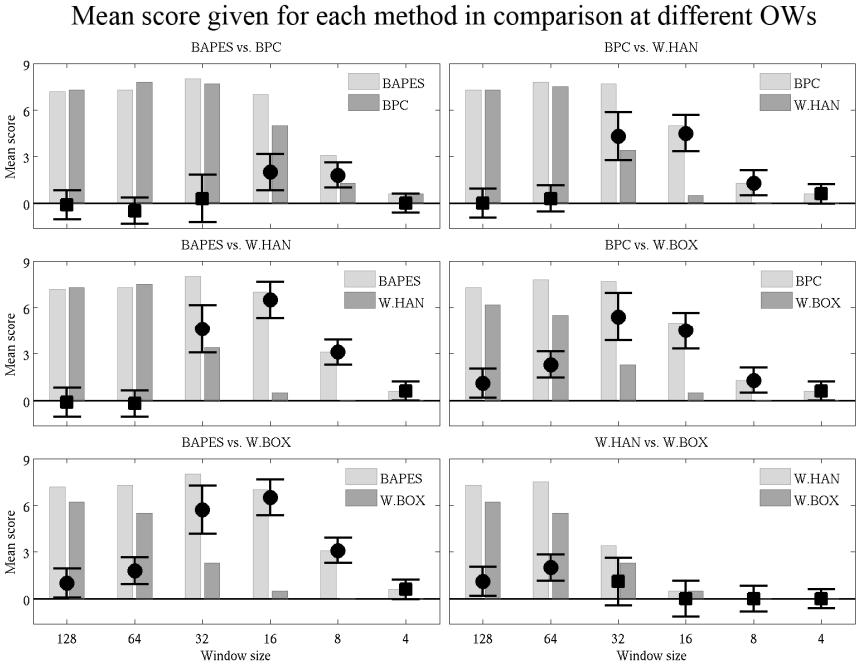

Figure 6: The mean of scores for each method in comparison over different OWs is shown with a histogram. The 95% confidence interval for the difference in means is shown as a bar and marked with a "■" if insignificant or with a "●" if significant. Comparisons to OW 2 are left out.

OW	Parameter	BAPES	BPC	W.HAN	W.BOX
128	FWHM [m/s]	0.029 (0.01)	0.026 (0.01)	0.034 (0.01)	0.029 (0.01)
	ratio [dB]	37.06 (3.19)	33.64 (3.16)	34.47 (3.20)	32.80 (2.45)
64	FWHM [m/s]	0.025 (0.01)	0.032 (0.01)	0.050 (0.01)	0.040 (0.01)
	ratio [dB]	35.81 (3.91)	29.89 (2.76)	31.53 (2.63)	29.31 (1.87)
32	FWHM [m/s]	0.034 (0.02)	0.033 (0.02)	0.074 (0.01)	0.055 (0.01)
	ratio [dB]	34.02 (4.47)	28.71 (2.94)	30.67 (4.63)	26.60 (2.25)
16	FWHM [m/s]	0.029 (0.01)	0.027 (0.01)	0.124 (0.00)	0.082 (0.01)
	ratio [dB]	33.27 (5.24)	29.03 (4.41)	29.63 (5.81)	22.99 (1.73)
8	FWHM [m/s]	0.034 (0.01)	0.033 (0.02)	0.230 (0.00)	0.159 (0.01)
	ratio [dB]	31.26 (5.17)	26.01 (4.18)	26.49 (5.33)	17.85 (0.81)
4	FWHM [m/s]	0.065 (0.02)	0.053 (0.03)	0.412 (0.01)	0.319 (0.00)
	ratio [dB]	26.73 (4.73)	22.23 (4.01)	20.51 (3.29)	13.20 (0.60)
2	FWHM [m/s]	0.145 (0.03)	0.113 (0.06)	0.688 (0.01)	0.688 (0.01)
	ratio [dB]	23.38 (4.13)	18.94 (4.18)	11.21 (0.51)	11.21 (0.51)

Table 2: Mean (and standard deviation) of FWHM and ratio given for each combination OW/method over ten volunteers.

OW	BAPES	BPC	W.HAN	W.BOX
128	72 (80 %)	73 (81.1 %)	73 (81.1 %)	62 (68.9 %)
64	73 (81.1 %)	78 (86.7 %)	75 (83.3 %)	55 (61.1 %)
32	80 (88.9 %)	77 (85.6 %)	34 (37.8 %)	23 (25.6 %)
16	70 (77.8 %)	50 (55.6 %)	5 (5.6 %)	5 (5.6 %)
8	31 (34.4 %)	13 (14.4 %)	0 (0.0 %)	0 (0.0 %)
4	6 (6.7 %)	6 (6.7 %)	0 (0.0 %)	0 (0.0 %)
2	0 (0.0 %)	0 (0.0 %)	0 (0.0 %)	0 (0.0 %)

Table 3: Each cell consists of the total sum of scores given by nine radiologists on 10 volunteers in the range 0 to 90 (and percentage) for the combination method/OW.

	BAPES	BPC	W.HAN	W.BOX	95% CI	p-value
128 emissions/estimate	7.2 (0.91)	7.3 (0.65)	7.3 (0.95)	6.2 (1.23)		
BAPES vs. BPC	x	x			(-1.03;0.83)	1.0
BAPES vs. W.HAN	x		x		(-1.03;0.83)	1.0
BAPES vs. W.BOX	x			x	(0.07;1.93)	0.03 ●
BPC vs. W.HAN		x	x		(-0.93;0.93)	1.0
BPC vs. W.BOX		x		x	(0.17;2.03)	0.01 ●
W.HAN vs. W.BOX			x	x	(0.17;2.03)	0.01 ●
64 emissions/estimate	7.3 (0.82)	7.8 (0.79)	7.5 (0.97)	5.5 (0.71)		
BAPES vs. BPC	x	x			(-1.34;0.35)	0.63
BAPES vs. W.HAN	x		x		(-1.04;0.64)	1.0
BAPES vs. W.BOX	x			x	(0.95;2.65)	<0.0001 ●
BPC vs. W.HAN		x	x		(-0.54;1.15)	1.0
BPC vs. W.BOX		x		x	(1.45;3.15)	<0.0001 ●
W.HAN vs. W.BOX			x	x	(1.15;2.85)	<0.0001 ●
32 emissions/estimate	8.0 (0.94)	7.7 (1.25)	3.4 (1.51)	2.3 (1.25)		
BAPES vs. BPC	x	x			(-1.24;1.84)	1.0
BAPES vs. W.HAN	x		x		(3.06;6.14)	<0.0001 ●
BAPES vs. W.BOX	x			x	(4.16;7.24)	<0.0001 ●
BPC vs. W.HAN		x	x		(2.76;5.84)	<0.0001 ●
BPC vs. W.BOX		x		x	(3.86;6.94)	<0.0001 ●
W.HAN vs. W.BOX			x	x	(-0.44;2.64)	0.31
16 emissions/estimate	7.0 (1.15)	5.0 (1.15)	0.5 (0.53)	0.5 (0.53)		
BAPES vs. BPC	x	x			(0.84;3.16)	0.0002 ●
BAPES vs. W.HAN	x		x		(5.34;7.66)	<0.0001 ●
BAPES vs. W.BOX	x			x	(5.34;7.66)	<0.0001 ●
BPC vs. W.HAN		x	x		(3.34;5.66)	<0.0001 ●
BPC vs. W.BOX		x		x	(3.34;5.66)	<0.0001 ●
W.HAN vs. W.BOX			x	x	(-1.16;1.16)	1.0
8 emissions/estimate	3.1 (1.10)	1.3 (0.94)	0 (0)	0 (0)		
BAPES vs. BPC	x	x			(0.99;2.61)	<0.0001 ●
BAPES vs. W.HAN	x		x		(2.29;3.91)	<0.0001 ●
BAPES vs. W.BOX	x			x	(2.29;3.91)	<0.0001 ●
BPC vs. W.HAN		x	x		(0.49;2.11)	0.0006 ●
BPC vs. W.BOX		x		x	(0.49;2.11)	0.0006 ●
W.HAN vs. W.BOX			x	x	(-0.81;0.81)	1.0
4 emissions/estimate	0.6 (0.84)	0.6 (0.70)	0 (0)	0 (0)		
BAPES vs. BPC	x	x			(-0.62;0.62)	1.0
BAPES vs. W.HAN	x		x		(-0.02;1.21)	0.062
BAPES vs. W.BOX	x			x	(-0.02;1.21)	0.062
BPC vs. W.HAN		x	x		(-0.02;1.21)	0.062
BPC vs. W.BOX		x		x	(-0.02;1.21)	0.062
W.HAN vs. W.BOX			x	x	(-0.62;0.62)	1.0
2 emissions/estimate	0 (0)	0(0)	0(0)	0(0)		

Table 4: The mean of scores is given on volunteer level in the range 0 to 9 (and standard deviation) for each combination method/OW indicated by "x". For each OW, comparison tests were performed with 95% CI in difference of means and p-value given. Significant findings are marked by a "●". No comparison is done for OW 2 as all methods were scored useless.

DISCUSSION

FWHM given in m/s is a measure of spectral resolution and should be as low as possible, while the ratio given in dB is a measure of spectral contrast and should be as high as possible. It is seen in Table 2 and Fig. 4 that on average for all OWs above 2, W.BOX performed with better resolution than W.HAN and W.HAN performed with better contrast than W.BOX. The adaptive methods outperformed WM in terms of resolution at all OWs below 128 and it is seen that BPC had a slightly better resolution than BAPES. In terms of contrast, BAPES was superior compared to both BPC and WM for all OWs. The W.HAN had better contrast than BPC for all OWs above 8.

In Fig. 2 examples of acquired spectrograms obtained with the four approaches at OW 128 and 16 are shown. Spectral resolution in the spectrogram corresponds to the width of the white curve representing estimated blood velocities, while the difference between the white curve and the dark surroundings corresponds to contrast. The spectrograms underline the results of the quantitative tests. At OW 128 the four approaches produced spectrograms of good quality while the estimators differed in performance at OW 16. At OW 16, it is seen that W.BOX estimated with a higher spectral resolution than W.HAN and the adaptive methods with higher spectral resolution than WM. Furthermore, it is seen that the contrast decreased from BAPES to BPC and WM. W.BOX performed poorest among the four methods in terms of contrast and a so-called ringing phenomenon at OW 16 can be seen.

Spectra for the methods are shown in Fig. 3. The side lobes representing leakage from the true velocity were suppressed, while the main lobe representing the true velocity was broadened for W.HAN compared to W.BOX. The pronounced side lobes for W.BOX at OW 16 correspond to the ringing phenomenon shown in Fig. 2. The adaptive methods had a narrower main lobe at OW 16 compared to WM and BAPES displayed better side lobe levels compared to both BPC and WM.

The overall result of the qualitative evaluation displayed in Table 3 and Fig. 5 shows that the radiologists preferred the adaptive methods over WM, BAPES over BPC and W.HAN over W.BOX. The inter- and intra-observer variability were additionally tested and showed moderate and good agreement, respectively, indicating consistent scores given by each radiologists with a base-line difference among the radiologists. In Table 4 and Fig. 6 the results of the statistical analyses on the mean of scores using Bonferroni adjusted tests for multiple comparisons are displayed. It is seen that at OW 128 and 64, BAPES, BPC and W.HAN performed equally well while W.BOX scored significantly less. When reducing the OW to 32, the adaptive methods BAPES and BPC performed better than W.HAN and W.BOX. However, BAPES was superior to BPC at OW 16 and 8. At OW 16 and 8 the conventional methods were scored useless. When the OW was decreased to 4 and 2 all four methods failed according to the radiologists.

For each method, the scores given at window sizes below OW 128 were compared to the score given at OW 128 to evaluate how robust each method was to reduction of OW. At OW 64 only W.BOX scored significantly worse, while W.HAN significantly decreased in score at OW 32. At OW 32, BPC scored as at OW 128 while BAPES actually scored significantly better. At OW 16, only BAPES was scored equal to OW 128. Hence, W.HAN at OW 64, BPC at 32 and BAPES at 16 can produce spectrograms, according to the nine radiologists, which are as acceptable as if they were produced at OW 128.

Moreover, the radiologists preferred contrast to spectral resolution when comparing scores given for W.BOX and W.HAN at OW 128 and 64 and in most modern scanners the Hanning weighting scheme is accordingly implemented for spectral blood estimation. However, when comparing BPC and W.HAN the improved resolution in BPC was preferred to the improved contrast in W.HAN. This is seen in Table 4 and Fig. 6 at OW 32 and 16. It indicates that it is not only the raised side lobe level in W.BOX, which reduces the quality of the spectrogram compared to W.HAN but also the accompanying ringing phenomenon.

Finally, the radiologists significantly preferred BAPES at OW 32 compared to BAPES at OW 128 ($p = 0.01$). The reason could be that the observers were disturbed visually by the high contrast and

spectral resolution of the spectrograms obtained with BAPES/OW 128 and somewhat preferred the smoothing of details as presented in spectrograms obtained with BAPES/OW 32.

The US examination of today can potentially be improved if the conventional WM for blood velocity estimation used in commercial scanners was to be replaced with one of adaptive spectral estimators BPC or BAPES. Consequently, either the temporal resolution of the spectrogram could be increased to obtain more information of the blood velocity profile, or the frame rate for the interleaved B-mode image could be increased to facilitate navigation under US examination. According to Gran et al. (2009), the adaptive methods are more computationally demanding than the conventional WM, and BAPES is more computationally heavy than BPC. However, when reducing the OW, the computational costs decrease as well. Therefore, the BAPES method implemented with an OW 16 or the BPC method with an OW 32 may be as tractable as WM with a much longer OW. It should therefore be possible to implement the methods into commercial scanners and convert the methods to an actual real-time modality.

CONCLUSION

In this paper the performances of two adaptive spectral estimators BPC and BAPES were investigated *in-vivo*. It was shown that the adaptive methods were superior to the conventional WM and that BAPES was superior to BPC. The quantitative tests showed that BAPES and BPC had improved spectral resolution and BAPES had improved spectral contrast compared to WM. According to the given scores given by nine radiologists, OW can be reduced to 32 when using BPC, and 16 when using BAPES method for estimating spectrogram without losing performance. The results indicate that the adaptive methods BPC and BAPES potentially can bring improvements to spectral blood estimation as an increase of the temporal resolution of the spectrogram or as an increase of the frame rate for the interleaved B-mode image. Further studies are needed to evaluate the adaptive spectral estimators in various *in-vivo* settings with different flow profiles, vessel geometries and scan depths using different transducers.

REFERENCE LIST

[1] P. D. Welch, The use of fast Fourier transform for the estimation of power spectra: A method based on time averaging over short, modified periodograms, IEEE Trans Audio Electroacoust., AU-15 (1967) 70-73.

[2] P. Stoica and R. Moses, Spectral analysis of signals, Prentice Hall, Upper Saddle River, N.J. 2005.

[3] J. B. Kruskal, P. A. Newman, L. G. Sammons, and R. A. Kane, Optimizing Doppler and color flow US: Application to hepatic sonography, Radiographics, 24 (2004) 657-675.

[4] A. J. S. Coats, C. Murphy, J. Conway, and P. Sleight, Validation of the beat to beat measurement of blood velocity in the human ascending aorta by a new high temporal resolution Doppler ultrasound spectral analyser, Br. Heart J, 68 (1992) 223-229.

[5] K. Ferrara and G. DeAngelis, Color flow mapping, Ultrasound Med Biol, 23 (1997) 321-345.

[6] N. Tanaka and S. Ohtsuki, Estimation of Doppler shift frequency using selected phase information for high frame rate color flow mapping, Journal of Medical Ultrasonics, 31 (2004) 5-12.

[7] F. Gran, J. Udesen, M. B. Nielsen, and J. A. Jensen, Coded ultrasound for blood flow estimation using subband processing, IEEE Trans Ultrason Ferroelec Freq Contr, 55 (2009) 2211-2220.

[8] N. Oddershede, F. Gran, and J. A. Jensen, Multi-frequency encoding for fast color flow or quadroplex imaging, IEEE Trans Ultrason Ferroelectr. Freq Control, 55 (2008) 778-786.

[9] J. A. Jensen, Spectral velocity estimation in ultrasound using sparse data sets, J Acoust Soc Am, 120 (2006) 211-220.

[10] J. Li and P. Stoica, An adaptive filtering approach to spectral estimation and SAR imaging, IEEE Transactions on Signal Processing, 44 (1996) 1469-1484.

[11] N. Feng, J. Zhang, and W. Wang, An adaptive clutter rejection method based on AR model in color flow imaging, ultrasonics, 44 Suppl 1 (2006) e85-e88.

[12] P. D. Wang, Y. Shen, and N. Z. Feng, A novel clutter rejection scheme in color flow imaging, ultrasonics, 44 Suppl 1 (2006) e303-e305.

[13] M. E. Allam and J. F. Greenleaf, Isomorphism between pulsed-wave Doppler ultrasound and direction-of-arrival estimation - part I: Basic principles, IEEE Trans Ultrason Ferroelec Freq Contr, 43 (1996) 911-922.

[14] M. E. Allam, R. R. Kinnick, and J. F. Greenleaf, Isomorphism between pulsed-wave Doppler ultrasound and direction-of-arrival estimation - part II: Experimental results, IEEE Trans Ultrason Ferroelec Freq Contr, 43 (1996) 923-935.

[15] A. Herment and J. F. Giovannelli, An adaptive approach to computing the spectrum and mean frequency of Doppler signals, Ultrason Imaging, 17 (1995) 1-26.

[16] P. Stoica and R. Moses, Introduction to spectral analysis, Prentice Hall, Upper Saddle River, N.J 1997.

[17] F. Gran, A. Jakobsson, and J. A. Jensen, Adaptive blood velocity estimation in medical ultrasound, Proc IEEE ICASSP, 1 (2007) 293-296.

[18] F. Gran, A. Jakobsson, and J. A. Jensen, Adaptive spectral Doppler estimation, IEEE Trans Ultrason Ferroelec Freq Contr, 56 (2009) 700-714.

[19] P. J. Vaikus and R. S. C. Cobbold, A comparative study and assessment of Doppler ultrasound spectral estimation techniques, Part 1: Estimation methods, Ultrasound Med Biol, 14 (1988) 661-672.

[20] P. J. Vaikus, R. S. C. Cobbold, and K. W. Johnston, A comparative study and assessment of Doppler ultrasound spectral estimation techniques, Part 2: Methods and results, Ultrasound Med Biol, 14 (1988) 673-688.

[21] J. A. Jensen and N. B. Svendsen, Calculation of pressure fields from arbitrarily shaped, apodized, and excited ultrasound transducers, IEEE Trans Ultrason Ferroelec Freq Contr, 39 (1992) 262-267.

[22] J. G. Proakis and D. G. Manolakis, Digital signal processing: Principles, algorithms and applications, Prentice Hall, Upper Saddle River, N.J. 2007.
[23] P. Stoica, A. Jakobsson, and J. Li, Matched-filterbank interpretation of some spectral estimators, Signal Processing, 66 (1998) 45-59.
[24] J. A. Jensen, O. Holm, L. J. Jensen, H. Bendsen, S. Nikolov, B. G. Tomov, P. Munk, M. Hansen, K. Salomonsen, J. Hansen, K. Gormsen, H. M. Pedersen, and K. L. Gammelmark, Ultrasound research scanner for real-time synthetic aperture image acquisition, IEEE Trans Ultrason Ferroelec Freq Contr, 52 (2005) 881-891.
[25] M. E. Tublin, R. O. Bude, and J. F. Platt, Review. The resistive index in renal Doppler sonography: where do we stand?, AJR Am J Roentgenol, 180 (2003) 885-892.
[26] D. G. Altman, Practical statistics for medical research, Chapmann & Hall/CRC, London 1991.
[27] J. R. Landis and G. G. Koch, The measurement of observer agreement for categorical data, Biometrics, 33 (1977) 159-174.
[28] J. L. Fleiss, Measuring nominal scale agreement among many raters, Psychol. Bull., 76 (1971) 378-382.

Appendix V

Validation of Transverse Oscillation Vector Velocity Estimation *In-Vivo*

Hansen K.L.[(1)], Udesen J. [(1)], Thomsen C. [(1)], Jensen J.A. [(2)], Nielsen M.B. [(1)]

1) Department of Radiology, Rigshospitalet, Blegdamsvej 9, DK-2100 Kbh. Ø, Denmark.
2) Center for Fast Ultrasound Imaging, Ørsted DTU, Bldg. 348, Technical University of Denmark, DK-2800 Lyngby, Denmark.

***Abstract*-Conventional Doppler methods for blood velocity estimation only estimate the velocity component along the ultrasound (US) beam direction. This implies that a Doppler angle under examination close to 90° results in unreliable information about the true blood direction and blood velocity.**

The novel method Transverse Oscillation (TO), which combines estimates of the axial and the transverse velocity components in the scan plane, makes it possible to estimate the vector velocity of the blood regardless of the Doppler angle.

The present study evaluates the TO method with magnetic resonance angiography (MRA) by comparing *in-vivo* measurements of stroke volume (SV) obtained from the right common carotid artery. Angle of insonation was 90° for the TO measurements. Eleven healthy volunteers were scanned with the TO method and MRA. The overall results were as follows: mean SV +/- STD for TO: 5.5 ml +/- 1.7 ml and for MRA: 5.8 ml +/- 2.0 ml with the full range for TO: 3.4 ml – 9.5 ml and for MRA 3.0 ml – 10.8 ml. The correlation between the SV estimated by TO and MRA was 0.91 ($p < 0.01$; 95 % CI: 0.69 to 0.98) with the equation for the line of regression MRA = 1.1•TO - 0.4. A Bland-Altman plot was constructed where the mean difference was 0.2 ml with limits of agreement at -1.4 ml and 1.9 ml (95 % CI for mean difference: -0.3 ml to 0.8 ml). The strong correlation and the low mean difference between the TO method and MRA indicates that reliable vector velocity estimates can be obtained *in vivo* using the presented angle independent 2-D vector velocity method. The results give reason to believe that the TO method can be a useful alternative to conventional Doppler systems bringing forth new information to the US examination of blood flow.

I. Introduction

The clinical US scanners today perform blood velocity estimation by using the autocorrelation approach where the actual velocity is a projection onto the US beam direction. However, the inherent limitations of the conventional Doppler system give rise to unreliable velocity estimations when the angle between the beam direction and the flow approaches 90° [1].

To circumvent the angle dependency, the promising TO method for vector velocity estimation has been proposed by Jensen and Munk [2-4] and a similar approach by Anderson [5]. The method introduces, along with the axial oscillation, an additional oscillation in the lateral direction of the pulse-echo field. The measured signals are therefore sensitive to both an axial and a transverse motion. Using special autocorrelation estimators [3], the axial and transverse velocity components can be determined to achieve angle independent 2D blood velocity estimates. Thus, the problem of conventional color Doppler in achieving a sufficient angle of insonation is alleviated.

The TO method has previously been evaluated in simulations and flow-phantoms [6;7] and examples of *in-vivo* sequences have been produced of the carotid artery [8;9]. However, the TO method has not yet been evaluated in a clinical study and performance compared to an independently and reliable velocity estimator.

In this paper the volume flow in the common carotid artery estimated with the TO method, is compared to volume flow measurement estimated with MRA. MRA is accepted as a gold standard for the quantification of the cerebral blood flow [10]. Furthermore, the assumptions of circular geometry of the examined vessel and rotationally symmetric blood flow used in the calculation of TO volume flow estimation were tested.

II. Materials and Methods

A. Patients

This prospective study was performed after approval by The Danish National Committee on Biomedical Research Ethics (Date:30-05-06, J.nr:(KF)07, 307579). Eleven healthy volunteers (seven males and four females, 24 – 44 years old, mean age: 32 years) entered the study after informed consent. The right common carotid artery was examined in all volunteers using US and MRA on two different days. The volunteer rested supine on the examination table 15 minutes before both examinations. All scans were carried out by an experienced radiologist.

B. Theory

The basis for vector velocity measuring with the TO method has been described previously [2-4;7]. In brief, the motion in the transverse direction is found by creating a double oscillation (an axial oscillation and a transverse oscillation) in the pulse-echo field from which two different frequencies can be found. The two frequencies can be manipulated to give the transverse vector velocity. The axial vector velocity is found exactly as in conventional Doppler systems from an axial oscillation. The two vector velocities, found from the same data set by changing the receive beamforming and using a special estimator, are combined to yield the 2D vector velocity of the moving scatterers. The emitted pulse giving rise to the two vector velocity components is identical to the pulse used in conventional US Doppler system. Details about the

measurement setup are described by Udesen et al. [9] and the estimators are described by Jensen [3].

C. TO setup

The recorded sequences of vector velocity images (VVI) were obtained with the experimental scanner RASMUS [11] and a linear array transducer both described by the parameters depicted in Table I. The post processing was performed with MATLAB 6.5 (Mathworks, Natick, MA, USA). All sequences of VVI were obtained from the right common carotid artery of the volunteers with angels of insonation of approximately 90°, i.e. when the conventional Doppler method fails to estimate any blood velocities. The vessel of interest was scanned approximately two cm upstream of the bifurcation to prevent confounding turbulence. For data analysis the stored 3 sec sequence was processed by an algorithm that automatically identified the vessel region in each frame from the B-mode image [9].

The volume flow per second in each VVI was estimated by integrating the delineated 2D vessel up to form a 3D vessel. The mean volume flow per second in each VVI was found as an average of the volume flows per second estimated to all different lateral positions in the VVI. This yielded a volume profile for every sequence. A detailed description of the calculations is given by Hansen et al [12].

D. MRA setup

MRA examinations were performed with a 1.5 T whole body scanner (Magnetom Vision, Siemens AG). A prospective ECG (electrocardiogram) triggered phase contrast sequence using a cervical coil was employed. Phase interval was 29 ms, pixel resolution 0.52 x 0.39 mm^2, FOV (field-of-view) 100 mm, slice thickness 6 mm and maximal velocity encoding V_{ENC} +/- 1.5 m/s.

TABLE I
SCANNER AND TRANSDUCER SETUP

Transducer	Linear array, BK 8812
Center frequency	5 MHz
Number of cycles pr. Pulse	8 cycles/pulse
Fprf	6 kHz
Sampling frequency	40 Mhz
Lateral wave length	1.0 mm
Apodization in transmit	Hanning
Apodization in receive	Two Hannings
Focus in transmit	18 mm
Focus in receive	Dynamic
F-number in transmit	3.3
F-number in receive	0.8
Number of firings pr. vel. est.	64 firings/vel. est.
Lateral distance between vel. est.	4 pitch
I_{spta}	293 mW/cm^2
MI	1.07
TIS	1.65

The scan plan for the volume flow measurements was selected to be perpendicular to the right common carotid artery and placed two cm upstream of the bifurcation as in TO. The volume flow estimation of the resulting MRA scanning was carried out in MATLAB 6.5 (Mathworks, Natick, MA, USA) using MRA DICOM (Digital Imaging and Communications in Medicine) formatted images. The MRA phase velocity maps (PVM) were recorded interleaved with anatomic images.

For every frame of the anatomic sequence, the circumferential vessel wall was computed by defining a threshold pixel value. The volume flow per second was calculated using the window on the corresponding PVM by adding all the pixel values within the vessel and multiplying with pixel area. Another region near the vessel on the flow sequence was selected to correct the phase off-set [13].

E. Assumption

When calculating the blood flow from VVI of the TO method, assumptions of circular geometry and rotationally symmetric blood flow are obligatory. The assumptions were tested by taking out lines from the MRA PVM for every angle. The lines of vector velocities were computed as if they were obtained with TO. Thus, for every angle a SV was calculated. This yielded a SV range for every volunteer which was compared to the actual MRA SV measurement where no assumptions were made.

F. Comparison

The comparison of the achieved volume flow profiles was made with respect to SV. This variable is less heart rate dependent and, thus, a more reliable parameter when comparing measurements obtained at two different occasions [14]. In ref. [12] the calculations of SV are detailed.

G. Statistics

An elementary statistical analysis was computed on the SV data for the two modalities finding mean value, standard deviation and SV range. The SV data obtained with TO were then compared to SV data obtained with MRA using linear regression analysis with two-tailed significance value given and $p<0.05$ considered significant. The correlation coefficient, regression equation, and confidence interval using Fisher's *r*-to-*z*-transformation were calculated. Finally a Bland-Altman plot was made to illustrate the difference of SV estimated by TO and MRA along with confidence intervals. All statistical analysis was performed within the MATLAB 6.5 (Mathworks, Natick, MA, USA) environment.

III. RESULTS

The mean SV +/- STD for TO was 5.5 ml +/- 1.7 ml with the range of 3.4 ml – 9.5 ml. Respective estimates for MRA was 5.8 ml +/- 2.0 ml with the range 3.0 ml – 10.8 ml.

The correlation between the SV estimated by TO and MRA is illustrated in Fig. 1 as a scatterplot. *R* was 0.91 ($p<0.01$; 95 % CI: 0.69 to 0.98) and the least squares (MRA = 1.1 * TO - 0.4) was found to be close to unity. The range of MRA SV

assuming rotationally symmetric flow and circular vessel geometry is shown as a bar for every volunteer in the scatterplot.

In Fig. 2 the Bland-Altman plot is constructed. The mean difference is 0.24 ml with limits of agreement at -1.41 ml and 1.90 ml (95 % CI for mean difference: -0.32 ml to 0.81 ml).

In Fig. 3 the ranges of SV as percentages of actual MRA SV for all volunteers are plotted giving a mean ratio of 24.3%. One volunteer presented a ratio between range of MRA SV and actual MRA SV of 48.3%. The angle dependent SV with a range of 3.2 ml to 5.1 ml for this volunteer is depicted in Fig 4. By examining the PVM of this particular volunteer, it was seen that a substantial asymmetric flow was present, while the vessel had approximately circular geometry.

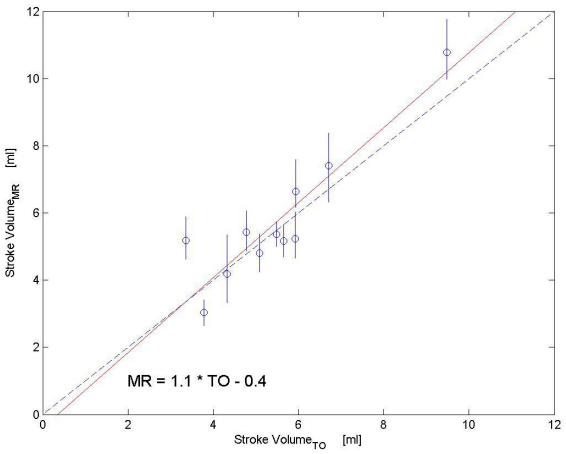

Figure 1. Correlation between MRA and TO. Line of best fit (solid line) and line of perfect fit (dashed line) are drawn. The range of MRA SV assuming circular geometry and rotationally symmetric flow is shown for every volunteer as a bar.

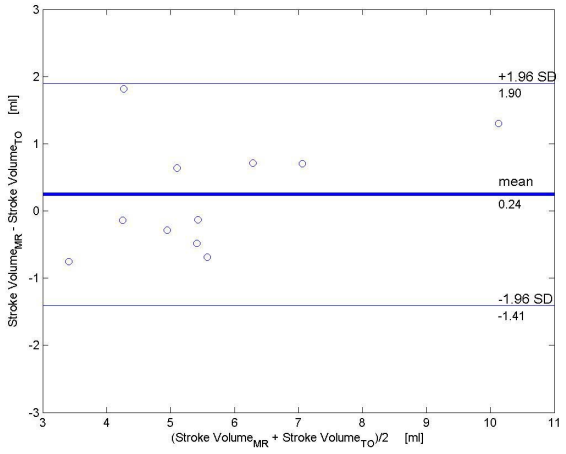

Figure 2. Bland-Altman plot of SV measured with MRA and TO showing mean (thick solid line) +/- 2 SD (thin solid line)

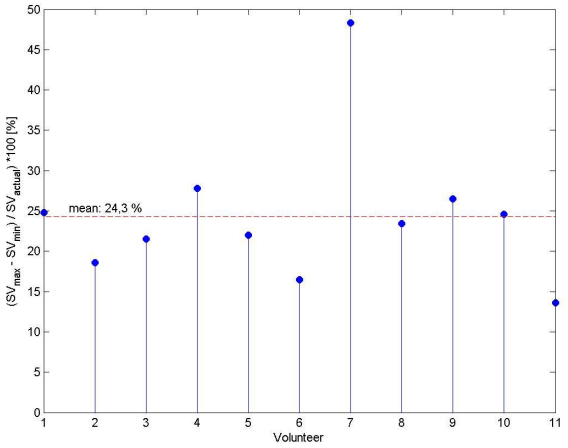

Figure 3. SV ratio was estimated by the range, found as the difference between the maximal and minimal angle dependent SV, divided with the actual MRA SV and given in percentage. The mean ratio was 24.3 %.

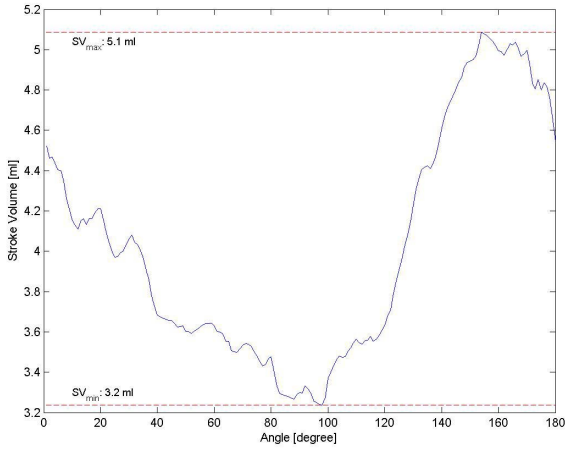

Figure 4. SV measured for every line of angle for one volunteer. The maximal and minimal angle dependent SV are shown as dashed lines.

IV. Discussion

The paper describes results of a comparison study between TO and MRA in an *in-vivo* setup. A strong linear correlation (R = 0.91, p<0.01) was found between the two modalities, when determining the SV in the right common carotid artery of 11 healthy volunteers. The TO underestimated the SV by 0.24 ml/stroke compared to MRA according to the Bland-Altman plot. Furthermore, the underestimation was illustrated by the slope of the regression equation (MRA = 1.1 * TO - 0.4). This is consistent with earlier results, which showed an underestimation of less than 10% for all angles between 50° to 90° [7]. Presumably one of the major reasons for the underestimation of SV obtained with TO is the stationary echo-cancelling filter, which cancels out echoes from stationary tissue. The blood scattterers with lowest vector velocities near the vessel boundaries are confounded with the stationary tissue and filtered out. Even though these vector velocities are

negligible, they correspond to a large cross sectional area and, thus, add up to a significant blood volume.

The common carotid artery was chosen as the vessel of interest, because it is usually a straight vessel and parallel to surface, which consequently favors an angle of insonation of 90°. Moreover, the vessel generally has a circular geometry and, thus, an expected symmetric flow profile. This was investigated and showed not to be the case for all 11 volunteers. There was a remarkable difference in SV over 180°, which shows that the assumption of circular geometry and rotationally symmetric flow profile is a simplification. By examining the different MRA PVM, it was evident that the asymmetric flow profile contributed far most in the angle dependent SV difference. Udesen found TO systematically to underestimate vector velocities in an experimental flow rig [7]. The estimates in this study found below the line of perfect fit in the scatterplot (Fig. 1) could be explained as an effect of the employed assumption which clearly gives rise to both under- and overestimation of the blood volume flow. For two volunteers the full range did not overlap the line of perfect fit while the estimates were found below the line. It indicates that the simplifying assumption of circular geometry and rotationally symmetric flow profile cannot entirely explain the differences between SV measured with TO and MRA.

To obtain reliable volume flow measurements by TO it was crucial to scan the vessel parallel to the longitudinal axis exactly through the middle of the vessel. According to the B-mode image where the diameter of the lumen was greatest and where *intima* most clearly was delineated. It is obvious that vessel *intima* is a reliable marker, when positioning the scan plane through the middle of the vessel. The layer structures are visible when the US beam direction is perpendicular to the planes of the layers. Vessels are not perfectly straight tubes so when scanning parallel to the longitudinal axis inevitably a part of the artery will be out of scan plane due to curvature. This results in slightly lowered averaged volume flow.

Also, it has to be taken into account that the heart rate, cardiac output, and SV alter between two consecutive scans. In this study up to one week occurred between compared TO and MRA scans. The SV is a more stable parameter to measure than cardiac output, but still it fluctuates and is to a certain point proportional to heart rate [14].

The limitation of this study is the small number of samples in the study population. This affects the correlation coefficient as well as the CI of all the statistical calculations. The examinations with the TO method are performed with the experimental scanner RASMUS [11] and calculated using MATLAB 6.5 (Mathworks, Natick, MA, USA) on a 100 CPU linux cluster. The cluster gives the most flexible environment for processing the data from an experimental point of view, but the processing time is considerable. One VVI sequence takes 3 sec to acquire, 10 hours to store and 48 hours to process. Obviously this affects the logistics and reduces the number of samples that can realistically be enrolled into the study population. However, TO is not a heavy method in terms of processing, since it is based on an autocorrelation estimator [1;2]. It should therefore be possible to implement the method into a commercial scanner and convert the method to an actual real-time modality.

V. Conclusion

Volume flow measurements were obtained *in-vivo* with the angle independent blood vector velocity method TO. The results validated against volume flow measurements obtained by MRA were found to be comparable for SV in terms of correlation coefficient and mean bias.

This study gives reason to believe that the TO method can be a useful alternative to conventional Doppler systems bringing forth new and relevant information to the US examination of the blood flow. However it remains to evaluate TO on a larger population using different transducers on different vessels at variable angles of insonation. Ultimately the TO method has to be evaluated on patients with existing pathology e.g. stenosis to conclude the usability of the method in clinical practice.

References

1] J. A. Jensen, *Estimation of Blood velocities using ultrasound: A signal processing approach*. New York: Cambridge University Press, 1996.

[2] J. A. Jensen and P. Munk, "A new method for estimation of velocity vectors," *IEEE Trans Ultrason Ferroelec Freq Contr*, vol. 45, pp. 837-851, 1998.

[3] J. A. Jensen, "A new estimator for vector velocity estimation," *IEEE Trans Ultrason Ferroelec Freq Contr*, vol. 48, pp. 886-894, 2001.

[4] P. Munk, *Estimation of the 2-D flow vector in ultrasonic imaging: a new approach. Master's thesis*.Copenhagen: Technical University of Denmark, 1996.

[5] M. E. Anderson, "Spatial quadrature: a novel technique for multidimensional velocity estimation," *Proc SPIE Med Imag*, pp. 1233-1238, 1997.

[6] J. Udesen and J. A. Jensen, "Experimantal investigation of transverse flow estimation using transverse oscillation," *Proc IEEE Ultrason Symp*, pp. 1586-1589, 2003.

[7] J. Udesen and J. A. Jensen, "Investigation of transverse oscillation method," *IEEE Trans Ultrason Ferroelec Freq Contr*, vol. 53, pp. 959-971, 2006.

[8] J. Udesen and J. A. Jensen, "An in-vivo investigation of transverse flow estimation," *Proc. SPIE - Progress in biomedical optics and imaging*, vol. 5373, pp. 307-314, 2004.

[9] J. Udesen, M. B. Nielsen, K. R. Nielsen, and J. A. Jensen, "Examples of In Vivo Blood vector velocity Estimation," *Ultrasound Med Biol*, vol. 33, pp. 541-548, 2007.

[10] S. O. Oktar, C. Yucel, D. Karaosmanoglu, K. Akkan, H. Ozdemir, N. Tokgoz, and T. Tali, "Blood-flow volume quantification in internal carotid and vertebral arteries: Comparison of 3 different ultrasound techniques with phase-contrast MR imaging," *AJNR Am J Neuroradiology*, vol. 27(2), pp. 363-369, 2006.

[11] J. A. Jensen, O. Holm, L. J. Jensen, H. Bendsen, S. Nikolov, B. G. Tomov, P. Munk, M. Hansen, K. Salomonsen, J. Hansen, K. Gormsen, H. M. Pedersen, and K. L. Gammelmark, "Ultrasound research scanner for realtime synthetic aperture image acquisition," *IEEE Trans Ultrason Ferroelec Freq Contr*, vol. 52, pp. 881-891, 2005.

[12] K. L. Hansen, J. Udesen, C. Thomsen, J. A. Jensen, and M. B. Nielsen, "In-vivo validation of Transverse Oscillation vector velocity estimation with MR angiography," *Ultrasound Med Biol*, submitted 2007.

[13] T. L. Chenevert, K. P. Fechner, and D. Y. Gelblum, "Improvements in MR angiography using phase-corrected data sets," *Magn Reson Med*, vol. 10, no. 1, pp. 38-49, Apr.1989.

[14] M. B. Higginbotham, K. G. Morris, S. Williams, P. A. McHale, R. E. Coleman, and F. R. Cobb, "Regulation of Stroke Volume during Submaximal and Maximal Upright Exercise in Normal Man," *Circ Res*, vol. 58, pp. 281-291, 1986.

Digital Object Identifier: 10.1109/ULTSYM.2008.0255

In-vivo evaluation of three ultrasound vector velocity techniques with MR angiography

Hansen K.L.[1,3], Udesen J.[2,3], Oddershede N.[2,3], Henze L.[3], Thomsen C.[1], Jensen J.A.[3], Nielsen M.B.[1]

1) Department of Radiology, Section of Ultrasound, Rigshospitalet, Blegdamsvej 9, 2100 Kbh. Ø, Denmark.
2) GN Resound, Lautrupsbjerg 9, 2750 Ballerup, Denmark.
3) Center for Fast Ultrasound Imaging, DTU Elektro, Bldg. 349, Technical University of Denmark, 2800 Lyngby, Denmark.

***Abstract* – In conventional Doppler ultrasound (US) the blood velocity is only estimated along the US beam direction. The estimate is angle corrected assuming laminar flow parallel to the vessel boundaries. As the flow in the vascular system never is purely laminar, the velocities estimated with conventional Doppler US are always incorrect. Three angle independent vector velocity methods are evaluated in this paper: directional beamforming (DB), synthetic aperture flow imaging (STA) and transverse oscillation (TO). The performances of the three methods were investigated by measuring the stroke volume in the right common carotid artery of eleven healthy volunteers, with magnetic resonance phase contrast angiography (MRA) as reference. The correlation between the three vector velocity methods and MRA were: DB/MRA R=0.84 (p<0.01); STA/MRA R=0.95 (p<0.01); TO/MRA R=0.91 (p<0.01). Bland-Altman plots were additionally constructed and mean differences for the three comparisons were: DB/MRA = 0.17 ml; STA/MRA = 0.07 ml; TO/MRA = 0.24 ml. The three US vector velocity techniques yield quantitative insight in to flow dynamics and can potentially give the clinician a powerful tool in cardiovascular disease assessment.**

I. Introduction

Magnetic resonance phase contrast angiography (MRA), and Doppler ultrasound (US) are the only non-invasive techniques for flow measurement in blood vessels. While the assessment of blood flow with MRA is time-consuming, the equipment is expensive and non-mobile, and the evaluation not performed in real time, Doppler US is an easily manageable and fast technique. The US equipment is mobile, relatively inexpensive, and evaluations are done in real time. However, one of the main limitations of the current Doppler systems is angle dependency which gives rise to incorrect estimates of velocity. It is impossible to predict the direction of a blood scatterer based on the B-mode image [1] as the flow profiles in the vascular system never are purely laminar and therefore impossible to angle correct.

Three different and promising vector velocity estimators have been suggested to alleviate the angle dependency found in conventional Doppler systems. The vector velocity methods are all characterized by the ability to estimate the instantaneous 2-D velocity of the blood scatterers in every point at every time to obtain quantitative velocity data. Directional beamforming (DB) was proposed by Jensen (2003), and Jensen and Bjerngaard (2003), synthetic transmit aperture flow imaging (STA) by Jensen and Nikolov (2002) and transverse oscillation (TO) by Jensen and Munk (1998).

The three vector velocity methods were validated *in-vivo* with MRA comparing volume flow in the right common carotid artery. MRA was chosen to be the reference as it is the gold standard for non-invasive cerebral blood flow measurement [6]. However, it should be noted that the true strength of the vector velocity techniques is expected to be in visualization of the non-laminar nature of blood flow.

II. Materials and Methods

A. Patients

This prospective study was performed after approval by The Danish National Committee on Biomedical Research Ethics. Eleven healthy volunteers (seven males and four females, mean age: 32 years, range: 24 – 44 years) entered the study after informed consent. The right common carotid artery was examined in all volunteers using US and MRA on four different days, using one full day for each ultrasound method.

B. Directional Beamforming

A focused pulse is emitted with the focal point placed below the region of interest (ROI) (Fig. 1a). Lines in ROI are beamformed along the flow direction. Cross-correlating the lines can directly give the displacement between emissions and, thus, the velocity [2;3]. The correct angle is found by searching all possible angles (for every 5º). The one with the highest correlation yields the correct flow angle as described by Kortbek and Jensen (2007).

C. Synthetic transmit aperture flow imaging

A STA image is acquired by emitting a spherical unfocused wave from a few elements and receiving the scattered signal with all elements. Since the position for the emission is known, the precise origin of the received scattered signal can be calculated from time-of-flight for all elements and used in focusing. The STA approach generates one low-resolution image for every emitted pulse. A high-resolution image is constructed by adding a number of consecutive low-resolution images. For every emission, a high-resolution image can be created by applying a recursive approach, where the oldest transmission event is replaced by the newest yielding a frame rate equal to pulse repetition frequency with focus in all image points.

An approach to estimate vector velocities, identical to DB is computed. Echo lines in a star-shaped pattern are created to

every point of interest and compared to find the right angle and magnitude of the motion. Details are given by Jensen and Oddershede (2006), and Oddershede and Jensen (2007).

D. Transverse Oscillation

The TO method tracks scatterer motion along two orthogonal axes by emitting a pulse identical to conventional Doppler. The motion along the *z*-axis is found exactly as in conventional Doppler US. An oscillation in the lateral direction is created by changing sensitivity of the receiving elements. The velocity along the *x*-axis is found from the phase shift in oscillation. By combining the velocity component along the *z*- and *x*-axis, vector velocities are achieved (Fig. 1b). Details are given by Udesen et al (2006).

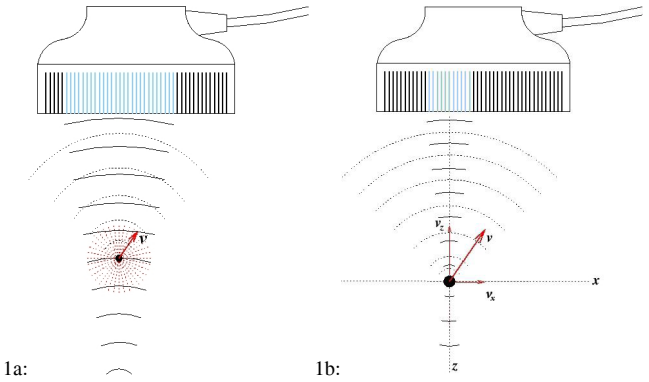

1a: 1b:

Figure 1: Magnitude and orientation of the scatterer motion are illustrated by the vector arrow v. The active elements in transmit are blue, the emitted signal is shown as solid black lines and the scattered signal as dotted black lines.

E. US setup

The vector velocity images (VVIs) obtained with the three US methods were recorded with the experimental scanner RASMUS [11]. The parameters for the three setups are shown in Table 1. The post processing was done offline with MATLAB 6.5 (Mathworks, Natick, MA, USA) on a 100 CPU Linux cluster.

TABLE I
SCANNER AND TRANSDUCER SETUP

	TO	DB	STA
Transducer (Linear array)	BK 8812	BK 8812	BK 8812
Center frequency	5 MHz	6.2 MHz	6.2 MHz
No. of cycles pr. pulse	8 cyc./puls	2 cyc./puls	2 cyc./puls
Fprf	6 kHz	6 kHz	21 kHz
Sampling frequency	40 MHz	40 MHz	40 MHz
Lateral wave length	1.0 mm	***	***
Apodization in transmit	Hanning	Hanning	Tukey
Apodization in receive	Two Hannings	Rectangular	Rectangular
Focus in transmit	18 mm	36 mm	None
Focus in receive	Dynamic	Dynamic	Dynamic
F-number in transmit	3.3	2.7	-0.75
F-number in receive	0.8	***	***
Lateral dist. between vel.est.	4 pitch	4 pitch	1 mm

All US sequences were recorded from the right common carotid artery two cm upstream of the bifurcation to prevent confounding turbulence. An identical approach was used for the three methods to calculate the volume flow from the recorded flow data. By knowing the vessel geometry in every frame, the vector velocity profiles could be calculated from the VVIs by setting the surroundings to zero and integrating the 2-D vessel up to form a 3-D vessel. This was only possible by assuming (i) circular vessel geometry, (ii) rotationally symmetric blood flow and (iii) a correctly placed window of insonation parallel to the longitudinally axis of the vessel, going exactly through the middle of the vessel. The volume flow to every frame was found by averaging over the whole image, thus, yielding a volume flow profile to every sequence.

F. MRA setup

MRA examinations were performed with a 1.5 T whole body scanner (Magnetom Vision, Siemens AG). A prospective ECG triggered phase contrast sequence using a cervical coil was employed. (Phase interval: 29 ms, echo time: 7 ms, flip angle: 30°, FOV: 100 mm, slice thickness: 6 mm, V_{ENC}: +/-1.5 m/s, , pixel resolution: 0.52 x 0.39 mm^2 in a matrix of 192 x 256 pixels interpolated up to 256 x 256 pixels).

The scan plane for the volume flow measurements was selected to be perpendicular to the right common carotid artery and placed two cm upstream of the bifurcation as in the US examinations. The MRA volume flow estimations were carried out in MATLAB 6.5 (Mathworks, Natick, MA, USA) using MRA DICOM images where the vessel was delineated by applying a window. The volume flow to each frame was found by adding the velocity values in the vessel and multiplying with pixel area, thereby, yielding a volume flow profile to every volunteer.

Details about the calculations used for volume flow estimation in US and MRA are described by Hansen et al. (2008).

G. Statistics

The stroke volume data obtained with DB, STA, and TO were each compared to stroke volume data obtained with MRA using linear regression analysis with two-tailed significance value given and $p<0.05$ considered significant. The correlation coefficients (R), regression equations (RE), and confidence intervals (CI) were calculated for each comparison. Paired two-tailed t-test was performed on each comparison. Finally Bland-Altman (B-A) plots along with CI were computed to illustrate the differences of estimated stroke volumes.

III. RESULTS

Stroke volume in the right common carotid artery was measured for the 11 volunteers with the three US methods and MRA. No significant differences were observed for any of the three comparisons (DB/MRA: $p=0.65$; STA/MRA: $p=0.24$; TO/MRA: $p=0.36$). In Fig. 2 the scatter plots are given showing the correlation between the each of the three US techniques and MRA with:

DB/MRA: $R= 0.84$ ($p<0.01$, 95% CI: 0.49 to 0.96, RE: MRA= 0.8*DB+1.2)

STA/MRA: R=0.95 (p<0.01, 95% CI: 0.82 to 0.99, RE: MRA= 1.2*STA–1.1)

TO/MRA: R=0.91 (p<0.01, 95% CI: 0.69 to 0.98, RE: MRA= 1.1*TO–0.4).

The resultant B-A plots are shown in Fig. 3. The mean difference (MD) [ml] (95% CI), with upper (UL) and lower limits (LL) of agreement [ml] are, DB/MRA: MD: 0.17 (-0.61 to 0.95), LL:-2.11, UL:2.44; STA/MRA: MD: -0.07 (-0.54 to 0.41), LL:-1.46, UL:1.32; TO/MRA: MD: 0.24 (-0.32 to 0.81), LL:-1.41, UL:1.90.

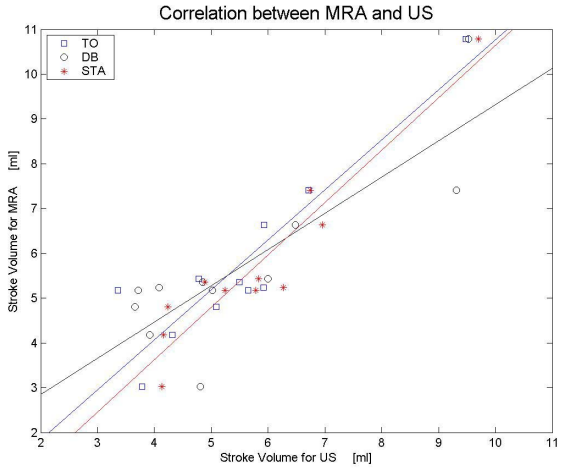

Figure 2: Graph showing the correlation between MRA and the three US methods. The line of best fit is drawn for each comparison.

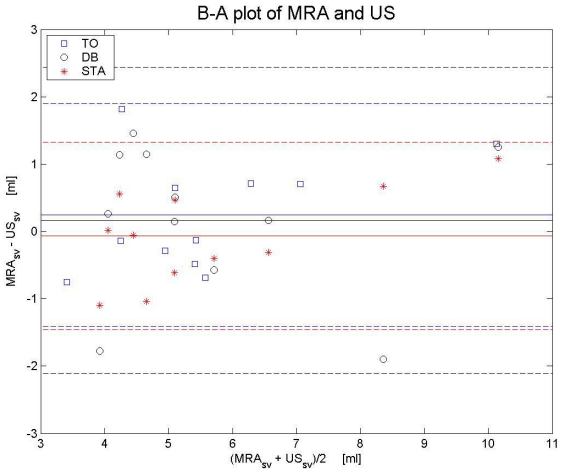

Figure 3: B-A plots of stroke volumes comparing MRA with each of the three US methods showing mean +/- 2 SD as solid and dashed lines, respectively.

IV. Discussion

The correlations of variables DB, STA and TO compared to MRA, when determining the stroke volume in the right common carotid artery of 11 healthy volunteers, were all significant and correlated well. The STA method performed most accurately among the three vector velocity methods. However, it is clear when examining CI that the differences in performance between STA, DB and TO were not significant.

According to the B-A plots (Fig. 3) the velocities were underestimated with the TO and DB method while overestimated with the STA method compared to MRA. The CI for the mean differences overlapped zero for all three methods and was narrowest for STA and broadest for DB (STA: 0.95 ml; TO: 1.13 ml; DB: 1.56 ml). This also applied to the limits of agreement (STA: 2.78 ml; TO: 3.31 ml; DB: 4.55 ml).

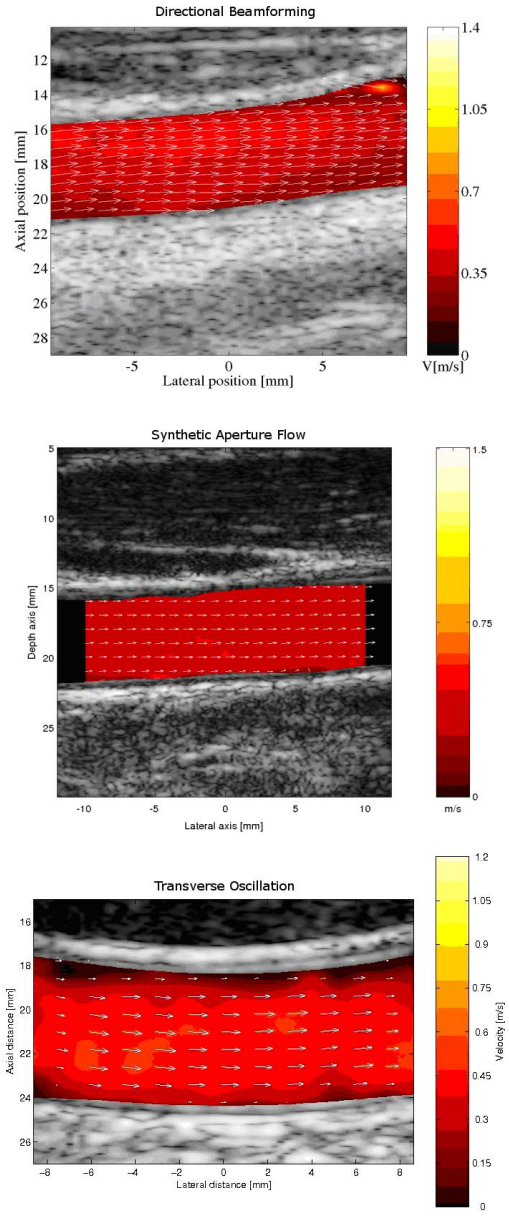

Figure 4: The frames are obtained from different volunteers and to different time. The vector arrows, superimposed onto color flow maps, delineate magnitude and direction of the moving blood scatterers.

A general problem in 2-D US velocity estimation and an important confounder to this study was the clutter filter, which cancelled out stationary echoes from vessel surroundings. The blood signal representing low velocities near the vessel wall

were cancelled out together with clutter signal and added up to a significant stroke volume loss.

The TO method is the most robust method in terms of echo cancelling as a result of the lateral oscillation and the estimates in this setup were obtained with only one filter applied. STA and DB use the same scheme for velocity estimation and both methods were employed with an adaptive filter approach. Nevertheless, the STA method has an advantage in terms of echo cancelling. This relies on the fact that the STA method uses continued data that can be echo cancelled with very long filters.

In the DB method the adaptive filter consisted of two different filters, one for systolic flow and one diastolic flow used for all volunteers. It was employed by manually setting a threshold value for each volunteer defining the systole and diastole.

Movements of the carotid artery during systole affected the estimation of scatterer motion near the vessel wall. While some volunteers had a stationary vessel during the heart beat, moving vessels were observed for others.

In the STA method two filters were designed to alleviate the problem; a filter applied on data from volunteers with a stationary vessel and another filter on data from volunteers with a moving vessel. For each volunteer the filter was manually chosen by examining the recorded data.

Other confounders to be mentioned were the placing of the US scan planes. It was crucial to scan the vessels parallel to the longitudinal axis exactly through the middle of the vessel. Furthermore, as vessels are not perfectly straight tubes, scanning parallel to axis, a part of the artery inevitably will be out of scan plane due to curvature. In either situation the result is expected to be a slightly lowered averaged volume flow when obtained with US. Also, it has to be taken into account that the heart rate, cardiac output, and stroke volume for each volunteer altered between the scans. The four measurements were accomplished within three weeks. Although the volunteers rested 15 min before each measurement, the flow dynamics were expected to fluctuate.

The Linux cluster gave the most flexible environment for processing the data from an experimental point of view, but the processing time was considerable. One VVI sequence took 3 sec. to acquire, 10 hours to store and up to 48 hours to process, where STA by far was the most demanding method. Obviously this affected the logistics and reduced the number of samples that realistically could be enrolled into the study population. However, all three methods can potentially be converted into real-time methods by implementation into commercial scanners, which will make it possible to design studies with larger sample size to produce unambiguous results.

V. Conclusion

In this study it was shown that reliable quantitative measurements could be obtained *in-vivo* with three different angle-independent 2-D vector velocity methods DB, STA, and TO.

The three methods open the possibility of estimating blood velocities in all vessels regardless of angle. Quantitative volume flow measurements could be usable information when evaluating the severity of stenosis of e.g. the internal carotid artery. Novel information about vorticis in bifurcations, turbulence in the heart, flow in tumour vessels and flow in greater vessels can be obtained and could be an aid to the clinician when examining patients with cardiovascular diseases, transplanted organs or malignancies.

Studies of visualizing non-laminar blood flow in complex vessel geometries are on-going to underline the true strength of the vector velocity methods. Future studies of the vector velocity methods DB, STA and TO are needed to conclude the usability in clinical practice.

Acknowledgement

This work was supported by grant 26-04-0024 from the Danish Science Foundation and by B-K Medical A/S, Herlev, Denmark.

References

[1] D.J. Philips, K.W. Beach, J. Primozich and D.E. Strandness, “Should results of ultrasound Doppler studies be reported in units of requency or velocity?” Ultrasound Med Biol, vol 15, pp. 205-212, 1989.

[2] J.A. Jensen, "Directional velocity estimation using focusing along the flow direction: I: Theory and simulaiton," *IEEE Trans Ultrason Ferroelec Freq Contr*, pp. 857-872, 2003

[3] J.A. Jensen and R. Bjerngaard, "Directional velocity estimation using focusing along the flow direction: II: Experimental investigation," *IEEE Trans Ultrason Ferroelec Freq Contr*, pp. 873-880, 2003.

[4] J.A. Jensen and S. Nikolov, "Transverse flow imaging using synthetic aperture directional beamforming," *Proc IEEE Ultrason Symp*, vol. 2, no. 1488, p. 1492, 2002.

[5] J.A. Jensen and P. Munk, "A new method for estimation of velocity vectors," *IEEE Trans Ultrason Ferroelec Freq Contr*, vol. 45, pp. 837-851, 1998.

[6] S.O. Oktar, C. Yucel, D. Karaosmanoglu, K. Akkan, H. Ozdemir, N. Tokgoz, and T. Tali, "Blood-flow volume quantification in internal carotid and vertebral arteries: Comparison of 3 different ultrasound techniques with phase-contrast MR imaging," *AJNR Am J Neuroradiology*, vol. 27(2), pp. 363-369, 2006.

[7] J. Kortbek and J.A. Jensen, "Estimation of Velocity Vector Angles Using the Directional Cross-Correlation Method," *IEEE Trans Ultrason Ferroelec Freq Contr*, vol. 53, pp. 2036-2049, 2007.

[8] J.A. Jensen and N. Oddershede, "Estimation of velocity vectors in synthetic aperture ultrasound imaging," IEEE Trans Med Imag, vol. 25, pp. 1637-1644, 2006.

[9] N. Oddershede and J.A. Jensen, "Effects influencing focusing in synthetic aperture vector flow imaging," *IEEE Trans Ultrason Ferroelec Freq Contr*, vol. 54, pp. 1811-1825, 2007.

[10] J. Udesen and J.A. Jensen, "Investigation of transverse oscillation method," *IEEE Trans Ultrason Ferroelec Freq Contr*, vol. 53, pp. 959-971, 2006.

[11] J.A. Jensen, O. Holm, L.J. Jensen, H. Bendsen, S. Nikolov, B.G. Tomov, P. Munk, M. Hansen, K. Salomonsen, J. Hansen, K. Gormsen H.M. Pedersen and K.L. Gammelmark, "Ultrasound research scanner for relatime synthetic aperture image acquisition" *IEEE Trans Ultrason Ferroelec Freq Contr, vol 52, pp. 881-891, 2005*

[12] K.L. Hansen, J. Udesen, C. Thomsen, J.A. Jensen, and M.B. Nielsen, "In-vivo validation of a blood vector velocity estimator with MR angiography," IEEE Trans Ultrason Ferroelec Freq Contr, In press 2008.

Digital Object Identifier: 10.1109/ULTSYM.2008.0257

Fast Blood Vector Velocity Imaging using ultrasound:

In-vivo examples of complex blood flow in the vascular system

Hansen K.L.[1,3], Udesen J.[2,3], Gran F.[2,3], Jensen J.A.[3], Nielsen M.B.[1]

1) Department of Radiology, Section of Ultrasound, Rigshospitalet, Blegdamsvej 9, 2100 Kbh. Ø, Denmark
2) GN Resound, Lautrupsbjerg 9, 2750 Ballerup, Denmark
3) Center for Fast Ultrasound Imaging, DTU Elektro, Bldg. 349, Technical University of Denmark, 2800 Lyngby, Denmark

Abstract – Conventional ultrasound methods for acquiring color flow images of the blood motion are restricted by a relatively low frame rate and angle dependent velocity estimates. The Plane Wave Excitation (PWE) method has been proposed to solve these limitations. The frame rate can be increased, and the 2-D vector velocity of the blood motion can be estimated. The transmitted pulse is not focused, and a full speckle image of the blood can be acquired for each emission. A 13 bit Barker code is transmitted simultaneously from each transducer element. The 2-D vector velocity of the blood is found using 2-D speckle tracking between segments in consecutive speckle images. The flow patterns of six bifurcations and two veins were investigated in-vivo. It was shown: 1) that a stable vortex in the carotid bulb was present opposed to other examined bifurcations, 2) that retrograde flow was present in the superficial branch of the femoral artery during diastole, 3) that retrograde flow was present in the subclavian artery and antegrade in the common carotid artery during diastole, 4) that vortices were formed in the buckets behind the venous valves in both antegrade and retrograde flow, and 5) that secondary flow was present in various vessels. The *in-vivo* results have revealed complex flow patterns not previously visualized with ultrasound imaging and indicate a flow complexity in both simple and complex vessel geometries.

I. Introduction

Color flow mapping (CFM) used for visualizing blood motion has two major limitations. The frame rate is low and the velocity estimates are angle dependent.

In conventional ultrasound (US) each frame consists of a number of lines. The frame rate is low as several pulse transmissions are necessary along each line to achieve a usable image. 2-D duplex mode (B-mode image combined with CFM) in commercial scanners are performed at frame rates down to 8-10 Hz. This is unsuitable for visualizing rapid temporal changes in the blood flow. The problem is aggravated in triplex mode (B-mode image, CFM and spectral Doppler) and will furthermore be a major hurdle in 3D duplex/triplex scanning.

The velocity estimate in conventional CFM is only found along the US beam direction i.e. in the axial direction [1]. In CFM no angle correction is performed and thus, no correct velocities are given. Consequently, CFM is only used as a qualitative method for visualizing flow. In spectral Doppler examination, the angle correction scheme is applied on velocities estimates found within the range gate. The spectral Doppler method is used quantitatively as it is believed that true velocities are obtained. However, it is impossible to predict the direction of a blood scatterer based on the B-mode image [2] as the flow profiles in the cardiovascular system never are purely laminar and therefore impossible to angle correct. Hence, incorrect blood velocities are always given with the conventional Doppler methods and valuable information of the complexity of the blood flow is never documented even though turbulence and vortices have predilection for atherosclerotic lesions [3].

A novel method for estimating blood motion with ultrasound has been proposed by Udesen et al. [4]. The method called Plane Wave Excitation (PWE) acquires, with a high frame rate, 2-D vector velocities of the blood using a 1-D linear transducer. The PWE method has previously been validated in simulations and flow-phantoms with promising results. Examples of *in-vivo* sequences have been produced of the carotid artery and results have been compared to MR angiography measurements with mean deviation of volume flow of 9 %.

This paper presents *in-vivo* vector velocity estimates of complex vessel geometries obtained with the PWE method. The results are compared to the literature and perspectives for vector flow are discussed.

II. Materials and Methods

A. Patients

This study was performed after approval by The Danish National Committee on Biomedical Research Ethics. Four healthy volunteers with no history of vascular or cardiac disease (three males and one female, 26 – 45 y, mean age: 34 y) entered the study after informed consent. Scan sequences were acquired of two carotid bifurcations, two femoral bifurcations, the bifurcation at the brachiocephalic trunk, the bifurcation of the subclavian artery as well as the internal jugular vein and the great saphenous vein, both with venous valves. The scans were all recorded with the volunteers in supine position except the scan of the great saphenous vein, where the volunteer was in standing position while performing dorsal and plantar flexion to simulate walking. All scans were carried out by an experienced radiologist (KLH).

B. The Plane Wave Excitation method

The PWE method is based on a number of well described techniques which all previously have been validated. A

thorough introduction to the PWE method is given in [4] based on a method previously suggested for elastography [5].

In PWE all elements of the transducer are excited at the same time thereby creating a pressure wave with a nearly plane front. The unfocused pulse covers the entire imaging plane with acoustic energy and a full speckle image is obtained for every emmision. To increase the penetration of the signal into the tissue, a 13 bit Barker code is used instead of a conventional pulse.

The angle independent vector velocity estimates are found when tracking speckle motion between consecutive speckle images by using a speckle tracking approach called sum of squared differences [6]. Using this approach no assumptions of laminar flow parallel to vessel boundaries are necessary for velocity estimation as no angle correction scheme is performed.

C. *Setup*

The experimental scanner RASMUS [7] and a 5 MHz linear array (BK-8804) transducer were used to acquire data. The post processing was done offline with MATLAB 6.5 (Mathworks, Natick, MA, USA) on a 100 CPU Linux cluster. The frame rate on the vector velocity images was 100 Hz.

III. Results

In Fig. 1 the vortex formation in the carotid bulb of two different volunteers is shown. In the left frame the internal carotid artery is seen as the superficial vessel while in the right frame it is seen as the profound vessel. For both volunteers a vortex with low velocities in the carotid bulb was present during the entire heart cycle. Apart from the vortical recirculation in the bulb no retrograde flow was present.

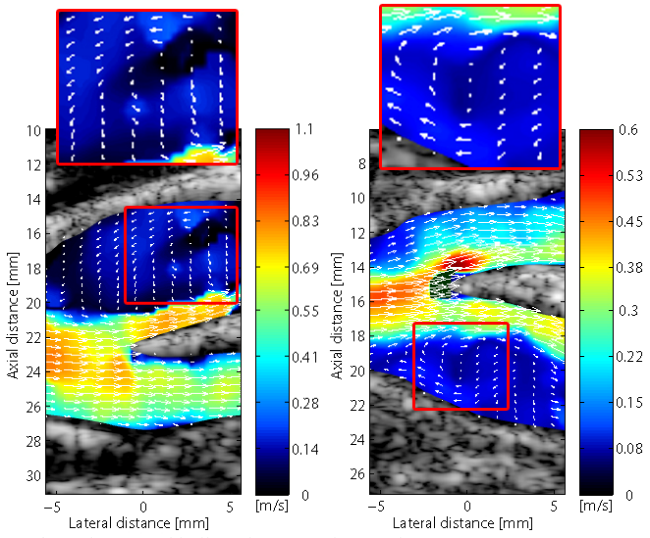

Fig.1: In the carotid bulb of the internal carotid artery a vortex was present during the entire heart cycle. For both volunteers the depicted frame was taken from the systole.

In Fig. 2 the brachiocephalic trunk is shown. In diastole the flow filled the common carotid artery (superficial vessel) from the subclavian artery (profound vessel). No vortex was present in systole but disturbed flow with vortices was seen in the subclavian artery when flow reversed in end systole and end diastole.

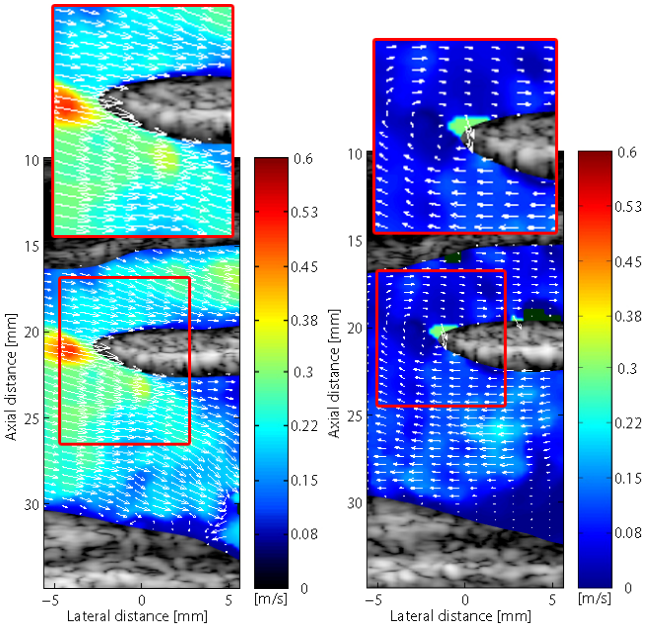

Fig. 2: No vortex was seen in the brachiocephalic trunk during systole (left frame). The blood flowed in diastole from the subclavian artery (profound vessel) to the common carotid artery (superficial vessel) (right frame).

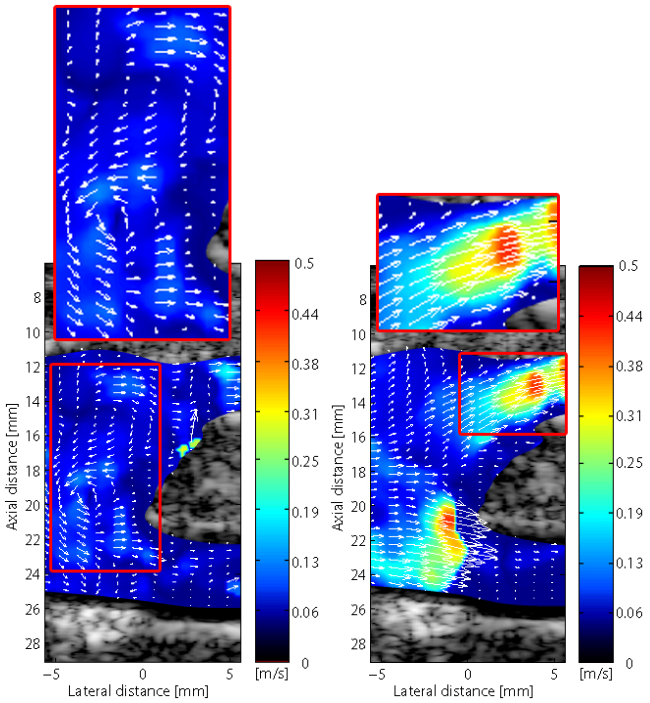

Fig. 3: In the subclavian artery vortices were present after peak systole and through out the diastole. Here is shown a frame taken from the beginning of the diastole (left frame). No turbulence in the vertebral artery (superficial vessel) and the thyrocervical trunk (profound vessel) was present during peak systole (right frame).

In Fig. 3 the bifurcation of the thyrocervical trunk and the vertebral artery is shown. Vortices in the subclavian artery scanned cross-sectionally were visible right after peak systole and through out the diastole (left frame). The secondary flow swept from the superficial part of the subclavian artery and downwards in an s-shaped pattern creating two vortices. During peak systole the flow propagated without turbulence to the vertebral artery (superficial vessel) and the thyrocervical trunk (profound vessel) as seen in the right frame.

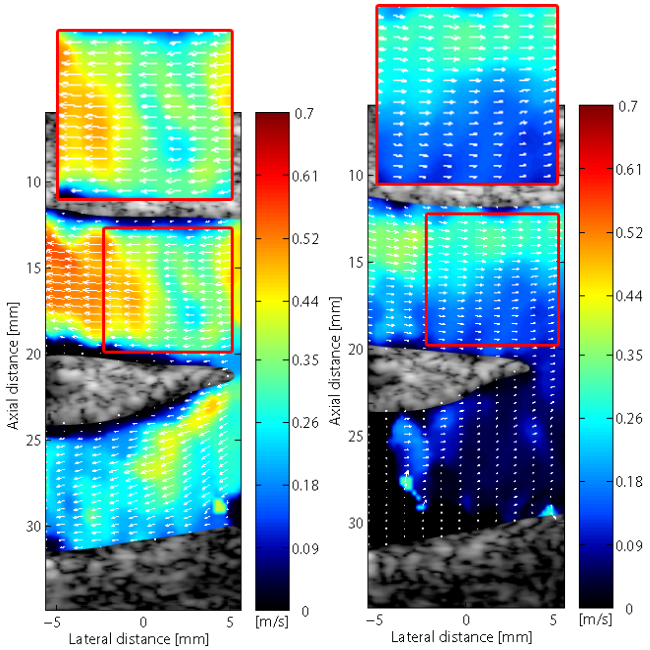

Fig. 4: In the femoral bifurcation no vortex was present during systole (left frame). Marked reversed flow in the superficial branch of the femoral artery was present during diastole (right frame).

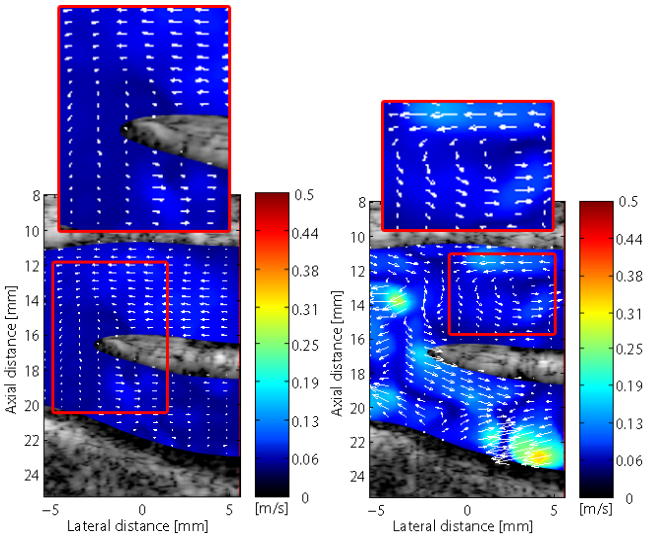

Fig. 5: In the superficial branch of the femoral artery retrograde flow was seen during diastole (left frame) Disturbed flow was seen in end systole and end diastole, when the flow reversed (right frame).

In Fig. 4 and Fig. 5 frames of two different femoral bifurcations are shown. For both sequences no turbulence was seen during the heart cycle but marked reversed flow was seen in the superficial branch during the beginning of the diastole. Similar to the brachiocephalic trunk shown in Fig. 2 disturbed flow was present with vortices when flow reversed. This can be seen in right frame of Fig. 5.

The venous valves of the great saphenous vein and the internal jugular vein were scanned. In Fig. 6, a venous bulb of the great saphenous vein is depicted. Although the valves were not visible, the effect of the valves on the flow was obvious. During opening of the valves the flow was squeezed to form a jet and vortices were formed in the buckets behind the valves (left frame). No retrograde flow was present and during the closed phase bidirectional blood motion was seen with the competent valves as a separator (right frame). The valves of the internal jugular vein are visible in Fig. 7. The flow pattern around the valves of the internal jugular vein was similar to the flow pattern observed in the great saphenous vein except that retrograde flow was observed due to incompetent valves. Vortices were formed in the buckets behind the valves and a jet was formed between the valves during the opened phase (left frame). During retrograde flow vortices were formed upstream of the valves and a jet was seen between the valves (middle frame). The common carotid artery was scanned cross-sectionally and a marked secondary flow was observed during systole (right frame).

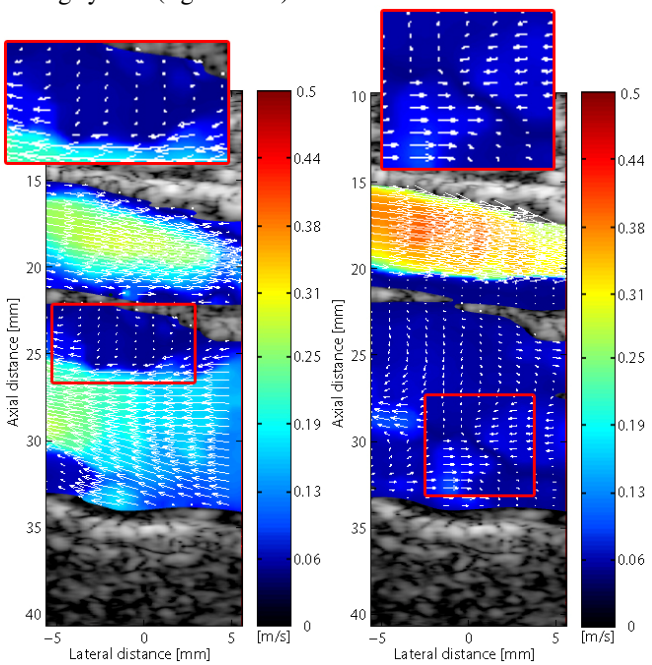

Fig. 6: In the great saphenous vein (profound vessel) a jet was formed between the valves and vortices was formed behind the valves during antegrade flow (left frame). No retrograde flow were present as the venous valves were competent (right frame). The femoral artery is seen as the superficial vessel in both frames.

IV. Discussion

Six bifurcations were examined on four volunteers. The two recorded carotid bifurcation showed a well-defined vortex in

the carotid bulb during the entire heart cycle. This is in accordance with earlier results obtained with US vector velocity examinations [8].

In the two femoral bifurcations and the brachiocephalic trunk reversed flows were observed in the diastole. The diastolic flow reversed in the superficial branches of the femoral artery with antegrade flow in the profound branches. In the brachiocephalic trunk the flow reversed in the subclavian artery and filled the common carotid artery. It is believed that antegrade flow in the peripheral circulation in diastole primarily is forwarded from the aorta due to the elastic forces of the aortic wall. In literature this is known as the *windkessel* effect [9]. The PWE results indicate that the blood reserve forwarded in diastole especially to the brain derives from other arteries than the aorta.

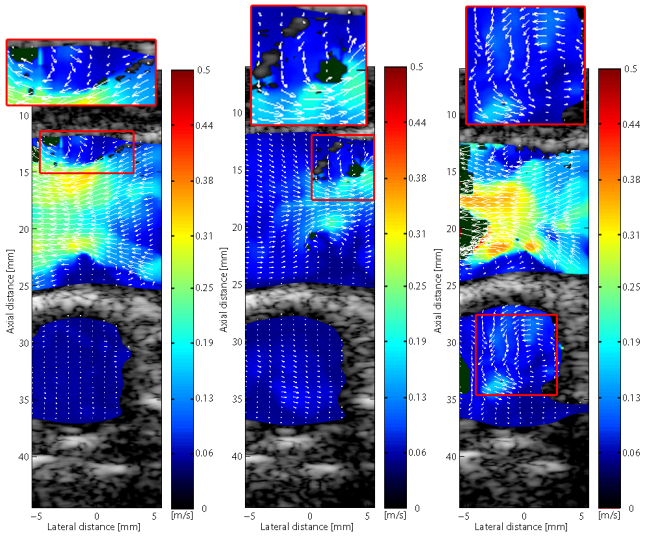

Fig. 7: In the jugular vein (superficial vessel) the flow was squeezed by the incompetent venous valves forming a jet during both antegrade and retrograde flow (left and middle frame, respectively). Vortices were formed in the buckets behind the valves during antegrad flow (left frame) and upstream of the valves during retrograde flow. In the carotid artery (profound vessel) secondary flow was seen during systole when scanned cross-sectionally (right frame).

With the PWE method instantaneous vector velocities of venous valves were recorded *in-vivo*. It was shown that competent valves in the great saphenous vein were present, and that vortices were formed behind valves in the buckets. This is in concordance with previous studies [10;11]. The examination of the internal jugular vein revealed the presence of incompetent valves and retrograde flow. The prevalence of incompetent valves of the internal jugular vein have been described to be as high as 36.8% to 38.4% of healthy persons [12]. The findings with the PWE method concerning valves in the great saphenous vein and the internal jugular vein confirm the literature. However, vortices on either side of the valves created by bidirectional flow have not been reported previously.

Secondary flow was seen in the common carotid artery (Fig.8) and in the subclavian artery (Fig 4.). Secondary flow has been predicted by computational fluid dynamics and magnetic resonance imaging [13;14] and connected atherosclerotic disease assessment [15] but not before has it been possible to visualize the secondary flow with US.

V. Conclusion

With the PWE method different vessel geometries have been examined and flow patterns described. The fast, angle independent, non-invasive, blood vector velocity method is unique compared to conventional imaging modalities in the ability to visualize complex flow patterns and has revealed new information in the field of blood dynamics.

References

[1] J.A. Jensen, *Estimation of Blood velocities using ultrasound: A signal processing approach*. New York: Cambridge University Press, 1996.

[2] D.J. Phillips, K.W. Beach, J. Primozich, and D.E. Strandness, "Should results of ultrasound Doppler studies be reported in units of frequency or velocity?," *Ultrasound Med Biol*, vol. 15, pp. 205-212, 1989.

[3] C. Cheng, D. Tempel, R. van Harperen, A. van der Baan, F. Grosveld, M. Daermen, R. Krams, and R. de Crom, "Atherosclerotic lesion size and vulnerability are determined by patterns of fluid shear stress," *Circulation*, vol. 113, pp. 2744-2753, 2006.

[4] J. Udesen, F. Gran, K.L. Hansen, J.A. Jensen, C. Thomsen, and M.B. Nielsen, "High frame-rate blood vector velocity imaging using plane waves: simulations and preliminary experiments," *IEEE Trans Ultrason Ferroelec Freq Contr*, vol. 55, no. 8, pp. 1729-1743, 2008.

[5] M. Tanter, J. Bercoff, L. Sandrin, and M. Fink, "Ultrafast compound imaging for 2-d motion vector estimation: application to transient elastography," *IEEE Trans Ultrason Ferroelec Freq Contr*, vol. 49, pp. 1363-1374, 2002.

[6] G.E. Trahey, J.W. Allison, and O.T. Ramm, "Angle independent ultrasonic detection of blood flow," *IEEE Trans Biomed Eng*, vol. 34, pp. 965-967, 1987.

[7] J.A. Jensen, O. Holm, L.J. Jensen, H. Bendsen, S. Nikolov, B.G. Tomov, P. Munk, M. Hansen, K. Salomonsen, J. Hansen, K. Gormsen, H.M. Pedersen, and K.L. Gammelmark, "Ultrasound research scanner for realtime synthetic aperture image acquisition," *IEEE Trans Ultrason Ferroelec Freq Contr*, vol. 52, pp. 881-891, 2005.

[8] J. Udesen, M.B. Nielsen, K.R. Nielsen, and J.A. Jensen, "Examples of In Vivo Blood vector velocity Estimation," *Ultrasound Med Biol*, vol. 33, pp. 541-548, 2007.

[9] G.G. Belz, "Elastic properties and Windkessel function of the human aorta," *Cadiovasc Drugs Ther*, vol. 9, pp. 73-83, 1995.

[10] Y. Qui, R.C. Quijano, S.K. Wang, and H.C. Hwang, "Fluid dynamics of venous valve closure," *Ann Biomed Eng*, vol. 23, pp. 750-759, 1995.

[11] F. Lurie, R.L. Kistner, B. Eklof, and D. Kessler, "Mechanism of venous valve closure and role of the valve in circulation: A new concept," *J Vasc Surg*, vol. 38, pp. 955-961, 2003.

[12] M. Nedelmann, D. Techner, and M. Dieterich, "Analysis of internal jugular vein insufficinecy - a comparison of two ultrasound methods," *Ultrasound Med Biol*, vol. 33, pp. 857-862, 2007.

[13] K.L. Lee, D.J. Doorly, and D.N. Firmin, "Numerical simulations of phase contrast velocity mapping of complex flows in an anatomically realistic bypass graft geometry," *Med Phys.*, vol. 33, no. 7, pp. 2621-2631, July2006.

[14] D.A. Steinman, B.T. Jonathan, M.L. Hanif, J.S. Milner, B.K. Rutt, and J.D. Spence, "Reconsturction of carotid bifurcation hemodynamics and wall thichkness using computational fluid dynamics and MRI," *Magnet Reson Med*, vol. 47, pp. 149-159, 2002.

[15] T. Shipkowitz, V.G.J. Rodgers, L.J. Frazin, and KB. Chandran, "Numerical study on the effect of secondary flow in the human aorta on local shear stresses in abdominal aortic branches," *J Biomech*, vol. 33, pp. 717-728, 2000.

Digital Object Identifier: 10.1109/ULTSYM.2008.0394

In-vivo validation of fast spectral velocity estimation techniques – preliminary results

Hansen K.L.[1,3], Gran F.[2,3], Pedersen M.M.[1,3], Holfort I.K.[3], Jensen J.A.[3], Nielsen M.B.[1]

1) Department of Radiology, Section of Ultrasound, Rigshospitalet, Blegdamsvej 9, 2100 Kbh. Ø, Denmark
2) GN Resound, Lautrupsbjerg 9, 2750 Ballerup, Denmark
3) Center for Fast Ultrasound Imaging, DTU Elektro, Bldg. 349, Technical University of Denmark, 2800 Lyngby, Denmark

Abstract – **Spectral Doppler is a common way to estimate blood velocities in medical ultrasound (US). The standard way of estimating spectrograms is by using Welch's method (WM). WM is dependent on a long observation window (OW) (about 100 transmissions) to produce spectrograms with sufficient spectral resolution and contrast. Two adaptive filterbank methods have been suggested to circumvent this problem: the Blood spectral Power Capon method (BPC) and the Blood Amplitude and Phase Estimation method (BAPES). Previously, simulations and flow rig experiments have indicated that the two adaptive methods can display sufficient spectral resolution for much shorter OWs than WM. The purpose of this paper is to investigate the methods on a larger population and letting a clinical expert evaluate the spectrograms. Ten volunteers were scanned over the right common carotid artery and four different approaches were used to estimate the spectrograms: WM with a Hanning window (WMhw), WM with a boxcar window (WMbw), BPC and BAPES. For each approach the window length was varied: 128, 64, 32, 16, 8, 4 and 2 emissions/estimate. Thus, from the same data set of each volunteer 28 spectrograms were produced. The artery was scanned using the experimental ultrasound scanner RASMUS and a B-K Medical 5 MHz linear array transducer with an angle of insonation not exceeding 60°. All 280 spectrograms were then randomised and presented to a radiologist blinded for method and OW for visual evaluation: useful or not useful. WMbw and WMhw estimated less useful spectrograms compared to the adaptive methods at OW below 64. The BAPES method performed better than BPC at OW of 16 and 8. Furthermore, BAPES was the only method that estimated spectrograms equally well for OW of 16 compared to OW of 128. All four approaches failed at OW of 4 and 2. The preliminary results indicate that the OW can be reduced to 32 when using the BPC method and to 16 when using the BAPES method for spectral blood estimation. This will liberate processing time in spectral US examination and could be used to increase the frame rate of the interleaved B-mode image.**

I. Introduction

The spectral Doppler (SD) method is a quantitative technique providing estimates of blood flow within a range gate on a single image line. The SD is displayed with a B-mode image in duplex mode in which the B-mode image is used for navigation for correct placement of the range gate. Alternatively SD is displayed in triplex mode with a B-mode image and color flow map.

A typical B-mode image consists of about 100 image lines. The blood flow estimated by SD is found by emitting focused pulses repeatedly along one of these image lines. The pulses reflected by blood scatterers, are received as echoes by the transducer, focused along the line by the scanner and compared to determine the axial blood scatterer movement. Knowing the movement of the scatterer and the time between lines yields the axial velocity [1].

The result of the SD estimation is angle corrected by the operator and presented as blood velocities plotted against time denoted as the power spectrum density (PSD). In most commercial scanners Welch's method (WM) is used for estimation of the PSD [2]. To obtain an acceptable spectral resolution with WM, a window of about 100 consecutive pulses is used for each velocity estimate. Clearly this affects the temporal resolution of the conventional PSD but more importantly it also affects the frame rate of the interleaved B-mode image. Due to the necessary emissions for the different modalities in use, whether the mode is duplex or triplex, the resulting frame rate is low and often decreased to the point where the information of the SD examination is impaired [3;4]. In practice the operator can experience difficulties in placing the range gate in the vessel of interest as the B-mode image used for navigation is not updated adequately.

Adaptive spectral techniques can potentially offer great improvement in spectral resolution and contrast compared to WM.

The Blood spectral Power Capon method (BPC) based on a minimum variance estimator has been proposed by Stoica et al [2;5] and the Blood Amplitude and Phase Estimation method (BAPES) method has been proposed by Gran et al. [6].

The algorithm used in BPC has previously been compared to the averaged periodogram used in WM [7;8]. Furthermore, BPC and BAPES have been evaluated in simulations using Field II [9], in a flow rig with steady laminar flow and in a single *in-vivo* experiment [10].

In this paper the two alternative methods BAPES and BPC are validated *in-vivo* against the conventional WM in a prospective, randomized, blinded trial. Ten volunteers were scanned on the common carotid artery. From each data set, spectrograms were found by using the different methods on a series of different observation windows (OW). The resulting spectrograms were randomized and presented to a radiologist blinded for method and OW for evaluation.

II. Materials and methods

A. Patients

This prospective study was performed after approval by The Danish National Committee on Biomedical Research Ethics. Ten healthy volunteers (nine males and one female, mean age: 29.1 years, range: 24-36 years) entered the study after informed consent. The right common carotid artery was examined in all volunteers using US. All scans were carried out by an experienced radiologist.

The conventional WM along with the two alternative spectral methods are presented in this section. WM is applied on data using two different weighting schemes: WM with a Hanning window (WMhw) and WM with a boxcar window (WMbw).

B. Spectral estimators

WMhw is the preferred conventional spectral estimator. It is well known in digital signal processing [11] that due to Hanning weighting of data the resulting spectrogram has a good contrast at the expense of spectral resolution. On the contrary spectrograms generated with the WMbw approach have a better spectral resolution but a decreased contrast.

The BPC method is an alternative method using adaptive filtration on data. Unique filters are designed to every velocity component in the data set. Hence, a unique matched filterbank is generated for each specific data set where the total power of the filters for each velocity of interest is minimized while not distorting the signal of interest. Thereby a highly improved PSD in terms of contrast and spectral resolution can be achieved compared to WM.

The BAPES method is based on a matched filterbank framework as BPC [2;12]. However, in the BAPES method the filtered noise power is minimized fulfilling the constraint that the signal of interest is not distorted. PSD acquired with the BAPES method has both increased contrast and spectral resolution compared to PSD acquired with the BPC method.

C. Spectrograms and spectra

Spectrograms for one volunteer with three systoles recorded are presented in Fig. 1 and Fig. 2 where estimated blood velocities were plotted against time. In Fig. 1, PSDs generated with an OW of 128 emissions/estimate are presented while an OW of 16 emissions/estimate was used to generate the PSDs presented in Fig. 2. The gaps in the PSDs represent the necessary pulse emissions used for generating the interleaved B-mode images.

The spectra from the PSDs to OW of 128 (Fig.1) and 16 (Fig. 2) taken to identical time are presented in Fig. 3. The spectra are plotted with amplitude given for each velocity component.

In Fig.1 and particular in Fig. 2 it is clear that the width of the white curve representing the estimated blood velocities is narrower e.g. more precise for WMbw than WMhw in terms of spectral resolution. It is seen when generating PSD using an OW of 16 (Fig. 2) that the adaptive methods estimates have a higher spectral resolution than WM and that estimates obtained with BAPES have a higher spectral resolution than estimates found with BPC.

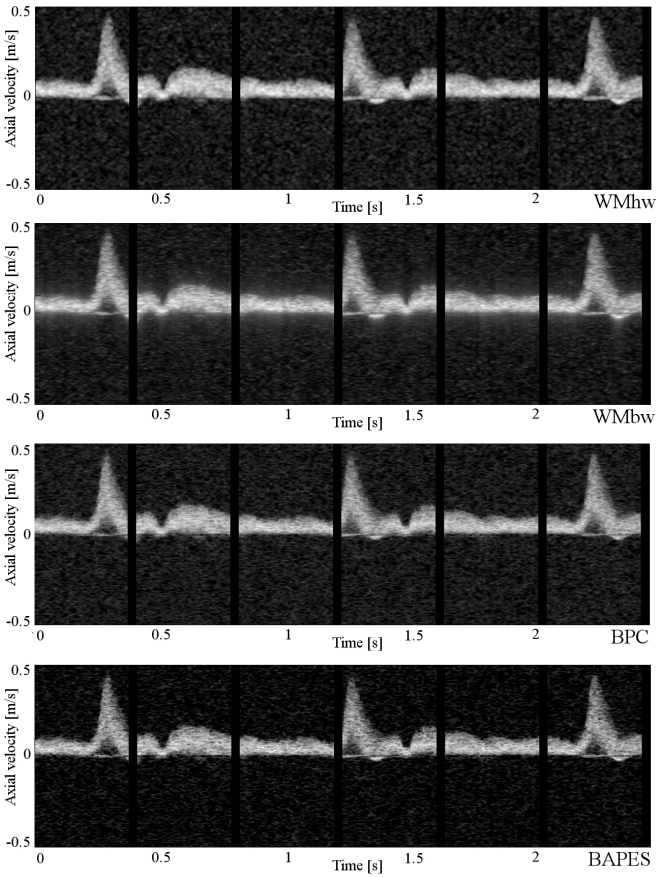

Figure 1: From the same volunteer PSDs are found using the four methods on an OW of 128. All methods display similar performance and it is easy to track the changes in the blood flow during the three systoles. However, WMbw estimates show slightly more spectral leakage as compared to WMhw, BPC and BAPES.

The decrease in contrast from BAPES to BPC and WM is seen in the PSDs as a more smeared appearance around the white curves. WMbw performs poorest among the four methods. The boxcar window results in a ringing phenomenon illustrated in Fig. 2.

The spectra for the methods at OW 128 and OW 16 are shown in Fig. 3. The side lobes representing leakage from the true velocity are suppressed, while the main lobe representing the true velocity is broadened for WMhw compared to WMbw. The pronounced side lobes for WMbw particular seen at OW 16 correspond to the ringing phenomenon shown in Fig. 2. Estimates obtained with BAPES display better side lobe levels and a narrower main lobe as compared to both BPC and WM.

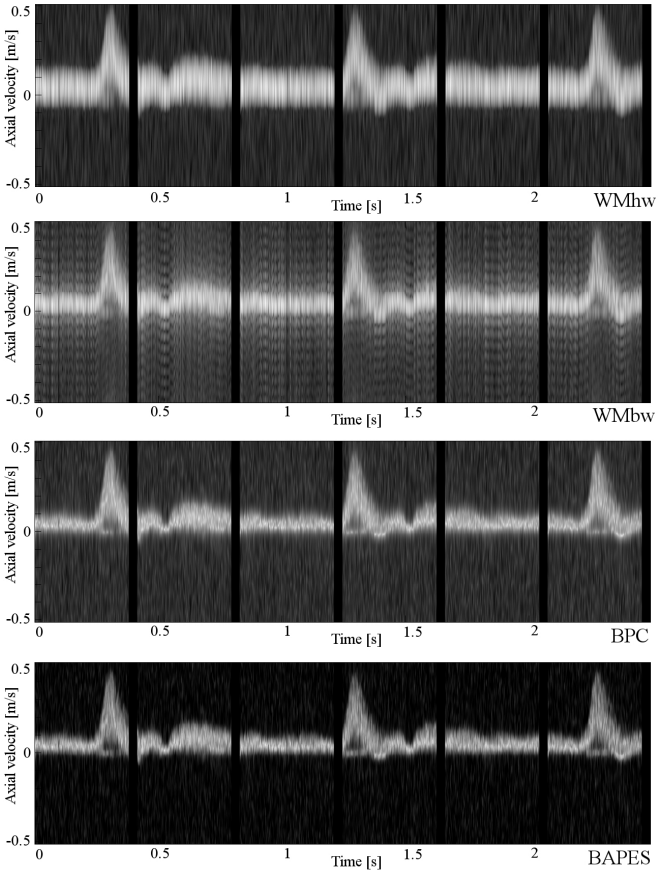

Figure 2: From the same volunteer are PSD found using the four methods with an OW of 16. It is no longer possible to rely on WM estimates due to significant spectral leakage. However, the BPC and BAPES still manage to represent the blood velocity.

D. Setup

Ten healthy volunteers were scanned on the right common carotid artery using the experimental scanner RASMUS [13] and a B-K Medical 8804, 7 MHz linear array transducer. Setup is given in Table 1.

One data set was recorded for each volunteer and post processed using the four different methods; WMhw, WMbw, BPC and BAPES. The post processing was done offline with MATLAB 6.5 (Mathworks, Natick, MA, USA) on a 100 CPU Linux cluster.

TABLE I
SCANNER AND TRANSDUCER SETUP

Parameter	Value
f_s	40 MHz
f_c	7 MHz
f_{prf}	1890 kHz
No. xmt.	64 elements
Apod. xmt.	Uniform
No. rcv.	64 elements
Apod. rcv.	Hanning

BPC and BAPES are both methods based on experimentally obtained data. However, the data was obtained in the same way as in conventional spectral Doppler systems. Thus, the adaptive methods for estimating blood velocities are within the limits of Food and Drug Administration (FDA).

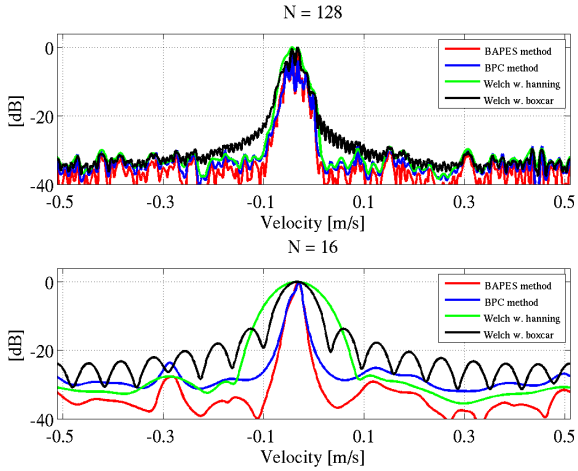

Figure 3: From the same volunteer to identical time a spectrum for each method at OW 128 and OW 16 is shown.

III. RESULTS

The results of the 280 evaluations are depicted in Fig. 4 where the usefulness of the four methods given in percentage is plotted against OW. It is seen that the four approaches perform almost equally good with OW of 128 and 64 while the WM approaches fail to produce useful spectrograms at OW of 32. BAPES is superior to BPC at OW 16 and all the methods fails at OW shorter than of 16.

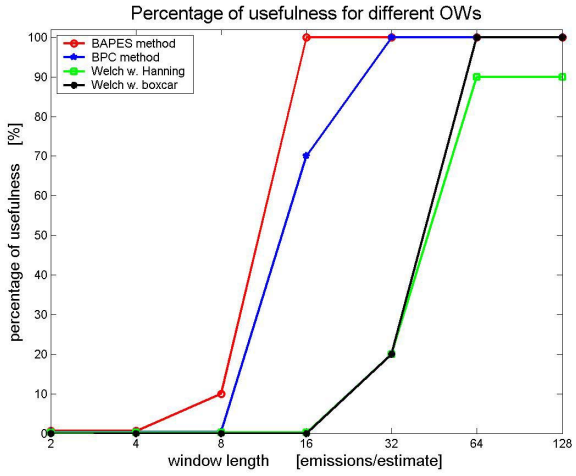

Figure 4: Evaluation of the generated PSDs given by a radiologist is shown as percentage of usefulness for different OWs.

IV. Discussion

The overall result shows that BAPES performed best among the four methods. At OW of 128 and 64, the methods performed equally well except WMhw that scored 90%. When reducing the OW to 32 the alternative methods BAPES and BPC performed better than WMhw and WMbw. However, BAPES was superior to BPC at OW of 16 and 8. At these OWs the conventional methods were useless. When the OW was decreased to 4 and 2 all four methods failed.

Only the BAPES method performed as well for OW of 16 compared to OW of 128.

The US examination of today can potentially be improved if the conventional WM for blood velocity estimation used in commercial scanners was to be replaced with one of adaptive spectral estimators BPC or BAPES. Consequently, either the temporal resolution of the spectrogram will be increased and give the US operator more information of the blood velocity profile. Or the improvement could be an increase in frame rate for the interleaved B-mode image in i.e. triplex scan mode. This will facilitate the navigation under examination so the placement of the range gate can be adjusted according to respiratory movements and be correctly placed in the vessel of interest.

According to Gran et al. (2008), the BAPES method is more computationally demanding compared to BPC which is heavier than the conventional WM. However, when reducing the OW, the computationally costs decrease as well. Therefore the BAPES method implemented with an OW of 16 or the BPC method with an OW of 32 may be as tractable as WM with a much longer OW. It should therefore be possible to implement the methods into commercial scanners and convert the methods to an actual real-time modality.

V. Conclusion

In this paper the performances of two adaptive spectral estimators BPC and BAPES were investigated *in-vivo*. The preliminary results indicated that the adaptive methods were superior to the conventional WM and that BAPES was superior to BPC.

According to the given judgements OW can be reduced to 32 when using BPC, and 16 when using BAPES method for estimating PSD without loosing performance.

Adaptive spectral estimation could potentially bring major improvements to duplex and triplex scan mode as an increase of the temporal resolution of the spectrogram or probably more interesting as an increase of the frame rate for the interleaved B-mode image.

Further studies are needed. An on-going study investigates the performance of adaptive spectral estimation in which spectrograms are evaluated by a number of radiologists to achieve results with statistical relevance. Other studies will concern the estimation of blood velocity estimation in different vessel geometries and scan depths.

Acknowledgement

This work was supported by grant 26-04-0024 from the Danish Science Foundation and by B-K Medical A/S, Herlev, Denmark.

References

[1] J.A. Jensen, Estimation of Blood velocities using ultrasound: A signal processing approach. New York: Cambridge University Press, 1996.

[2] P. Stoica and R. Moses, Spectral analysis of signals Prentice Hall, Upper Saddle River N.J., 2005.

[3] J.B. Kruskal, P.A. Newman, L.G. Sammons, and R.A. Kane, "Optimizing Doppler and color flow US: Application to hepatic sonography," Radiographics, vol. 24, pp. 657-675, 2004.

[4] K. Ferrara and G. DeAngelis, "Color flow mapping," Ultrasound Med Biol, vol. 23, pp. 321-345, 1997.

[5] P. Stoica and R. Moses, Introduction to spectral analysis Prentice Hall, Upper Saddle River N.J, 1997.

[6] F. Gran, A. Jakobsson, and J.A. Jensen, "Adaptive blood velocity estimation in medical ultrasound," Proc IEEE ICASSP, vol. 1, pp. 293-296, 2007.

[7] P.J. Vaikus, R.S.C. Cobbold and K.W. Johnston, "A comparative study and assesment of Doppler ultrasound spectral estimation techniques, Part 2: Methods and results," Ultrasound Med Biol, vol. 14, pp. 673-688, 1988.

[8] P.J. Vaikus and R.S.C. Cobbold, "A comparative study and assesment of Doppler ultrasound spectral estimation techniques, Part 1: Estimation methods," Ultrasound Med Biol, vol. 14, pp. 661-672, 1988.

[9] J.A. Jensen and N.B. Svendsen, "Calculation of pressure fields from arbitrarily shaped, apodized, and excited ultrasound transducers," IEEE Trans Ultrason Ferroelec Freq Contr, vol. 39, pp. 262-267, 1992.

[10] F. Gran, A. Jakobsson, and J.A. Jensen, "Adaptive spectral Doppler estimation," IEEE Trans Ultrason Ferroelec Freq Contr, vol. submitted 2008.

[11] J.G. Proakis and D.G. Manolakis, Digital signal processing: Principles, algorithms and applications, 4. ed. Upper Saddle River, New Jersey, USA: Pearson Prentice Hall, 2007.

[12] P. Stoica, A. Jakobsson and J. Li, "Matched-filterbank interpretation of some spectral estimators," Signal Processing, vol. 66, pp. 45-59, 1998.

[13] J.A. Jensen, O. Holm, L.J. Jensen, H. Bendsen, S. Nikolov, B. G. Tomov, P. Munk, M. Hansen, K. Salomonsen, J. Hansen, K. Gormsen, H. M. Pedersen, and K.L. Gammelmark, "Ultrasound research scanner for realtime synthetic aperture image acquisition," IEEE Trans Ultrason Ferroelec Freq Contr, vol. 52, pp. 881-891, 2005.